

# Label-free Analytics by Transmission Localized-SPR and its Application to Small Molecules Monitoring in Serum

THÈSE N° 6454 (2014)

PRÉSENTÉE LE 21 NOVEMBRE 2014

À LA FACULTÉ DES SCIENCES ET TECHNIQUES DE L'INGÉNIEUR  
CHAIRE SWISS-UP EN INGÉNIERIE - LABORATOIRE D'ÉLECTRONIQUE POUR LES SCIENCES DU VIVANT  
PROGRAMME DOCTORAL EN BIOTECHNOLOGIE ET GÉNIE BIOLOGIQUE

ÉCOLE POLYTECHNIQUE FÉDÉRALE DE LAUSANNE

POUR L'OBTENTION DU GRADE DE DOCTEUR ÈS SCIENCES

PAR

Giulia CAPPI

acceptée sur proposition du jury:

Prof. N. Stergiopoulos, président du jury  
Prof. C. Guiducci, Prof. L. Benini, directeurs de thèse  
Dr M. I. Boamfa, rapporteur  
Prof. O. Martin, rapporteur  
Dr S. Tombelli, rapporteuse



ÉCOLE POLYTECHNIQUE  
FÉDÉRALE DE LAUSANNE

Suisse  
2014



To my family



# Acknowledgements

I first want to acknowledge my supervisor, Prof Carlotta Guiducci, not only for giving me the opportunity to work in her group but also for four years full of interesting science and great social life apart from work. Her motivation and encouragement to tackle outstanding challenges, the multidisciplinary approach and the many different scientific facets of the CLSE were a source of creativity and inspiration.

I want to thank my thesis committee Prof Luca Benini, Dr Marius Boamfa, Prof Olivier Martin, Dr Sara Tombelli and Prof Nikolaos Stergiopoulos for their detailed and valuable feedback on my work. Especially, my co-advisor Luca Benini, for his guidance during my thesis, Olivier Martin for his constant interest in the progress of this thesis and Marius Boamfa for his advices that facilitated many of my decisions.

Furthermore, I acknowledge the collaboration with the department of Clinical Pharmacology at the Centre Hospitalier Universitaire Vaudoise, which provided me with the motivating perspective of where my work could go. Without the help from Marco Bianchessi, Yessica Moncada and Federica Guerinoni at STMicroelectronics this project would have not progressed as quickly. For the sample preparation in the Center of Micro- and Nanotechnology (CMi) at EPFL, the staff not only ensured the constant availability of the tools but also provided many useful hints. Furthermore, I want to thank Andrea and Shourya of the NAM laboratory, for the helpful discussions about the details of the plasmonic detection and nanostructures.

I enjoyed going to work every day because of Anna, Enrico, Enrica, Fabio and Samuel, because they are not only skilled co-workers but also became close friends over time. It is not usual to find a working place with such a helpful and collaborative atmosphere that is productive and fun at the same time. I especially enjoyed our lab weekends to several of the most beautiful places in Switzerland, the afterwork at Satellite and our beach volley tournaments. As well, I want to thank the previous lab members and students, Elena, Marco, Valeria, Nadia, Fabrizio and Michael, and the new arrived, Andrea and Enrico, that contributed to make the lab a great working environment. Thank you Homeira for your great support in all administrative questions and your help with the EPFL bureaucracy.

During the four years in Lausanne I met many wonderful people and friends, some of which I want to acknowledge here. First of all my housemates, Luisa and Enrica, and my previous ones, Camilla and Maude, for the nice and familiar atmosphere that made our collocation a real home. Annalisa, Il Manni, Il Mazzilli, Sara, Enrica, Ivan, Patty, Simo, Max, Maria Elena and all the others that I am sure I forgot, for the evenings, hikings and visits around Switzerland, thank you all for making these PhD years unique!

## Acknowledgements

---

Also, I want to thank my long-time friends in Rome and Crema, that, despite the distance, took part of my life here in Lausanne, supported me in good as well in difficult moments, and warmly welcomed me every time I went back home: Franciolla, Lara, Valeria, Antonella, Micaela, Francesco, Alessandro, Viviana, Cristina, Il Macri, Veronica, thanks for being great friends and for always finding the time to talk and see each other, despite my usual last minute notice.

In addition, my friends from the Netherlands, Antonio, Roberto and Pablo, that, no matter in which part of the world they are, are always present for me.

A special and lovely thank to Martin, for being beside me and supporting me during the last year, in the difficult and stressful moments of the thesis preparation, as well as being with me in the happy ones. Thank you for always finding time for me, for your energy and enthusiasm, and for all the experiences we are sharing together.

Finally, thanks to all my family, without you Crema wouldn't be so much a home for me. I would like to express my warmest gratitude to my parents, Danila and Carlo, and my sister Federica, for all your support, encouragement and love. It would have been impossible to reach such a result without you, and it is to you that I wish to dedicate this thesis.

*Lausanne, 17 Octobre 2014*

Giulia

# Abstract

In the frame of therapeutic drug monitoring and personalized medicine, point-of-care systems (POCs) that can help overcome long waiting times for results and costly procedures of clinical tests are highly desirable. At present, the detection of low-molecular-weight molecules with portable systems remains a challenge. In addition, measurements in serum have always been more complicated with respect to buffer solutions due to the occurrence of non-specific binding.

This thesis presents a portable transmission-localized SPR (T-LSPR)-based setup that is intended to work as a POC for the detection of small molecules in serum. As a biorecognition element, a selected DNA aptamer specific to tobramycin (467 Da) has been used to functionalize a gold nanoislands (NIs) fluorine-doped tin oxide (FTO) covered glass that acts as a biosensor.

As a proof of concept, real-time detection in TE buffer was performed by monitoring concentrations down to  $0.5 \mu\text{M}$  and enabling the observation of association and dissociation phases. The extracted parameters match those obtained with a high-end commercial SPR system.

Concentrations of tobramycin in undiluted serum down to  $10 \mu\text{M}$  were measured. The interesting effect of the serum is that it masks the association kinetics of the tobramycin to the DNA aptamer. The quantification of the captured tobramycin is calculated at the beginning of the dissociation phase and leads to a linear calibration curve for the concentrations in the clinical range tested. The reason why the binding of tobramycin is hindered by the serum remains under investigation.

The T-LSPR system employs low-cost, off-the-shelf components that make it possible to scale down the system to a palm size. The CMOS image sensor, employed as a light detector, forced the choice of the NIs to have resonance in the visible spectrum in order to match the sensitivity of the light detector. Despite the low sensitivity of the NIs FTO-coated glass slides, justified by the irregularity in size and pattern of the NIs and of the FTO substrate, the NIs exhibit extremely high stability in high-ionic solutions, standing continuous regeneration cycles without altering their sensing properties and without denaturation of the DNA aptamer on their surface.

An algorithm for the extraction of the plasmon peak location of the resonance was developed. To increase the speed of data elaboration and to allow the real-time display of the results, hue was studied and used as an alternative parameter for plasmonic evaluation.

**Keywords:** localized surface plasmon resonance, nanoislands, label-free, small molecule,

## Acknowledgements

---

point-of-care, DNA aptamer.



## Sommario

La medicina personalizzata necessita del monitoraggio terapeutico dei farmaci, per il quale i sistemi Point-of-Care (POC) sono altamente desiderabili per ovviare alla lunga attesa dei risultati e ridurre i costi dei test clinici. Tuttavia, ad oggi la rilevazione di molecole a basso peso molecolare, come la maggior parte dei farmaci attualmente in uso, con sistemi portatili rimane ancora difficoltosa. In particolare, misure condotte direttamente in siero sanguigno sono ancora più complicate rispetto alle soluzioni tampone a causa delle interferenze da legami aspecifici. Questo lavoro presenta un sistema portatile POC, basato sul fenomeno della risonanza plasmonica di superficie in trasmissione (T-LSPR), per la quantificazione di farmaci in siero.

Come elemento di riconoscimento del biosensore, un aptamero a base di DNA specifico per la molecola modello tobramicina (un antibiotico dal peso molecolare di 467 Da) è stato utilizzato per funzionalizzare delle nanoisole d'oro (NIs) depositate su vetro ricoperto di ossido di stagno fluorurato (FTO).

Il sistema T-LSPR ha mostrato che misurazioni di concentrazioni fino a  $0,5 \mu\text{M}$  in tampone sono possibili in tempo reale, permettendo quindi di osservare le fasi di associazione e dissociazione. I parametri di cinetica di legame estratti corrispondono a quelli ottenuti con un sistema di risonanza plasmonica di superficie commerciale.

Concentrazioni di tobramicina fino a  $10 \mu\text{M}$  sono state misurate con il sistema T-LSPR in siero non diluito. Nonostante il siero mascheri la cinetica di associazione della tobramicina all'aptamero, la quantificazione della tobramicina catturata è calcolabile all'inizio della fase di dissociazione, generando una curva di calibrazione lineare per le concentrazioni nel range clinico testato. Il motivo per cui il fenomeno di associazione sia mascherato dal siero è ancora oggetto di studio.

Il sistema T-LSPR utilizza componenti standard a basso costo che permettono di ridurre notevolmente le dimensioni del sistema. Il sensore di immagine CMOS, impiegato per determinare le variazioni del plasmone, impone l'utilizzo di NIs con risonanza nello spettro del visibile. Le NIs hanno una sensibilità minore rispetto a strutture regolari che viene però compensata da un'elevata stabilità in soluzioni ad elevate concentrazioni ioniche, consentendo cicli di rigenerazione senza alterazione delle proprietà di rilevamento né rilascio dell'aptamero sulla loro superficie.

È stato sviluppato un algoritmo per l'estrazione della posizione del picco di risonanza plasmonica. Al fine di aumentare la velocità di elaborazione dei dati e per consentire la visualizzazione in tempo reale dei risultati, la tinta è stata studiata e utilizzata come parametro

## Acknowledgements

---

sostitutivo per la valutazione del picco di risonanza.

**Parole chiave:** risonanza plasmonica di superficie, nanoisole, piccole molecole, point-of-care, aptameri a DNA.

# Contents

<b>Acknowledgements</b>	<b>i</b>
<b>Abstract (English/Italiano)</b>	<b>iii</b>
<b>List of figures</b>	<b>ix</b>
<b>Introduction</b>	<b>1</b>
<b>1 Motivation and state of the art</b>	<b>3</b>
1.1 Definition of personalized medicine . . . . .	3
1.2 Relevance and impact of point-of-care systems in the healthcare field . . . . .	4
1.3 Concept of optical detection and affinity biosensors . . . . .	5
1.4 Molecules and assays . . . . .	7
1.5 Kinetics of biomolecular interactions . . . . .	8
1.6 Aptamers . . . . .	9
1.7 Summary and thesis organization . . . . .	11
<b>2 SPR-based analytical platforms</b>	<b>13</b>
2.1 SPR for biosensing . . . . .	13
2.1.1 Measurement schemes . . . . .	14
2.2 Application areas . . . . .	15
2.2.1 Laboratory platforms . . . . .	15
2.2.2 Mobile platforms . . . . .	16
2.3 Localized SPR-based platforms . . . . .	17
2.4 Transmission LSPR . . . . .	18
2.5 Research on LSPR as biosensors in POC systems . . . . .	18
2.6 Sensing of small molecules in buffer and serum . . . . .	19
2.7 Biosensing with aptamers . . . . .	20
<b>3 Principle of SPR based detection</b>	<b>23</b>
3.1 Propagating SPR . . . . .	23
3.1.1 Excitation schemes . . . . .	23
3.1.2 Main characteristics of propagating plasmons . . . . .	25
3.2 Localized SPR . . . . .	26
3.2.1 Main characteristics of localized plasmons . . . . .	27

## Contents

---

3.3	Sensitivity and figure of merit . . . . .	28
<b>4</b>	<b>Nanoislands chip fabrication</b>	<b>31</b>
4.1	Nanostructures for Localized SPR . . . . .	31
4.2	Stability of the LSPR nanostructures . . . . .	32
4.3	Sensor based on gold nanoislands . . . . .	33
4.4	Surface modification of the nanoislands . . . . .	34
<b>5</b>	<b>Peak shift determination with T-LSPR setup</b>	<b>37</b>
5.1	T-LSPR based setup . . . . .	37
5.1.1	Setup description . . . . .	38
5.2	The algorithm for peak extraction . . . . .	40
5.3	Repeatability of the peak wavelength determination . . . . .	41
5.4	Measurement of the peak shift due to a ssDNA layer formation . . . . .	43
5.5	Summary . . . . .	44
<b>6</b>	<b>Plasmon shift determination in array format with CMOS image sensor</b>	<b>45</b>
6.1	Optical setup for real-time detection . . . . .	45
6.2	Microfluidic plasmonic chip for molecular analytics . . . . .	46
6.3	Data analysis . . . . .	47
6.4	Adaptation of the algorithm to the new setup . . . . .	47
6.5	Hue calculation . . . . .	48
6.6	Stability of the NIs layer in aqueous solution . . . . .	50
6.7	Refractive index sensing in bulk . . . . .	50
6.7.1	Calibration curve and figure of merit . . . . .	52
<b>7</b>	<b>Real-time direct detection of small molecule binding in saline buffer and in serum</b>	<b>55</b>
7.1	NIs surface functionalization and samples preparation . . . . .	55
7.2	Handling of solutions by microfluidics . . . . .	56
7.3	Small molecule analysis with a custom made T-LSPR system and DNA aptamers	56
7.4	Real-time sensing of tobramycin in TE buffer . . . . .	58
7.5	Real-time sensing of tobramycin in undiluted serum . . . . .	60
<b>8</b>	<b>Conclusions and future perspectives</b>	<b>63</b>
	<b>Bibliography</b>	<b>67</b>
	<b>Curriculum Vitae</b>	<b>81</b>

# List of Figures

1.1	Representation of a drug's therapeutic range (left) and steady-state level reached after constant, repeated drug administration (right). . . . .	4
1.2	Schematic of an optical transducer hosting a biorecognition element on its surface (left) that changes its optical parameters upon analyte binding (right). . . . .	6
1.3	The profile of the SPR response versus time gives an indication of the association and dissociation steps of the binding interaction. Figure adapted from Biacore GE. . . . .	8
1.4	SELEX process: 1) Oligos pool (initially a library of randomized oligos). 2) Binding to the support via the immobilized analyte. 3) Elution via change in the buffer. 4) Amplification of the eluted oligos via polymerase chain reaction. . . . .	10
2.1	SPR sensor based on angular modulation (top left), polarization modulation (top right), wavelength modulation (bottom left), and intensity modulation (bottom right). . . . .	14
2.2	Examples of commercial platforms based on SPR detection. . . . .	16
2.3	Examples of commercially available portable platforms based on SPR detection. . . . .	17
3.1	Plasmon peak location shift due to binding of biomolecules on the sensor surface (left) and response curve of the biosensor over time (right). . . . .	24
3.2	Schematic of prism coupling for surface plasmon excitation (left) and illustration of the corresponding phase matching condition (right). . . . .	24
3.3	Comparison of propagating (left) and localized (right) SPR-based biosensors. . . . .	25
3.4	Scattering of light of a plasmonic nanoparticle. . . . .	27
3.5	Biomolecular interaction occurring within a short distance from the metal surface and occupying a small portion of the plasmon (left). Biomolecular interaction occurring within the whole extent of the surface plasmon (right). . . . .	29
4.1	(A) SEM image of a thin gold layer evaporated on a FTO glass substrate. (B) SEM image of gold NIs formation after thermal annealing [1]. . . . .	34
4.2	(A) Extinction spectrum of a sample after gold evaporation. (B) Extinction spectrum of a sample after evaporation and subsequent annealing [1]. . . . .	34

## List of Figures

---

- 5.1 Example of a typical gold NIs spectrum (dashed line) measured with a UV-Vis-NIR spectrophotometer Jasco V-570 in transmittance mode with a scan speed of 200 nm/min, bandwidth 1 nm. The solid line represents the curve shift after NIs surface modification with organic molecules. The three crosses indicate the transmittance values measured with the LEDs system plotted at the LEDs effective wavelength. The dotted lines represent the LEDs spectral emissions normalized at their respective maximum emission values and filtered by the photodiode characteristic after passing through the layer of gold NIs. . . . . 38
- 5.2 (A) Digital rendering of our transmission setup. (B) Frontal view showing the location of the light sources, sample and photodetector. (C) Schematic view of the setup. . . . . 39
- 5.3 Fitting of the LEDs experimental data. The three stars represent the intensity measured by enlightening the sample with the LEDs and they are plotted at the LEDs effective wavelengths. The dashed curve represents the typical plasmon peak shape ( $T_{NI}(\lambda)$ ) and the two double arrows,  $\delta_x$  and  $\delta_y$ , indicate the direction in which the curve is shifted in order to fit the experimental data.  $\delta_x^*$  and  $\delta_y^*$  are the optimal values extracted by the algorithm that correspond to the best data fitting. . . . . 42
- 5.4 (A) The measurement and extraction of the peak location of a NIs coated slide has been repeated 6 subsequent times. The maximum deviation among the 6 measurements is 1.1 nm. Each measurement has an error bar between 1.2 nm and 1.3 nm given by the standard deviation over the 40000 samples. (B) The NIs-coated slide has been removed from the sample holder and place it back in between each of the 6 measurements [1]. . . . . 42
- 5.5 Peak shift of a NIs sample before (solid line) and after surface modification with ssDNA (dotted line) as extracted by means of our LEDs-based setup and extraction algorithm. Transmission is calculated with respect to a FTO-coated slide. . . . . 43
- 6.1 A) Digital rendering of the components of the optical setup. B) Side view with relative distances in scale among the components. C) Picture of the T-LSPR setup. 46
- 6.2 Picture of the microfluidic plasmonic chip. . . . . 46
- 6.3 Schematic representation of a NIs FTO glass slide indicating the spots on surface and the areas exposed to the microfluidic channels (right). Example of image acquired by the CMOS camera (left). The ROIs are selected during the data processing. 1) Reference FTO surface. 2) Aptamer spots. 3) MCH control spots. 47

6.4	Example of a typical gold NIs spectrum (blue dashed line) measured with a UV-Vis-NIR spectrophotometer Jasco V-570 in transmittance mode with a scan speed of 200 nm/min, bandwidth 1 nm. The solid line black line represents the white LED emission. The dashed blue, green and red lines represent the RGB filters of the CMOS image sensor normalized at their respective maximum values and the continuous blue, green and red lines are the same curves convoluted with the LED spectrum. . . . .	48
6.5	Hue calculation for different light intensities. The pink and cyan lines represent the light intensity for a NIs and a bare FTO spot on surface, respectively, modified by changing the LED feeding current. The corresponding hue is represented by the red and blue lines and it is independent on the luminous intensity of the light. . . . .	49
6.6	Bulk Refractive Index response of the NIs FTO-coated glass slide to glucose/sucrose solutions injections with increasing RI values expressed in hue variation. The blue and red vertical lines indicate when the glucose/sucrose solution and the ultra pure water reach the sensor's surface, respectively. . . . .	50
6.7	Bulk Refractive Index response of the NIs FTO-coated glass slide to glucose/sucrose solutions injections with decreasing RI values. The blue and red vertical lines indicate when the glucose/sucrose solution and the ultra pure water reach the sensor's surface, respectively. . . . .	51
6.8	Bulk Refractive Index response of the NIs FTO-coated glass slide to glucose/sucrose solutions injections with increasing RI values expressed in peak location shift (nm). The blue and red vertical lines indicate when the glucose/sucrose solution and the ultra pure water reach the sensor's surface, respectively. . . . .	52
6.9	Bulk Refractive Index sensitivity expressed in peak location wavelength (left) and in hue variation (right). . . . .	53
7.1	70 $\mu$ l Tobramycin 10 $\mu$ M in TE 1X delivered to the DNA aptamers and to a control MCH on surface at 5 $\mu$ l/min. Peak location (black line) and hue (red line) are extracted from the same RGB data collected by the CMOS image sensor. The red and blue vertical lines represent the start of the association and dissociation phases, respectively. The light blue area represents the regeneration step thanks to NaCl solution. The control spot does not show any specific response to the injection of Tobramycin indicating that the small molecule drug is recognized and bound to the DNA aptamer only. . . . .	57
7.2	Correlation between hue shift and peak location shift in TE buffer (left) and in serum (right). . . . .	57

## List of Figures

---

7.3	Real-time association and dissociation of Tobramycin recognized by the selected DNA aptamer (blue line) attached to the surface. 70 $\mu$ l of tobramycin in concentrations of 0.5 $\mu$ M, 1 $\mu$ M, 2 $\mu$ M , 5 $\mu$ M and 10 $\mu$ M in TE 1X are delivered to the surface at 5 $\mu$ l/min. The green line represents the control measurement performed with a layer of MCH on the NIs, which allows to cancel out the signal of the bulk effect and to verify the occurrence of non-specific binding. The blue and red vertical lines indicate the start of the association and dissociation phases, respectively. The light blue areas correspond to the injection of NaCl as a regeneration step. . . . .	58
7.4	Kinetics association and dissociation of tobramycin for the different concentrations tested. . . . .	59
7.5	Hue variation for different concentrations of tobramycin averaged over 4 independent DNA aptamer spots on the same NIs FTO glass slide (black dots) and for the MCH control spot (red squares). . . . .	60
7.6	Real-time association and dissociation of tobramycin recognized by the selected DNA aptamer attached to the surface. 70 $\mu$ l of tobramycin in the concentrations of 10 $\mu$ M, 20 $\mu$ M, 40 $\mu$ M, 60 $\mu$ M and 80 $\mu$ M in undiluted serum, alternated with control injections serum without tobramycin, are delivered to the surface at 10 $\mu$ l/min. The black and red vertical lines indicate the start of the association and dissociation phases, respectively. The light blue areas correspond to the injection of NaCl as a regeneration step. . . . .	61
7.7	Hue variation for different concentrations of tobramycin averaged over 2 independent DNA Aptamer spots on the same NIs FTO glass slide normalized over NaCl injections. . . . .	62



# Introduction

In terms of clinical treatment, dose adjustment that is precisely tailored to the patients allows for more efficient healing and reduces side effects. It is crucial to follow the drug concentration in patients' blood quite frequently (that is, at different time-points) in order to assess the personalized pharmacokinetics and pharmacodynamics relative to the drug in use, and thus to extrapolate dosage corrections.

Drug concentration monitoring is currently performed mainly in highly specialized laboratories, leading to long waiting times for results and costly procedures. In particular, low-molecular-weight drugs are mainly measured with mass spectrometry techniques.

Accordingly, there is a need for automated and compact analytical systems combining multiple functions that allow for potentially better therapy and increased autonomy of patients. The need for those systems, known as point-of-care systems (POCs), is steadily increasing because clinical analytical facilities are crowded and expensive, and moving treatments outside allows for in-situ diagnosis and more personalized approaches [2].

For common targets such as glucose or pregnancy tests, there are already portable systems available; however, the detection of small molecules (<kDa) remains a challenge. The miniaturization and integration of the experimental setup is not always possible and it depends on the principle of detection employed [3]. Among other detection techniques, such as imaging, flow cytometry, immunoassays, electrochemical detection, magnetic detection [4], POCs based on optical detection are preferred because they are relatively immune to electromagnetic interference and they permit multiple measurements in an array configuration [5, 6].

During the last few decades, antibodies have been the preferred way to detect medical analytes. However, only a few antibodies are available for small drugs detection and their production is often costly and suffers from high batch variability. Recently, aptamers have become increasingly popular in small-molecule detection, as they can be directly synthesized and modified while showing similar high affinity binding than their specific analytes. Moreover, aptamers offer higher thermal and chemical stability (especially DNA-aptamers) with respect to antibodies, which makes them particularly suitable for biosensing applications based on molecular recognition.

Currently, low-molecular-weight molecules are often detected by means of competitive assays,

## List of Figures

---

sandwich assays or conjugated analyte molecules [7, 8, 9]. In the literature, mainly fluorescence [10] and electrochemical detection [11, 12, 13] systems have been used to characterize the kinetics of small molecules. For instance, the colorimetric detection of Xia et al. [14] employs aptamers to detect a small molecule (cocaine) through inhibition assay via conjugated polyelectrolyte. Optical [15, 16, 17] and electrochemical [18, 19, 20, 21] detection systems allow for measurements in pure or diluted serum only for target molecules above the kDa range (mainly proteins and cancer biomarkers).

Despite their sensitivity, the extra manipulation of the molecules can alter their behavior and recognition properties. Label-free optical biosensors measure the change in the refractive index (RI) in the proximity of the sensor's surface, without any manipulation of the molecules, leaving them and their properties unaltered. However, low-molecular-weight drugs are very difficult to monitor because of the low RI change they produce.

Therefore, a system that is suitable for being scaled down as a portable device while reducing the complexity of the system itself, of the biosensor, and of the sample preparation would be desirable.

The choice of the biosensor represents one of the most critical features. In the literature, a variety of plasmonic nanostructures with high sensitivity have been presented. However, the major concern for biosensing application is the stability of the nanostructures when put in contact with solvents and under continuous flow. To overcome this limitation, the nanostructures are often passivated with protective layers or deposited on the substrate via an adhesion layer to improve their stability.

A portable label-free optical detection system based on transmission-localized surface plasmon resonance (T-LSPR) employing gold nanoislands deposited on a fluorine-doped tin oxide covered glass is presented here. This system is able to measure the binding kinetics of a small molecule, tobramycin, via direct assay to a selected DNA aptamer in undiluted serum. Because of the label-free measurement system and the direct assay, sample preparation and elaboration are reduced at minimum.

# 1 Motivation and state of the art

The objectives of the thesis are to design and develop an optical detection system suitable as a point-of-care (POC) device and to investigate its performance for real-time monitoring of biomolecular interaction. The study includes design, optimization and characterization of such a device and real-time measurements performed in an undiluted serum environment. The system is based on localized surface plasmon resonance (LSPR) and is intended to be compact and simple. In addition, thanks to the non-connected pattern of the biosensor's nanostructures, it can perform array measurements.

This thesis is developed in the frame of the Nano-Tera Program, which was addressed to develop therapeutic monitoring of drug concentrations in blood samples and drug dosage adjustments tailored to the patient. At present, specific blood tests are performed only in highly specialized laboratories, often leading to costly procedures and a long waiting time for results.

## 1.1 Definition of personalized medicine

Nowadays, the need for early detection of disease and rapid time to results for clinical tests have increased interest in developing new diagnostic tools and medical care support. Current medicine develops and administers drugs to patients to treat illness and non-physiological conditions. However, since drugs generally tend to target as many patients as possible, the same drug can be differently tolerated and can have different effects on the healing process.

Personalized medicine consists of using the patient's genetic profile and clinical data to select a personal therapy or medication and administer it at the proper dosage. The administration of a drug needs to be dosed such that its concentration stays within a therapeutic range.

The therapeutic range of a drug defines the concentration at which the patient has the clinical benefits, while reducing the adverse effects. The size of the range is determined by the minimal effective concentration and maximal toxic concentration of the drug. If the drug concentration in blood is below the desired level, there will be no pharmacological effect. On the contrary,

excessive dosage can lead to an adverse response and side effects (Figure 1.1).

The time window in which the drug concentration stays in the therapeutic range is the duration of action of the drug. Patients are given multiple doses to stay within the therapeutic range for the duration of the treatment. After several constant dosages at constant intervals it reaches a level called *steady state*, which is when the amount of drug accumulated in the body is equal to the amount of drug the body expels. The therapeutic windows vary among the population, depending on age, sex, metabolism, and health. Therefore, it is important to control the dosage amount and frequency in a drug therapy.

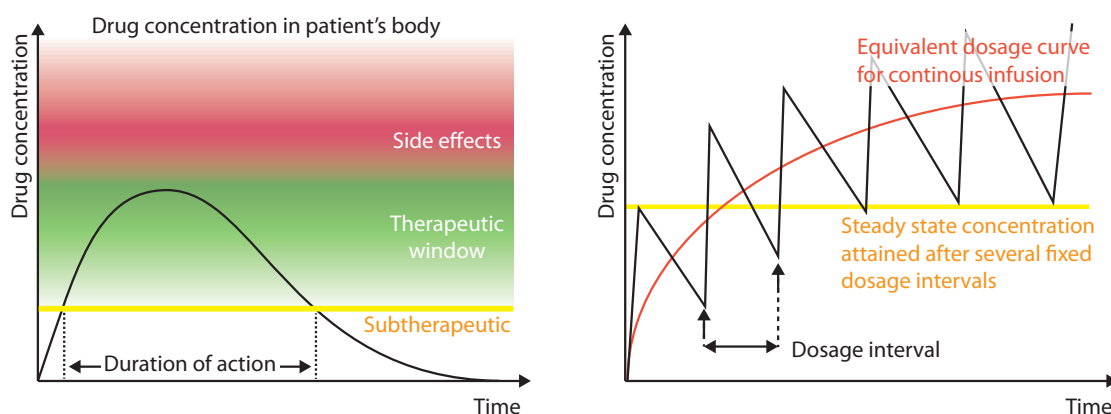


Figure 1.1: Representation of a drug's therapeutic range (left) and steady-state level reached after constant, repeated drug administration (right).

In personalized medicine, pharmacokinetics and pharmacodynamics are used for dose monitoring and adjustment. In particular, pharmacokinetics evaluates the drug concentration in blood, which is drug dose versus drug concentration. Pharmacodynamics refers to the concentration of biomarkers in blood, which is drug concentration versus drug effect.

At present, specific tests are mainly done in a few highly specialized laboratories, leading to a long wait for results. These tests are costly and require trained personnel. Therefore, there is a need for automated, compact analytical systems that combine the ability to observe the presence of a molecule in a sample and adjust its dose accordingly. These functions are coupled with communication capabilities to be connected with doctors and pharmacokinetic parameter databases for further refinement in dosage adjustment procedures [2].

Point-of-care (POC) systems satisfy these criteria.

## 1.2 Relevance and impact of point-of-care systems in the health-care field

Health monitoring systems combining multiple functions represent a potential for better therapy and increased patient autonomy. The need for those systems, referred to as POCs, is

### 1.3. Concept of optical detection and affinity biosensors

---

steadily increasing because clinical analytical facilities are crowded and expensive. Moving treatments outside the hospital allows for in-situ diagnosis and more personalized approaches. POCs are rapidly expanding because of the more readily available technology to produce them and their portability and ease of use.

There are already examples of POCs currently used in daily life. Some applications require sporadic tests (allergy, pregnancy), while others may require multiple monitoring (as for example glucose blood). In order to develop and implement on a large-scale, POCs need to be miniaturized and integrated, while providing autonomy, user-friendliness, high throughput, and automated reagent delivery.

The integration of microfluidic modules for delivering the reagents assures minimal contamination and only a small amount of sample volume needed, with consequent reduction of reagent consumption, leading to overall cost reduction [22].

The growing interest in POCs is evidenced by the broad applications already available, such as a POC performing ELISA tests for HIV diagnosis in Rwanda [23], a mobile phone-mounted light microscope [24], a POC mounted on smart phone for evaluating and correcting misaligned eyes [25], and many other examples [26, 27, 28, 29, 30].

Nevertheless, miniaturization and integration of the experimental setup is not always possible. It depends on the detection method that is used [3]. Among other detection techniques, such as imaging, flow cytometry, immunoassays, electrochemical detection and magnetic detection [4], POCs based on optical detection are preferred because they are relatively immune to electromagnetic interference and they permit multiple measurements in an array configuration [5, 6]. An overview of optical detection techniques is given in the next paragraph.

### 1.3 Concept of optical detection and affinity biosensors

POCs require a biosensor, in which the biomolecular event takes place. Biosensors based on optical affinity are devices consisting of a biorecognition element for molecules with affinity toward specific target molecules and an optical transducer that translates the binding event into an output signal (Figure 1.2) [31].

As schematically represented in Figure 1.2, the biorecognition element is typically covalently bound to the sensor surface, while the analyte to be detected is delivered to the surface. In cases of affinity matches between the biorecognition element and the delivered analyte, a change in the optical signal is detected.

Biosensors are classified according to their analytical capability (the ability to monitor a single or several parameters on the same device), reusability (if they are disposable or support multiple uses), and assay format (if they are label-based or label-free).

Label-based affinity biosensors require labeling the target molecule under study with a dye

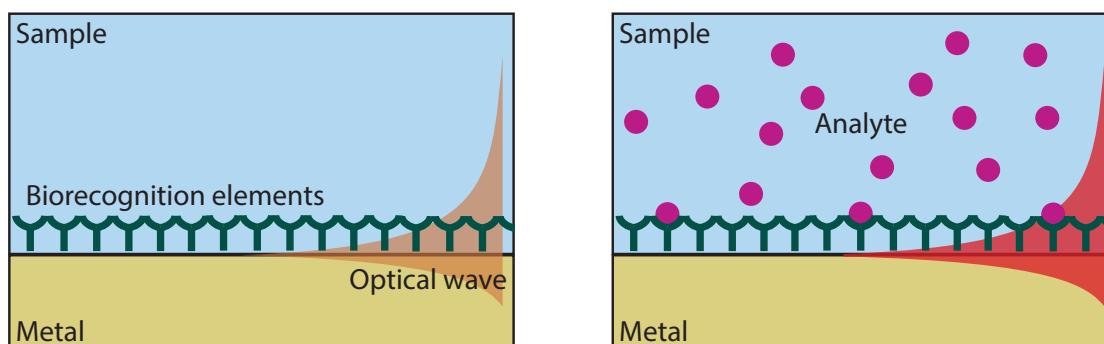


Figure 1.2: Schematic of an optical transducer hosting a biorecognition element on its surface (left) that changes its optical parameters upon analyte binding (right).

or a fluorescent marker. This step is time-consuming, costly, and could alter the targets' recognition properties. However, this method is widely used because of its high sensitivity at low concentrations and high throughput [32, 33, 34, 35, 36, 37, 38]. On the other hand, label-free biosensors do not require any manipulation of the molecules prior to the binding experiment, leaving the molecules and their properties unaltered.

Examples of applied optical detection principles that measure changes in the refractive index (RI) in proximity of the surface of the sensor include interferometric sensors and sensors based on spectroscopy of guided waves (grating coupler, resonant mirror, SPR sensors) [39, 5, 40].

The main features of label-free biosensors are the ability to perform direct assays, or detect the analyte in one-step, and real-time measurements with continuous monitoring of the binding events. This work focuses on localized SPR detection based sensors.

The performance of a biosensor can be expressed in terms of:

- **Sensitivity:** The entity of output signal variation signal in relation to the binding event occurring on the sensor surface
- **Specificity:** The ability of the biorecognition element to recognize the molecule of interest and discriminate it from other molecules in the solution
- **Limit of detection (LOD):** The minimum detectable quantity of analyte that can be discriminated from the noise of the measurement

Effective biosensors detect the target in physiologic concentrations and do so without any additional processing of the target biological fluid. They operate with small volumes and control multiple parameters. Together with the implementation of a module for signal processing, data transmission, powering and end-user interface, they can contribute to the increasing use of POCs for personalized medicine.

### 1.4 Molecules and assays

The quantification procedure to detect the activity or the amount of a substance is referred to as *biological assay*. The type of assay adopted in SPR optical detection systems depends on the molecules under study. The main applications are the study of biomolecule interaction (antigen-antibody, protein-protein, protein-DNA, DNA hybridization) association and dissociation rates, specificity, detection and identification of chemical and biological analytes (drugs, hormones, toxins, bacterial pathogens) [6].

The choice of the assay type is an essential part of the detection system. Most frequently used assay formats that produce a measurable signal are:

- Direct detection: Employed for medium- and large-size analytes
- Sandwich assay: Used for small- and medium-size analytes at small concentrations
- Indirect detection (competition, inhibition): Employed for small analytes at very low concentrations

The direct assay consists of a one-step recognition event of a probe immobilized on the surface that specifically binds the analyte in solution. The produced change in RI is directly proportional to the amount of analyte bound to the probe. The binding interaction kinetics has an exponential time dependence. As the interaction progresses, there are fewer available sites, until equilibrium between the association and dissociation processes is reached. The time needed to reach equilibrium depends on the concentration of the analyte, leading to a faster interaction for a larger amount of analyte.

The sandwich-assay format consists of two steps. In the first step, the analyte is delivered to the surface and bound to the biorecognition element on surface. In the second step, another molecule, specific to the previously bound analyte, is delivered to the surface and recognizes the analyte, thus increasing the total number of molecules on surface and increasing the change of RI.

In the competition assay, the surface is covered with the biorecognition element. The sample solution delivered to the surface contains a mixture of the analyte and an analyte conjugate. The difference in signal between a reference solution that contains only conjugated analyte and the sample solution indicates the amount of analyte in the sample. High analyte concentrations in the sample result in low signals.

The inhibition assay requires the binding of the analyte on the surface. The sample solution that contains the analyte is mixed with biorecognition elements in excess. The biorecognition element binds both to the analyte in solution and to the analyte previously bound to the surface. The difference in signal between a blank solution that does not contain the analyte and the sample solution indicates the amount of analyte in the sample. High analyte concentrations result in low signals.

## 1.5 Kinetics of biomolecular interactions

Quantitative information about the kinetic association and dissociation constants can be extracted from the observation of a binding interaction in real time. This provides information regarding complex formation and stability.

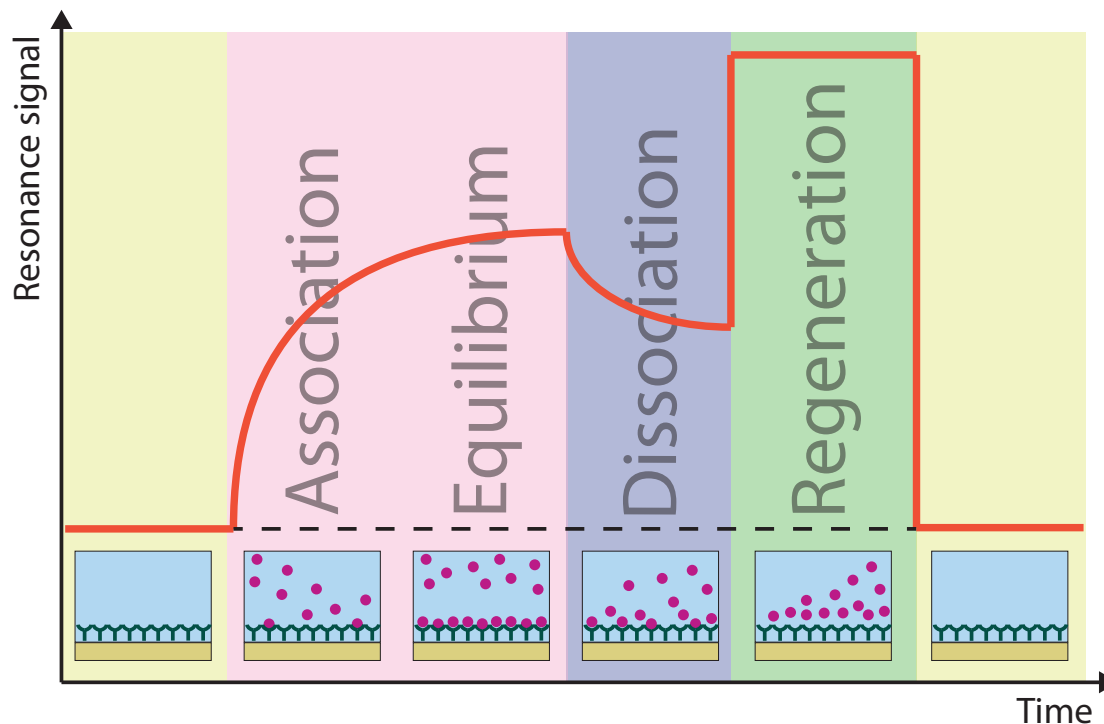


Figure 1.3: The profile of the SPR response versus time gives an indication of the association and dissociation steps of the binding interaction. Figure adapted from Biacore GE.

The majority of the binding interactions are bi-molecular (or two molecules), the analyte A, and its capturing probe B, that react together to form the complex AB. The relationship can be written as:



The association ( $k_{ON}$ ) and dissociation ( $k_{OFF}$ ) rates determine the rates of the complex formation and breakdown.

The Langmuir kinetic model is based on four assumptions:

- The surface of the adsorbent is uniform
- Adsorbed molecules do not interact
- All adsorptions occur with the same mechanism



- Only a monolayer is obtained at the maximum adsorption

The total amount of captured analytes increases until there are no longer free capturing probes (saturation coverage) or it is not possible to further increase the target density.

At equilibrium:

$$\frac{K_{OFF}}{K_{ON}} = \frac{[AB]}{[A][B]} = K_D \quad (1.2)$$

in which the square brackets indicate the concentrations of A and B.

The equilibrium constant  $K_D$  indicates the strength of the binding between A and B in terms of how easy it is to separate the complex AB. Analyte concentrations must be accurately known to determine correct association rate constants. When high concentrations of A and B are required to form AB,  $K_D$  is high, indicating a low strength of the binding. On the contrary, a small  $K_D$  indicates a strong binding.

Depending on the type of interaction, the experimental conditions need to be optimized in terms of:

- surface density
- analyte concentration
- flow rate

The flow rate is particularly important for the mass transport effect. In order to bind to the ligand, the analyte in solution must be transported from the bulk of the solution to the sensor's surface. The analyte transportation rate to the surface depends on the dimensions of the flow cell and the diffusion properties of the analyte. Under laminar flow conditions, it is proportional to the cube root of the flow rate. If the rate of transport is much faster than the association rate between analyte and ligand, the analyte/ligand binding is determined by the kinetics constants. If the mass transport is much lower than the association rate, the analyte/ligand binding is limited by the rate of the analyte transport, and the binding kinetic information is lost or only partially available. Optimal assay conditions are high flow rates and low surface-binding capacity.

## 1.6 Aptamers

The ability to detect small drug molecules has always been a challenge, due to the low molecular weight and the small change in the refractive index they cause, often leading to competitive assays, sandwich assays, or other combinations [8, 7, 9]. Aptamers are oligonucleotide sequences that bind to a specific target molecule. The characteristics of aptamers make them

## Chapter 1. Motivation and state of the art

particularly attractive in diagnostic and therapeutic applications. They also represent a new topic of interest in biosensing systems [21, 12, 41, 10, 11, 42, 43].

During the last decades, antibodies have been the preferred way to detect analytes. However, aptamers are steadily conquering more space in small molecule detection, and they proved to be suitable for applications based on molecular recognition. One of the great advantages of aptamers is that they can be directly synthesized and modified to specifically recognize any target molecule with high affinity and specificity [44].

Aptamers are selected through a process called *systematic evolution of ligands by exponential enrichment* (SELEX) [45]. The SELEX process is an in-vitro technique for selecting and amplifying oligonucleotide libraries. The process starts with a random sequence library of chemically synthesized DNA containing approximately  $10^{14}$  to  $10^{15}$  individual molecules. The complexity of the library depends on the number of randomized nucleotide positions.

The iterative process starts with the incubation of a random DNA sequence library with the target of interest in a certain buffer at a certain temperature. During this step, a small fraction of the random sequences will interact with the target. These sequences are physically separated from the rest of the library. The selected sequences are then amplified to enrich their number in the library and used to repeat another cycle of selection and subsequent amplification. After several repetitions of these cycles of selection/amplification, the affinity saturation is reached and the selected sequences are cloned and sequenced to obtain the sequence information of each member.

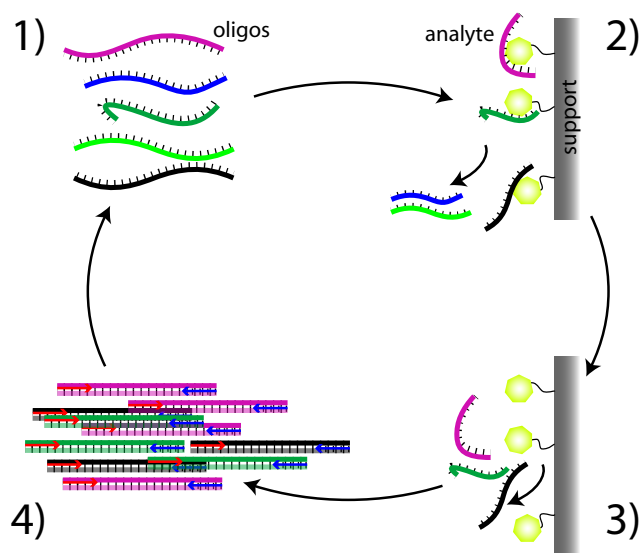


Figure 1.4: SELEX process: 1) Oligos pool (initially a library of randomized oligos). 2) Binding to the support via the immobilized analyte. 3) Elution via change in the buffer. 4) Amplification of the eluted oligos via polymerase chain reaction.

The great interest in aptamers comes from the fact that their properties can be changed on demand, such as to obtain aptamers that work in non-physiological buffers or at non-

physiological temperatures. Aptamers are very stable and can stand long-term storage, but they can denature. However, this is a reversible process, and they can be regenerated in few minutes. The SELEX process guarantees high accuracy and reproducibility in the chemical synthesis for producing aptamers, as only small variations are expected from batch to batch of production. Affinity and specificity are the most important characteristics in a diagnostic assay, as it relies on the affinity and strength of the aptamer-target interaction [46].

The present work focuses on relevant clinical and diagnostic tests involving the detection of small molecule drugs. We studied the behavior of a small molecule drug, Tobramycin, that is an antibiotic of 467 Da used to treat lung infections. A variety of selected DNA aptamers to specifically recognize tobramycin, have been created and studied in our laboratory [47].

## 1.7 Summary and thesis organization

This thesis is organized as follows.

This chapter discusses the importance of a POC system and the main requirements related to the healthcare field, together with reviewing some of the fundamentals of biomolecules interaction and surface detection. The second chapter gives an overview of the analytical platforms based on SPR, the commercial existing systems, and the progresses of the research. The third chapter introduces the principles of SPR-based detection, discriminating between propagating and localized plasmons. In particular, it presents the features related to biosensing. Chapter Four includes the fabrication of the plasmonic nanostructures for the biosensor chip and the characterization tests of their stability and repeatability. Chapter Five presents the first prototype of the transmission-localized SPR-based setup. It explains the principle of the discrete light system employed, and the extraction and reconstruction of the plasmonic information. Chapter Six describes the optimized, current version of the setup, featuring a CMOS camera for parallel detection. It includes the adaptation to the current version of the previously mentioned algorithm, and introduces and validates the hue for a faster evaluation of the real-time response of the system to biomolecular interactions. In addition, the chapter presents a characterization of the biosensor's bulk refractive index sensitivity. Chapter Seven shows the experiments conducted with the transmission-LSPR setup. The detection of a low molecular-mass drug, tobramycin, is performed in different matrices, including undiluted serum.

Several results presented in this thesis have been described by the author in [1, 48].



## 2 SPR-based analytical platforms

SPR has been widely studied and is a stable, established technology for recognizing binding events. The surface plasmon phenomenon was first observed in 1902 by R.W. Wood and then characterized by Kretchmann, Otto and Raether in 1968 [31]. Liedberg first employed a SPR setup for biosensing purposes in 1983 [49]. Since then, the field has rapidly developed thanks to advancements in immobilization techniques and optical measurement approaches [50]. In particular, thanks to improved solutions for immobilizing receptors on the metal surface and coating techniques, previous limitations due to adsorption of non-specific molecules and reduced receptor activity have been overcome.

### 2.1 SPR for biosensing

Nowadays, SPR-based detection systems represent a well-established, commercialized technology. SPR is a label-free technique that allows the observation of real-time kinetics for binding processes. SPR is a very sensitive, powerful method for detecting biomolecular binding of different species, such as proteins, oligonucleotides, and viruses [51]. One of the main reasons for its robust development is the versatility of SPR-based sensors. In principle, they can detect any analyte, as long as a biorecognition element specific to the analyte exists. Because they are based on RI changes in the proximity of the surface, analytes do not have to exhibit any particular features, such as fluorescence or adsorption and scattering bands, as their mass should be enough to cause a detectable change in RI.

SPR sensors are sensitive to changes of the RI in the proximity of the surface, independently from what is causing this change. In principle, any molecule can lead to a RI change, therefore SPR sensors cannot discriminate between different molecules. In addition, changes in RI could come from interfering effects, or changes in RI not caused by the analyte, such as non-specific binding or background RI variations due to sample temperature and composition fluctuations. Therefore, the specificity of SPR detection systems is assured by the biorecognition element. The biorecognition element should specifically recognize only the analyte of interest and prevent non-specific binding to other molecules with similar structures to the analyte under

study.

### 2.1.1 Measurement schemes

Surface plasmon waves modify their propagation constant according to the bulk and the surface RI at a metal dielectric interface (see Chapter 3). Most techniques detect changes in the light reflected by a thin metal layer. This is the case with the prism-coupled attenuated total reflection method (ATR), the fiber SPR, the waveguide SPR, the grating-coupled SPR, and the magneto-optic [52, 53].

SPR sensors are classified as angle-, wavelength-, intensity-, phase-, or polarization-modulation-based, depending on which characteristic is measured (Figure 2.1) [54, 55].

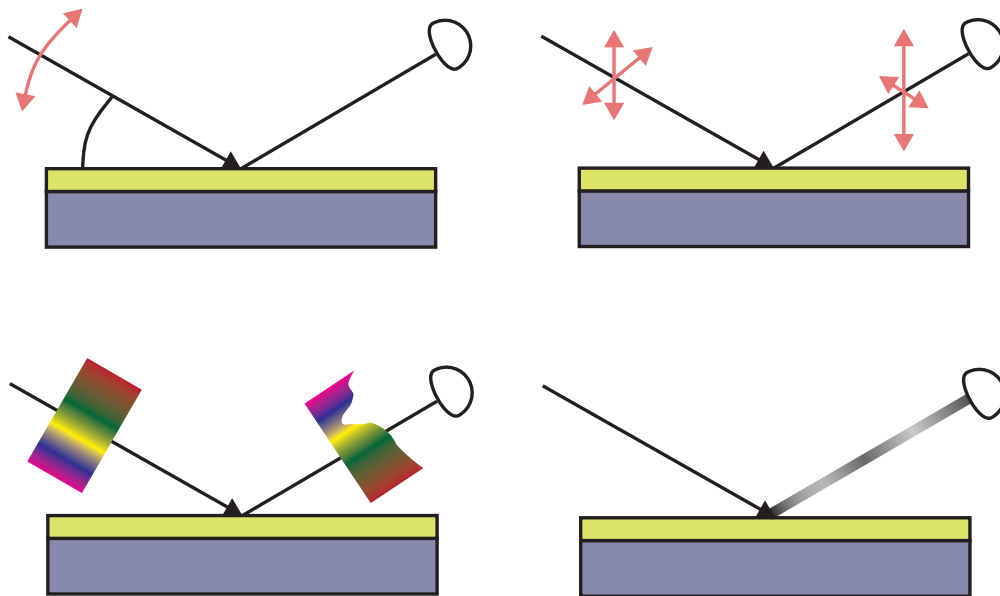


Figure 2.1: SPR sensor based on angular modulation (top left), polarization modulation (top right), wavelength modulation (bottom left), and intensity modulation (bottom right).

- In SPR sensors with angular modulation, the coupling strength between the excitation light and the surface plasmon at a fixed wavelength and multiple angles of incidence of the exciting light is measured, and the angle of incidence yielding to the strongest coupling (dip in the reflected light) is determined.
- In SPR sensors with wavelength modulation, the coupling strength of the exciting light and the plasmon is measured at a fixed angle of incidence and multiple wavelengths, and the wavelength yielding the strongest coupling is determined.
- In SPR sensors based on intensity modulation, the exciting light is at a fixed wavelength and a fixed angle of incidence, and the changes in intensity of the light interacting with the plasmon are measured.

- In SPR sensors based on phase modulation, the shift in phase of the exciting light coupling with the surface plasmons are measured at a fixed wavelength and a fixed angle of incidence.
- In SPR sensors based on polarization modulation, changes in the polarization of the light coupling with the surface plasmons are measured at a fixed wavelength and a fixed angle of incidence.

## 2.2 Application areas

Many optical SPR setups have been proposed [50]. So far, SPR-based systems cover a wide range of applications, such as proteins, antibodies, drugs, and DNA strands. The widespread use of SPR instrumentation comes from the improvements in monitoring multiple sites in parallel, functionalization for high-density biochips, microfluidics for delivery of biomolecules to the sensor surface, functionalization for specific molecular coatings, sample preparation, and the analyte extraction device.

SPR development targets two specific areas of application: Laboratory platforms for high-throughput screening and high sensitivity; and mobile platforms for *in situ* detection.

### 2.2.1 Laboratory platforms

Commercial SPR systems are generally based on the traditional prism-coupled SPR configuration, which is based on angular spectroscopy, wavelength spectroscopy, or intensity modulation methods [56].

The traditional biosensing approach consists of simultaneously measuring two sensing channels, one with the biorecognition element specific to the analyte under study (signal channel) and one with no specificity (reference channel). At least two sensing channels are needed to reference for interfering effects that could lead to a false evaluation of the signal. Increasing the number of channels in a SPR system can increase the number of parallel interactions that can be monitored at the same time.

Techniques based on SPR detection require rather complex optical systems with limited parallelism. The main limitations of those systems are that they are costly, bulky, require trained personnel, and are mainly designed for use in the lab.

At present, the highest number of different sensing sites on standard SPR has been achieved on the Biacore 4000 [57], which features 16 sensing sites divided over four channels. SPIRIT, from Seattle Sensor Systems [58], based on SPREETA sensing chips [59], features four SPR detectors with triplicate measurement and 12 channels. SR7000DC SPR system, from Reichert Technologies [60], can perform SPR in combination with electrochemistry, fluorescence, photochemistry, mass spectrometry, and liquid chromatography. Many other SPR systems

## Chapter 2. SPR-based analytical platforms

---

can be found in [61, 50].



Figure 2.2: Examples of commercial platforms based on SPR detection.

To scale up the number of simultaneous sensing areas per experiment, imaging SPR (iSPR) systems have been developed. The iSPR measures the spatial refractive index changes on a surface on which an array of biomolecules has been immobilized. It relies on the use of CMOS or CCD image sensors [62, 63, 64, 65, 66, 67, 68, 69, 70]. Commercially available systems, such as SPRi-PlexII™ from Horiba (up to 400 biomolecular interactions) [71], or IBIS MX96 (2x48 spots) provide monitoring of several hundred of independent biomolecular interactions [72]. Such systems are equipped with sophisticated optics, so are rather bulky and expensive.

### 2.2.2 Mobile platforms

The interest in scaling down the systems and making them compact and portable as a POC is demonstrated by the large number of instruments available: Spreeta from Texas Instruments [73], SPRmicro from K-MAC [74], and other systems from companies such as Horiba, Sensia, Toto, and Xuzhou Shengpu (Figure 2.3) [75]. They employ LEDs (TI Spreeta) or lasers (e.g., BiochipAnalyzer, SPRnano) as excitation sources and offer up to eight channels (SPRnano). While the portable iSPR from K-MAC, based on intensity interrogation and featuring 2 CCD, weighs 30 kg, Möbius Advanced Technology offers a handheld SPR platform. Such small-scale devices usually do not rely on laser sources, but employ LEDs to excite the SPR.

Research on portable SPR-based systems is very active, as in the case of C. E. Furlong's group, who presented a system with 24 parallel sensing areas [59], and the group of Homola, which proposed different SPR setups. One of their systems is based on angular interrogation that employs a gold-coated diffraction grating to achieve very high sensing resolution ( $3 \times 10^{-7}$  refractive index unit (RIU)) [76], with 10 parallel channels on a disposable cartridge [77]. Another example by the same group is a portable six-channel SPR system based on a special diffraction grating called a *surface plasmon coupler and disperser* [78].

A recent review [79] highlighted the most significant contributions in the field of photonics and lab-on-a-chip. Efforts continue to make systems compact, portable, and possibly integrated. Scaling down is possible only by avoiding bulky, moving elements, which most commercial



systems have.

However, further scaling down of SPR-based systems is limited by the difficulties in scaling the optical excitation system. This is why LSPR-based systems are being heavily investigated as an alternative to the classical propagating SPR-based methods [80, 81, 82, 83].



Biochip Analyzer,  
K-MAC



SPRmicro,  
K-MAC



SPREETA, Texas  
Instrument

Figure 2.3: Examples of commercially available portable platforms based on SPR detection.

## 2.3 Localized SPR-based platforms

Pushed by the need to reduce the dimensions of SPR optical systems, metallic nanoparticles supporting LSPR have been investigated. In principle, LSPR allows for increasing the spatial resolution of a biosensor, as the non-connected pattern of the nanoparticles impedes the propagation of the plasmon along the surface [84].

Although LSPR sensors are one to two orders of magnitude less sensitive than propagating SPR [85, 86], they dramatically reduce the complexity and bulk of the optical instrumentation. However the fabrication of the sensors supporting nanostructures for LSPR can be more expensive.

The intense research on the sensing nanostructures made the production costs of the nanofabrication process constantly drop. As the sensitivity of LSPR systems greatly depends on the characteristics in size, geometry, materials and interparticle spacing [87, 88, 89], research mainly focused on identifying the optimum configuration to achieve the best sensitivity. In this frame, a great variety of structures exhibiting LSPR have been exploited, including metallic nanoparticles, metal nanopatterns exhibiting a LSPR, and novel materials of greater sensitivity [90, 91, 92, 52, 93, 94].

Pushed by the need for POC bio-analytical systems, previous works have reported electronic-based compact implementations of reflectance-based systems for LSPR. Nevertheless, these reflectance-based setups still require specific optical elements that are difficult to realize on an integrated system. Neuzil et al. [7] presented a palm-sized biodetection system featuring four LEDs and a photodiode collecting the light reflected from the sensor surface. The system has been tested with different RI solutions.

### 2.4 Transmission LSPR

The LSPR phenomenon can be observed either in reflectance, as with standard propagating SPR, or in transmission configuration (T-LSPR). Clearly, a transmission approach is particularly suitable for developing compact, or even integrated, measurement setups, which only require alignment among light source, sample, and detector. The transmission configuration may greatly facilitate the development of miniaturized, highly parallel, fully integrated SPR systems. In contrast, in a reflectance-based system, moving elements are needed to observe, for example, the changes in the reflectance angle of the light used to excite the sample.

In particular, the principle of T-LSPR has been extensively studied in the works of the Rubinstein group since 2000. T-LSPR has characterized molecular binding events, such as biotin-streptavidin, on discontinued metal layers on inert transparent substrates [95, 96, 97]. Moreover, Hutter and Pileni [98] reported detecting DNA hybridization on a layer of gold nanoparticles of 2.5 nm on glass.

### 2.5 Research on LSPR as biosensors in POC systems

In recent years, interest shifted from creating the most sensitive structures [99, 100, 101, 102, 103, 104] to practicality and real-world applications. Reliability and long life of the sensor are the main requirements for POC systems [105]. The implementation of LSPR biosensors with a liquid sample-handling interface that operate with small detection volumes in normal incidence condition allowed for development of simple, miniaturized instrumentation.

Malic et al. presented a system with microfluidic channels integrated with blazed nanograting structures into thermoplastics substrates [106]. The system was tested with different concentrations of glycerin in water and CD44 glycoprotein at clinically relevant concentrations. Despite the high sensitivity structures and their integration with the microfluidics, they used a spectrophotometer for transmission detection that limited the biosensor throughput to sequential measurements. However, it is planned to implement a CCD camera to perform multiplexed SPR imaging spectroscopy.

Another example of integration of microfluidics with T-LSPR gold nanoparticle structures was presented by the Borghs group [107]. This system addresses the detection of transmittance changes at a single wavelength of biotin/anti-biotin recognition experiments, rather than observing the plasmon peak shift.

Gallegos et al. [108] provides another integration example, in which a label free biodetection of protein and antibody is performed by a module containing optical components directly connected to the CMOS camera of a smart phone that acted as a spectrophotometer by measuring the transmission spectrum of the photonic crystal biosensor.

Recently, systems based on Extraordinary Optical Transmission (EOT) have been presented

## 2.6. Sensing of small molecules in buffer and serum

---

[109, 110, 111, 112, 113]. EOT systems give a plasmonic response that is more stable and highly reproducible, thanks to array nanostructures surrounded by planar gold, such as nanoholes, nanocavities, nanoslits, or nanogratings arrays [114, 69, 115, 116]. In this case, surface plasmon oscillations can be either propagating or localized surface plasmons, but the nanoholes simplify the detection system by transmittance configuration.

An example of an EOT-based system is presented by the Altug group. They employed direct coupling of perpendicularly incident light to the plasmonic excitations through nanohole arrays on thick metal films and image on a CMOS camera. The nanohole array is very highly sensitive to RI changes. However, the system has only been tested with biomolecules in dry conditions. In addition, fabricating the nanostructures based on e-beam lithography requires cost-intensive, time-consuming clean-room processes [111].

S. H. Oh's group gives another example of an integrated system [117] that employs EOT on a gold nanohole array integrated with an ITO electrode, which concurrently acts as a nanoplasmonic sensor and as a gradient-force generator for dielectrophoresis studies. The same group presented a system featuring 50 channels in parallel with microfluidics [70] that combined EOT with iSPR. Despite the high parallelism reached, it was a rather complicated system that employed a high resolution imaging spectrophotometer and a CCD camera that required precise alignment.

The presented research works are indicative examples of the variety of integrated structures that can be found. In some cases, the detection systems represent a proof of concept before the realization of a stand-alone system. In other cases, the systems are rather complicated or complex fabrication processes are needed. This thesis examines the possibility of a transmission LSPR setup scaled down in a simple, low-cost configuration, due to the flexibility allowed by the choice of the nanostructures, as discussed in the next chapter.

## 2.6 Sensing of small molecules in buffer and serum

Small molecule detection with a label-free optical system has always been challenging, due to the low molecular weight and their associated small refractive index change. They are often detected by means of competitive assays, sandwich assays, or conjugated analyte molecules [7, 8, 9].

In literature, fluorescence [10] and electrochemical detection [118, 11, 12, 13, 119] systems have mainly been used to characterize the kinetics of small molecules. Optical [15, 16, 17] and electrochemical [18, 19, 20, 21] detection systems allow for measurements in pure or diluted serum only for target molecules above the kDa range (mainly proteins and cancer biomarkers). The R. E. Kunz group presented a bulk refractometric system based on an optical waveguide [120] that is able to extract the calibration curves and kinetics of biotin (244 Da), even though the system is rather complicated and difficult to scale down as a portable system.

Other works based on sandwich-assay detection employ biomolecules conjugated to nanoparticles. As already discussed in section 1.3, biomolecule labeling requires an additional operational step that, other than being costly and time-consuming, can alter the physiological properties of the molecule itself. Hutter and Pileni used LSPR-based gold islands on glass in combination with extra gold nanoparticles to form a sandwich assay and overcome the difficulties in detecting small biomolecules [98]. However, the detection was performed by immersion of the island-covered glass into buffer with thiolated DNA and measured with a commercial spectrophotometer, without focusing on the implementation of a new detection system.

The C. E. Furlong group [9] detected small molecules (cortisol in saliva) via competition assay using a commercially available portable SPR system (SPREETA 2000) that still needed temperature stabilization. Other works used more complex methods to amplify the SPR response [121].

The S. Maerkl group published another relevant work reporting measurements in serum [105]. They employed gold nanorods on glass and integrated plasmonics and microfluidics monitoring in real time 32 sensing sites in parallel. They tested the system for the detection of cancer biomarker (proteins), both in a direct and in a sandwich format, in a 50% serum matrix down to 500 ng/mL concentration. Although the system is, in principle, scalable as a POC, it employs a bright field transmission microscope that is far from a miniaturized POC system.

At present, label-free direct detection of small molecules in serum remains a challenge. The manipulation of the small molecules with conjugated analytes or signal-enhancing particles may alter the properties of the molecules themselves, while the multi-step detection via sandwich or competitive assay requires extra preparation and prolongs the time of the assay (1.3).

### 2.7 Biosensing with aptamers

Aptamers are an emerging topic of interest, as they can be created to recognize a specific biomolecule (section 1.6). Works studying properties of aptamers and employing them in biomolecular recognition assays without any chemical modification of the target have been presented [46, 122, 123, 124, 125]. The direct characterization of small molecule-binding aptamers is very challenging because high sensitivity is needed to detect low molecular weight substances.

The K. Plaxco group presented a label-free system based on electrochemical interrogation of a small molecule (cocaine) via structure-switching aptamers in a 50% blood serum matrix with a limit of detection of 10  $\mu$ M [11]. They took advantage of the conformational change of the aptamers upon binding of the small molecule that make the sensor unaffected by non-specific binding and easy to regenerate by immersion in buffer. However, the main focus remains on the sensor and the biorecognition aptamer, rather than an innovative detection system.

Another interesting system from the same group, based on colorimetric detection, employs aptamers to detect a small molecule (cocaine) down to 1.25 pM [14]. In this case, the detection is not label-free, as they used inhibition assay via a conjugated polyelectrolyte.

SPR-based systems have characterized kinetics and equilibrium-binding properties of aptamers to small molecules [126]. A sandwich or a competitive assay is usually preferred for small molecule detection with SPR-based systems. The Y. Du group [8] described the preparation of an array chip for high-throughput detection based on aptamers. They immobilized plasmonic nanoparticles on a hydrophilic-hydrophobic patterned glass slide and enhanced the LSPR signal thanks to gold NPs coupled to the aptamers. LSPR information was then read with a laboratory microplate reader, so this system was not portable or suitable for personalized medicine.

Jang et al. presented a nanocube-enhanced SPR system based on sandwich assays that used aptamers for detecting cardiac biomarkers [127]. DNA aptamers were functionalized on a gold surface and the antibody was conjugated with gold nanocubes. Although this approach was very sensitive, as the aptamers are tested in undiluted human serum and concentrations down to aM are measured, the complicated manipulation of both aptamer and antibody is not convenient for a POC.

Each of the presented research efforts only implements one key aspect of the problem. For a system to be suitable as a POC for personalized medicine in a real-life application, all of these aspects must be combined. Therefore, it is highly desirable to have the advantages of label-free direct detection into a portable, low-cost platform. The work presented here is an important step for real-time detection of small molecules in undiluted serum by DNA aptamers via direct assay with a portable, label-free, optical detection system into real-life applications.



## 3 Principle of SPR based detection

The electromagnetic field of light incident on metal particles or thin metal films can excite the free electrons inside the metal to collectively move, forming charge density waves, the so called surface plasmon resonance (SPR). A SPR biosensor's performance highly depends on the underlying principle, its chemical interface and bio-functionalization, as well as the optical, electrical and structural features of the reading instrumentation. This chapter gives an overview on the concept of propagating SPR and on the Localized SPR, mainly focused on the sensing features.

### 3.1 Propagating SPR

Surface plasmon polaritons (SPP) are travelling charge density waves associated with an electric field propagating along the metal-dielectric interface and decaying exponentially in the perpendicular direction to the interface. Most of the energy is confined to the metal surface, making an SPR sensor highly sensitive to the changes that occur in the proximity of its surface [52]. Binding of molecules to the surface causes changes in the local refractive index (RI) and shifts the absorption spectrum peak towards longer wavelengths [128, 129, 130, 88]. Hence, this shift, measured as the change of the absorption curve's peak wavelength, can give quantitative information about the molecular layers on the surface (Figure 3.1) [131].

#### 3.1.1 Excitation schemes

Direct excitation of SPPs by light beams is not possible unless special techniques to achieve matching conditions between SPP and light are employed. This is usually achieved through coupling devices, mainly by total internal reflection in a prism coupler, wave diffraction in grating structures, or dielectric waveguides [52]. On planar metal-dielectric interfaces, the

### Chapter 3. Principle of SPR based detection

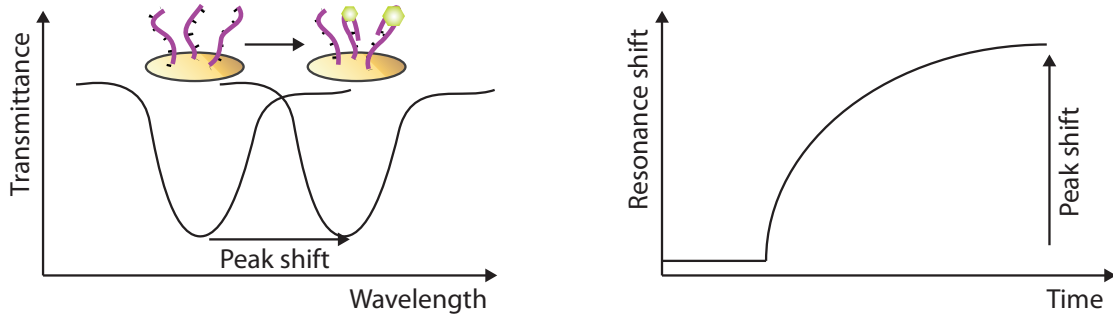


Figure 3.1: Plasmon peak location shift due to binding of biomolecules on the sensor surface (left) and response curve of the biosensor over time (right).

wavevector of SPPs,  $k$ , is larger than the one associated with the incident light.

$$k = \frac{\omega}{c} \sqrt{\epsilon_i} \quad (3.1)$$

is the wavevector of light propagating in a medium  $i$  of relative permittivity  $\epsilon_i$ ,  $\omega$  angular frequency and  $c$  speed of light. In free space the wavevector becomes  $\frac{\omega}{c}$  or  $\frac{2\pi}{\lambda_0}$ , where  $\lambda_0$  is the incident wavelength. However, the propagating SPR at the interface between a metal and a dielectric has a wavevector of  $k = \frac{\omega}{c} \sqrt{\epsilon_m}$ . Due to the fact that the dielectric constant of metals  $\epsilon_m$  is higher than the one of any dielectric material, special excitation schemes have to be applied in order to reach the matching condition (Figure 3.2).

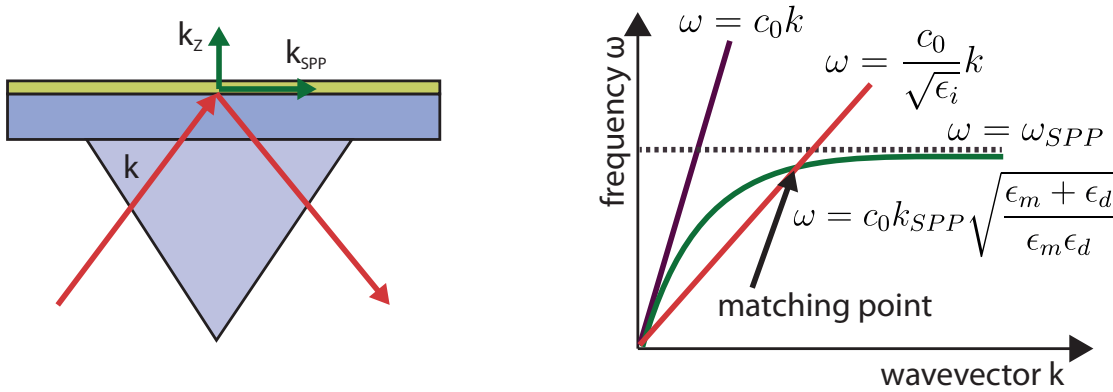


Figure 3.2: Schematic of prism coupling for surface plasmon excitation (left) and illustration of the corresponding phase matching condition (right).

A typical coupling device used to match the wavevector is a prism, in which the light is shined above a critical angle such that total internal reflection at the interface of the two media is obtained.

The amplitude of the wavevector  $k$  is expressed as:  $k^2 = k_{SPP}^2 + k_{z_i}^2$ , with two components,



one parallel to the plane of propagation,  $k_{SPP}$ , and one in the direction perpendicular to the interface,  $k_z$ . In order to excite the SPP, the component of the light wavevector that is parallel to the interface has to be enhanced by a factor of  $\sqrt{\epsilon} \sin \theta$  to match that of the surface plasmon ( $\epsilon$  is the permittivity of the prism coupler and  $\theta$  the angle of excitation).

Under these resonant conditions, a sharp minimum is observed in the reflected light. The wavelength for which this minimum is measured, can excite the SPPs most efficiently and is called resonance wavelength.

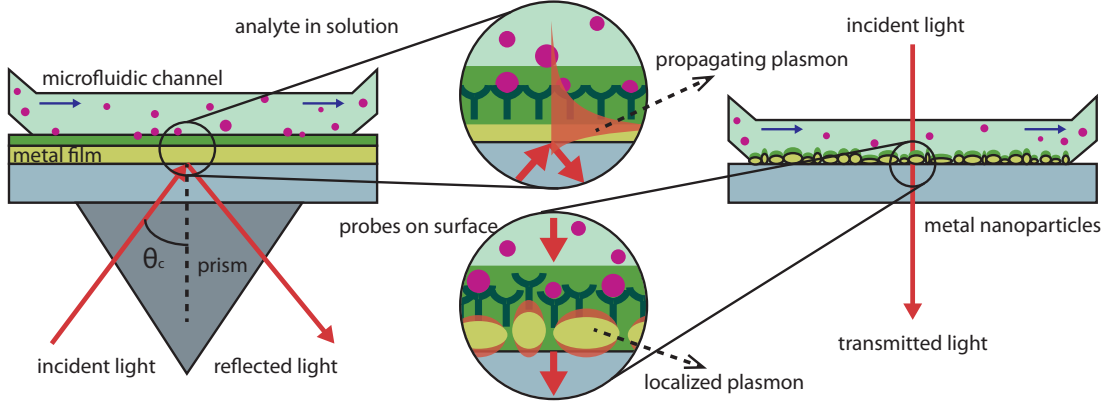


Figure 3.3: Comparison of propagating (left) and localized (right) SPR-based biosensors.

### 3.1.2 Main characteristics of propagating plasmons

A SPR sensor based on propagating plasmons is characterized by three main parameters: electric field enhancement, propagation length and penetration depth. The electromagnetic (EM) field is confined at the metal-dielectric interface and decreases exponentially in both media, depending on their permittivity.

If the excitation condition is fulfilled, the oscillating charges are in resonance with the external driving field and cause a strong enhancement of the electric field at the metal-dielectric interface. This resonance frequency depends on the thickness and optical properties of the materials, and on the different complex permittivity between the metal (higher) and the dielectric (lower).

The component parallel to the plane of propagation  $k_{SPP}$  is expressed as:

$$k_{SPP} = \frac{\omega}{c} \sqrt{\frac{\epsilon_m \epsilon_d}{\epsilon_m + \epsilon_d}} \quad (3.2)$$

where  $\epsilon_m$  and  $\epsilon_d$  are the dielectric permittivity of the metal and of the dielectric, respectively. The dielectric permittivity of a metal is a complex quantity

$$\epsilon_m = \epsilon'_m + j\epsilon''_m \quad , \quad (3.3)$$

### Chapter 3. Principle of SPR based detection

---

as a result the SPP wavevector has a complex nature

$$k_{SPP} = k'_{SPP} + jk''_{SPP} \quad , \quad (3.4)$$

where the imaginary part describes the SPR wave attenuation due to metal absorption and radiative losses. This means that the field intensity decays exponentially with a characteristic decay distance of  $\frac{1}{2k''_{SPP}}$ . The SPP propagation length  $\delta_{SPP}$  is defined as

$$\delta_{SPP} = \lambda_0 \frac{(\epsilon'_m)^2}{2\pi\epsilon''_m} \sqrt{\left(\frac{\epsilon'_m + \epsilon_d}{\epsilon'_m\epsilon_d}\right)^3} \quad , \quad (3.5)$$

where  $m$  refers to the metal and  $d$  refers to the dielectric [52]. For distances further than  $\delta_{SPP}$  the plasmon is strongly attenuated.

The plasmon propagation length affects the spatial resolution of the sensor and it is typically in the range of 3-30  $\mu\text{m}$ , depending on the characteristic of the system and exciting light [132]. In order to resolve two features on the same surface, they must be separated by a minimum distance corresponding to at least ten times the propagation length.

The wavevector amplitude  $k_{z_i}$  is imaginary and thus expresses the exponential decay of the EM field in the  $z$  direction. The penetration depth  $\delta_i$  is defined as the distance at which the intensity of the EM field inside the medium  $i$  (metal or dielectric) decreases to  $1/e$  of its original value at the interface.

$$\delta_i = \frac{\lambda_0}{2\pi} \sqrt{\left| \frac{\epsilon'_m + \epsilon_d}{\epsilon_i^2} \right|} \quad , \quad (3.6)$$

where  $\epsilon_i$  refers to  $\epsilon'_m$  or  $\epsilon_d$  depending on the direction considered for the decay of the EM field. The plasmon penetration depth in the dielectric affects the sensitivity of the sensor and it is typically in the range of 100-500 nm, depending on the characteristic of the system and exciting light [85].

## 3.2 Localized SPR

Localized surface plasmons (LSPs) are excited in metallic nanostructures that have characteristic dimensions smaller than the wavelength of the incident light. They are non-propagating charge density waves occurring on suspended nano-sized metal particles and on metallic nano-patterns [133, 134, 135, 136, 137, 138]. Excitation of LSP results in a peak in the extinction spectrum that depends on the metal, on the geometry and on the properties of the surrounding dielectric [87, 139, 140, 141, 142, 143, 89, 144]. A regular, periodic pattern of nanoparticles on a surface exhibits an extinction peak (caused by both absorption and scattering) in the visible and near-infrared range that can be narrowed by enhancing the regularity of the patterns [145]. Changes in the local refractive index cause the plasmon peak to shift in wavelength.

The penetration depth of LSPs is defined as the distance from the particle surface for which the surface sensitivity is half the bulk sensitivity [52, 146, 147]. The LSPs evanescent field extends into the dielectric medium typically in the range of 10-40 nm, depending on the nanoparticles' size, pattern and materials.

The main advantages of Localized Surface Plasmon Resonance (LSPR) over SPR include increased spatial resolution thanks to the non-connected pattern, simpler instrumentation required for detection, and no need for temperature stabilization due to the lower bulk RI sensitivity [86]. On the other hand, the fabrication of the nanostructures can be very costly compared to thin film deposition.

#### 3.2.1 Main characteristics of localized plasmons

The properties of LSPs can be modeled by assuming a spherical particle with dielectric permittivity  $\epsilon(\lambda)$  and with radius smaller than the wavelength of the exciting light. The incident field  $E_0$  is considered to be homogeneous over the whole particle's surface. A collective electron motion is excited in the particle when light is incident.

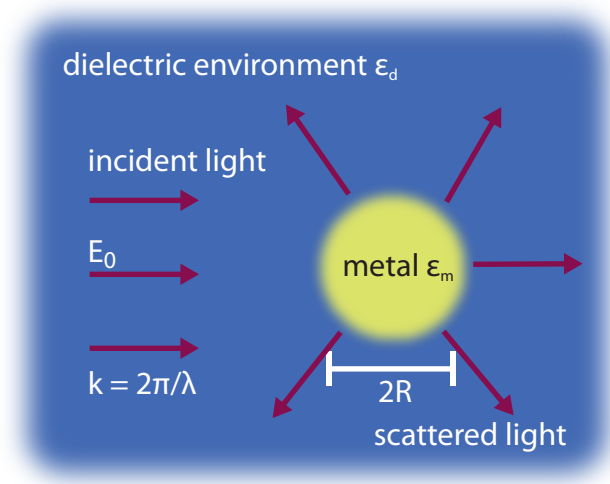


Figure 3.4: Scattering of light of a plasmonic nanoparticle.

The scattering efficiency of the particle exposed to homogenous electric field is expressed by

$$Q(\lambda) = \frac{8}{3} x^4 \left| \frac{\epsilon_m(\lambda) - \epsilon_d}{\epsilon_m(\lambda) + 2\epsilon_d} \right|^2, x = \frac{2\pi R}{\lambda} \quad (3.7)$$

where  $\epsilon_m$  and  $\epsilon_d$  are the dielectric permittivities of the metal and the dielectric, respectively,

and the first coefficient  $\frac{8}{3}x^4$  is related to the particle size with respect to  $\lambda$  [148]. The resonance condition depends on the permittivity of the background medium and it occurs when  $\epsilon_m(\lambda) = -2\epsilon_d$ .

Larger particles exhibit smaller and less sharp resonance, due to the fact that electrons have to travel a longer distance. As the particle symmetry decreases, that is particles with more complex shapes, the spectral features become more complex leading to multiple resonances.

### 3.3 Sensitivity and figure of merit

The sensitivity of a SPR based sensor is described as its ability to resolve small changes of RI in the proximity of the surface. In order to be able to detect a binding event, the interaction must occur within the extent of the plasmon. The sensitivity is then defined as:

$$S = \frac{\Delta\lambda_{peak}}{\Delta n} \quad (3.8)$$

where  $\Delta\lambda_{peak}$  is the shift in wavelength of the plasmonic resonance, while  $\Delta n$  is the variation in RI.

Sensitivity can be distinguished into bulk sensitivity,  $S_B = \frac{\Delta\lambda_{peak}}{\Delta n_{medium}}$ , that is changes in the RI occurring homogeneously in the whole medium surrounding the nanoparticles, and surface sensitivity,  $S_S = \frac{\Delta\lambda_{peak}}{\Delta n_{layer}}$ , that is the changes occurring within a layer at the surface of the particle [149].

The surface RI sensitivity is equal to the bulk sensitivity times a fill factor,  $\eta(0-1)$ , that indicates the fraction of LSP field volume filled by the layer (Figure 3.5). In other words, for a fixed layer thickness, larger particles exhibit lower surface refractive index sensitivity [131, 150]. In the case of biomolecular interaction that occupies the whole extent of the plasmon, the induced RI variation produces a change in the real part of the propagation constant  $k_{SP}, Re\{\Delta k\}$ , which is directly proportional to the RI change  $\Delta n$ :

$$Re\{\Delta k\} \cong k_0 \Delta n \quad , \quad (3.9)$$

where  $k_0$  denotes the free-space wavevector [131]. In order to compare different type of sensors, the Figure of Merit (FOM) is defined as:

$$FOM = \frac{S}{FWHM} \quad (3.10)$$

where  $S$  is the sensitivity and FWHM is the full width at half maximum of the resonance plasmon. The higher the FOM, the better the sensor. This means that high-performance sensors should have high sensitivity and a sharp plasmon resonance (narrow FWHM).

The theoretical study presented in [85] compares the sensing performance of propagating

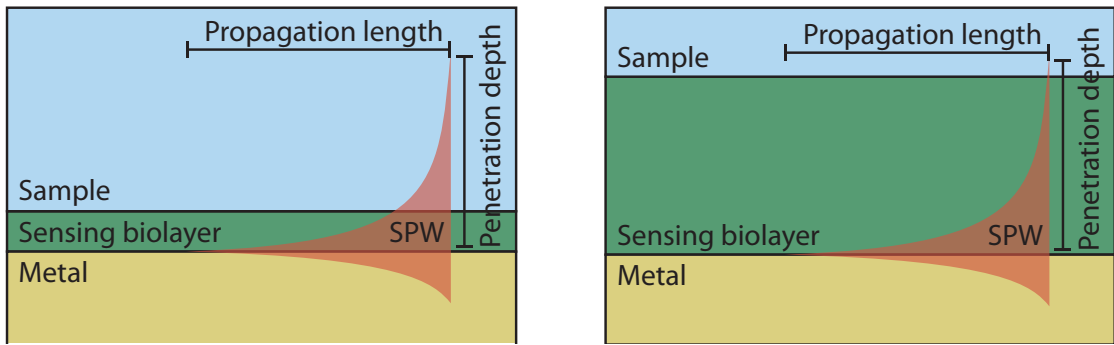


Figure 3.5: Biomolecular interaction occurring within a short distance from the metal surface and occupying a small portion of the plasmon (left). Biomolecular interaction occurring within the whole extent of the surface plasmon (right).

SPR and localized SPR sensors. Continuous metal layers and gold nanorods are simulated in order to extract and compare their FOM. The propagating SPR supported by the metal layer exhibits decay lengths varying between 100 and 500 nm, while for single nanorods the simulated distance is reduced to 50-80 nm from the nanoparticles surface, depending on the particles' geometry. This results in a one order of magnitude higher bulk RI sensitivity of the propagating SPR with respect to the LSPR.

Analysis of the sensitivity shows for both propagating and localized SPR a linear increase with increasing wavelengths. This is due to the larger penetration depth of the plasmons into the dielectric for longer resonant wavelengths, thus providing a larger volume that is sensitive toward RI changes.

The surface sensitivity has been simulated by modeling a 1 nm thick uniform coating over the nanostructures. Both for propagating and localized SPR, the surface sensitivity decreases for longer resonant wavelengths due to the larger penetration depth of the plasmon into the dielectric (see Figure 3.5). Also experiments confirmed a 15 % higher surface sensitivity for LSPR with respect to propagating SPR. Thus, for a nanoplasmonic sensor biosensing detection should be carried out within 10-15 nm from the surface. Beyond that distance, the sensitivity is strongly decreased.

Also Svedendahl et al. [86] did a comparison between the RI sensing capabilities of propagating and localized SPR. They conducted measurements on 50 nm thick gold films and on gold nanodisks featuring 120 nm diameter and 30 nm height. The same experimental conditions and excitation wavelength of 700 nm were used in both cases. Water/glycol mixtures were tested, obtaining bulk RI sensitivities of 3300 nm/RIU for the propagating SPR and 178 nm/RIU for LSPR, that correspond to a FOM of 54 and 2, respectively. The higher bulk RI sensitivity and FOM are due to the larger penetration depth of the plasmon into the dielectric, in fact propagating SPR exhibits a 246 nm decay length, while the nanodisks exhibit a 30 nm decay length because of their stronger electromagnetic field confinement around the nanoparticles.

### **Chapter 3. Principle of SPR based detection**

---

In this work, gold Nanoislands (NIs) evaporated on fluorine-doped tin oxide (FTO) on glass have been employed (See Chapter 4). These nanostructures form a non-connected pattern with irregular distribution on the surface due to the irregularity of the surface itself and the random formation process. As a result, the plasmon resonance is broad (FWHM= 150 nm) leading to a reduction of the FOM of the sensor. Nevertheless, they are extremely stable in solvents. The details of the fabrication process and the sensing characteristics are described in the next chapter.

## 4 Nanoislands chip fabrication

This chapter overviews the fabrication of the LSPR structures and some of their major limitations in biosensing applications. Then, the fabrication process of the gold nanoislands biosensor employed in this thesis is presented. Its application for the real-time sensing of small molecules with the T-LSPR setup is presented in chapter 7.

### 4.1 Nanostructures for Localized SPR

In the last decades, the progress of nanofabrication made it possible to create nanostructures with arbitrary geometries and nanometer precision [144, 151, 152]. Generally, nanofabrication techniques can be divided into two main categories: top-down and bottom-up approaches.

Top-down approaches, which consist of gradually removing material from a base substrate until the desired shape is reached, include commonly used techniques such as lithography, electron-beam lithography and focused ion-beam milling [101], which offer freedom in design and high precision.

Bottom-up techniques build on a base substrate the desired nanostructures by assembling atoms, molecules or particles using diverse techniques, such as for example soft lithography, nanosphere lithography (NSL) and direct evaporation. Such self-assembly approaches, in contrast to for example e-beam fabrication, often do not rely on expensive machines or serial processes and have thus been heavily used for biosensors development [146, 153, 154].

In NSL fabrication processes, self-assembled colloidal nanoparticles are utilized as either deposition or etching masks to pattern periodic nanostructures [130, 87, 88]. The nanoparticles have a regular size and are confined to a surface at a fixed interparticle spacing determined by the size of the nanosphere mask.

The group of R. Van Duyne extensively used this technique, for example to fabricate triangular silver nanoparticles (NPs) [130]. They tested the NPs' sensitivity with alkanethiols of different chain length and demonstrate that such NPs undergo structural changes when exposed to

various solvents, which significantly affect the LSPR (see discussion in the next section 4.2).

S. Zhu et al. [142] use NSL to create rhombic and triangular NP arrays and compared their sensitivity to bulk RI changes and surface modification with biotin-streptavidin. They reported a higher spatial resolution and a higher sensitivity for the rhombic NPs, even though the measurements were conducted in dry conditions.

The group of S. H. Oh investigated an inexpensive and high-throughput fabrication method for nanoapertures used in EOT systems. They use a template-stripping procedure to pattern periodic nanohole arrays [110, 117]. A silicon template is made via nanoimprint lithography and reactive ion etching and features periodic arrays of deep circular trenches. Then a silver film is deposited into the silicon template. The metal surface is then coated with a thin layer of epoxy and covered with a glass slide. Then the metal layer is peeled off the template while the mold remains reusable.

P. Chung and coworkers [101] presented a procedure for the fabrication of nanodimple arrays by using a spin-coated double-layer colloidal crystal as structural template.

In the case of direct metal evaporation onto substrates [98, 95, 141], the morphology of the islands film is determined by the evaporation conditions and the post deposition treatment [129], and determines the shape, intensity and position of the plasmon resonance.

However, the major concern in the creation of nanostructures for biosensing is their stability in wet environment, that is the mandatory condition to perform real-time measurements of biomolecular binding events.

### 4.2 Stability of the LSPR nanostructures

In biosensing applications, nanostructures with stable and reproducible optical properties are mandatory and define an efficient LSPR sensor.

Metal NPs fabricated on bare glass, mica or quartz substrates exhibit poor adhesion when immersed in solvents [129, 97]. The structural instabilities of the particles in solvents cause a change in their optical response. Often adhesion layers and coatings with organic or inorganic layers are employed to protect the nanostructures and improve their stability in wet environment [155].

Motivated by the poor stability of gold island films in water and other solvents, the group of Rubinstein proposed a method to stabilize gold island films on glass while maintaining a high sensitivity of the surface plasmon to analyte binding events [97]. Gold islands are coated with a thin silica layer of about 1.5 nm deposited by a sol-gel procedure on an intermediate mercaptosilane monolayer.

Another similar method is based on the coating of the gold nanostructures deposited on glass



with an amorphous silicon-carbon alloy overcoating deposited in a controlled manner via plasma-enhanced chemical vapor deposition [156].

The group of G. Borghs synthesized gold nanoparticles in solution and immobilized them on quartz substrates by a silane layer as molecular glue [157]. The nanoparticles have been tested with biotin/anti-biotin experiments, before which the NP-coated substrates were further modified with a self-assembled monolayer (SAM) of thiols (16-mercapto hexadecanoic acid).

Even if coating the nanostructures with a passivation layer is an effective method to protect the nanostructures in wet environment, it is an additional step required in the biosensor preparation and, depending on the passivation layer, it changes the surface chemistry than can be applied. In addition, the SAM layer occupies a fraction of the sensitive detection region determined by the plasmon extent in the dielectric medium, thus reducing its sensitivity (Figure 3.5).

As an alternative, the group of Rubinstein proposed a non-connected gold pattern of 2.5 nm thickness evaporated on polystyrene slides (cut out of petri dishes) instead of glass and obtained good adhesion in various solvents and tested on their islands with biotin-streptavidin binding assay [96]. With the same objective, also S. Szunerits and co-workers [129] replaced the glass substrate with indium tin oxide (ITO).

In the present work, gold nanoislands (NIs) are formed on fluorine-doped tin oxide (FTO) coated glass slides, as explained in the next paragraph.

### 4.3 Sensor based on gold nanoislands

The gold NIs employed in this work were realized by direct thermal evaporation and by subsequent mild thermal annealing (200°C overnight). No seed-mediated growth or additional adhesion layers were employed [158], thus involving a reduced-complexity process. NIs were formed on FTO coated glass slides. The usage of FTO coated glass instead of plain glass significantly improves the stability of gold NIs. In fact, gold penetrates in the porous SiO<sub>2</sub> layer during thermal annealing [159]. FTO coated slides are characterized by excellent adhesion properties while showing high optical transmittance and conductivity. The latter is desirable to perform comparative characterization techniques such as electrochemical and Scanning Electron Microscopy.

As a substrate, 5.3 cm × 1.2 cm FTO-coated glass slides were prepared by 20 minutes sonication in a 1:1 solution of 2-propanol and acetone, followed by abundant rinsing with ultra pure water and drying with pure nitrogen.

A layer of 5 nm of gold was evaporated on one surface at RT at  $3 \times 10^{-6}$  mbar at a rate of 0.0016 nm/sec. The layer thickness was monitored by a built-in quartz balance. Vacuum evaporation was followed by a thermal annealing overnight at 200°C.

## Chapter 4. Nanoislands chip fabrication

Figure 4.1 shows the evaporated gold layer before (A) and after (B) the annealing process. After mild heating, gold reorganizes in small clusters giving rise to a well-defined plasmonic peak (Figure 4.2B). Conversely, the extinction spectrum of the FTO-coated slide right after evaporation does not feature a well-defined peak (Figure 4.1) corresponding to a connected pattern.

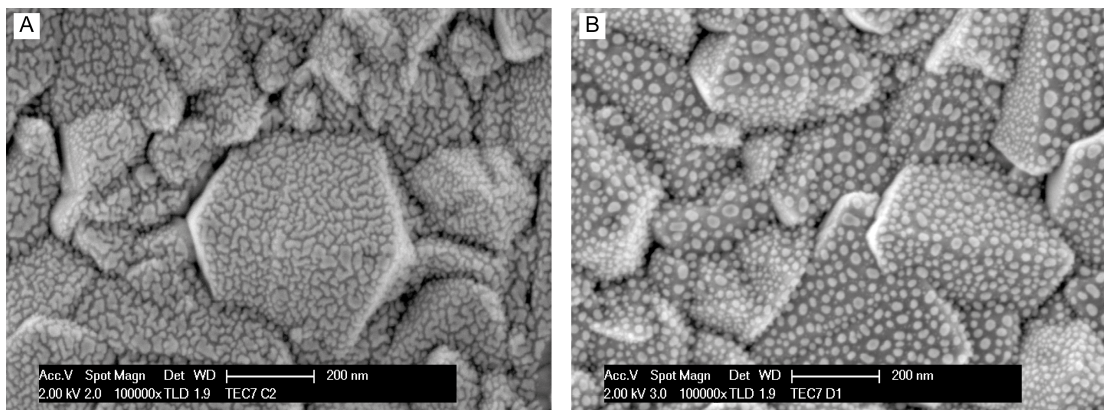


Figure 4.1: (A) SEM image of a thin gold layer evaporated on a FTO glass substrate. (B) SEM image of gold NIs formation after thermal annealing [1].

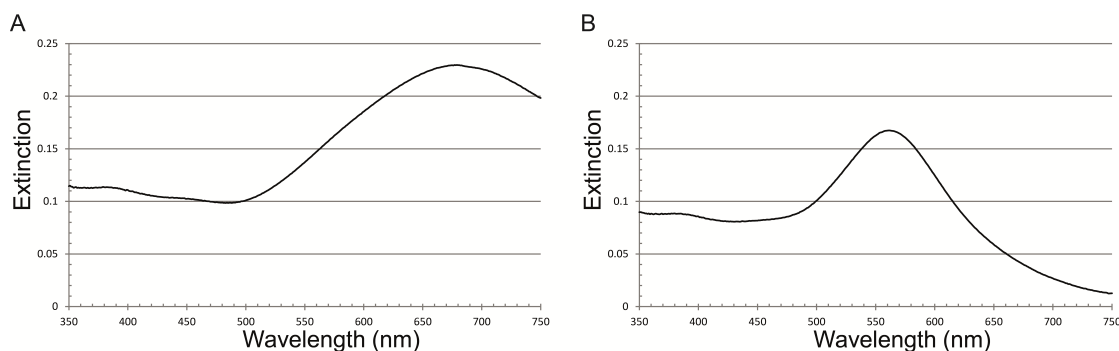


Figure 4.2: (A) Extinction spectrum of a sample after gold evaporation. (B) Extinction spectrum of a sample after evaporation and subsequent annealing [1].

### 4.4 Surface modification of the nanoislands

The gold NIs FTO-coated slides were functionalized using the following protocol.

DNA probes immobilization on gold was achieved by sulfur-gold bond. The NIs FTO-glass slides were incubated at room temperature for 16 hours in a PBS buffer solution containing the 5'-thiolated-CAG TGA GGC GTG GCC AGG G-3'-oligonucleotide (ssDNA).

After the incubation, the samples were rinsed with PBS buffer and ultra pure water and then gently dried with pure nitrogen. The light extinction of the samples was measured prior and

after surface ssDNA immobilization.

A reference slide was prepared to estimate the peak shift due to NIs aging and modification in liquid environment. We immersed NIs FTO-coated glass slides for 24 hours in PBS buffer, the same buffer used for the ssDNA immobilization process.

The sample was rinsed with ultra pure water and dried with pure nitrogen.

The formation of the ssDNA layer on surface is verified by means of a commercial spectrophotometer (Ocean Optics 2000+) by recording the NIs FTO-coated glass slides transmission spectra prior and after surface modification. A complete characterization of the formation of the ssDNA layer on surface is described in the next chapter.



## 5 Peak shift determination with T-LSPR setup

We aim at the observation of the plasmon peak location due to biomolecular binding events on a sensor surface. In this chapter the first prototype of a portable T-LSPR setup and the algorithm used for the extraction of the plasmon peak location are presented.

The setup is an electronic-based implementation of T-LSPR that avoids bulky equipment such as spectrophotometers and monochromators, while exhibiting excellent repeatability in the peak wavelength determination. It is based on light emitting diodes (LEDs) as a light source, a photodiode as a detector and on on-board signal amplification.

The peak location is extracted by a fast iterative curve-fitting algorithm, which is suitable for implementation on a limited-power computing platform (e.g. a 32bit microcontroller).

The system was tested in dry conditions on DNA-modified gold NIs evaporated on FTO-coated glass slides but in principle it is suitable for any transparent surface exhibiting a LSPR effect.

### 5.1 T-LSPR based setup

Our low-cost measurement approach is based on the observation that the information content of the complete transmittance curve is limited and that the key parameter of interest in T-LSPR measurement is the peak shift of the surface plasmon. Thus, we developed an ad-hoc technique for measuring the surface plasmon peak shift observed in transmittance using low-cost components and a highly streamlined optical setup.

We measure the peak shift by illuminating the sample with a limited number of different color LEDs. Since the intensity of the peak changes as well as the location, at least three LEDs whose spectra cover the peak region are needed to identify the peak shift. The peak location is estimated from the three measured intensities by means of an innovative interpolation technique that will be discussed in section 5.2.

A typical surface plasmon transmission spectrum of gold NIs evaporated on a transparent

## Chapter 5. Peak shift determination with T-LSPR setup

slide is plotted in Figure 5.1 (dashed curve, left axis); it has been measured with a UV-Vis-NIR spectrophotometer Jasco V-570 in transmittance mode with a scan speed of 200 nm/min and a bandwidth of 1 nm. Transmittance is normalized with respect to bare FTO slides. The peak is located between 550 nm and 595 nm and red-shifts upon modification of the NIs with layers of organic molecules (solid line).

The peak wavelengths of the LEDs spectral distributions are chosen to be across the SP peak and are respectively of 525 nm, 590 nm and 650 nm. Moreover, the NIs layer modifies the LEDs spectra when the light passes through it, resulting in an altered (filtered) spectral distribution (Figure 5.1, dotted lines, right axis). The three crosses indicate the transmittance values measured with the three LEDs light sources.

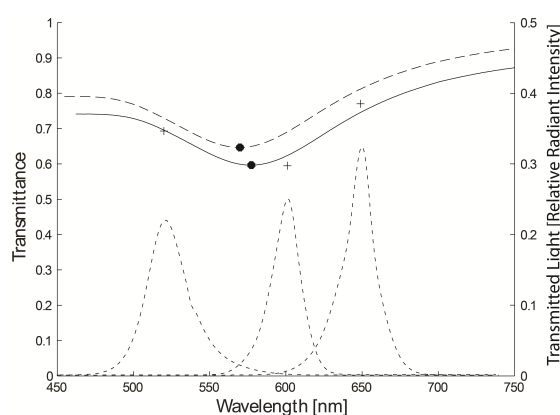


Figure 5.1: Example of a typical gold NIs spectrum (dashed line) measured with a UV-Vis-NIR spectrophotometer Jasco V-570 in transmittance mode with a scan speed of 200 nm/min, bandwidth 1 nm. The solid line represents the curve shift after NIs surface modification with organic molecules. The three crosses indicate the transmittance values measured with the LEDs system plotted at the LEDs effective wavelength. The dotted lines represent the LEDs spectral emissions normalized at their respective maximum emission values and filtered by the photodiode characteristic after passing through the layer of gold NIs.

### 5.1.1 Setup description

We selected Kingbright 1.0 mm × 0.5 mm SMD LEDs with a 120° viewing angle characterized by a Full Width at Half Maximum (FWHM) of 30 nm, 20 nm and 28 nm, respectively. At a forward current of 20 mA the LEDs have a luminous intensity of 110 mcd to 300 mcd for pure green, 50 mcd to 150 mcd for yellow, and 70 mcd to 220 mcd for red. LEDs light intensity emission has been monitored over 60 minutes. Despite an initial transient of about 10 seconds, the emitted light showed for all the LEDs constant drifts of  $-10^{-7}$  V/s,  $-3 \times 10^{-7}$  V/s,  $-2 \times 10^{-7}$  V/s for green, yellow and red, respectively. Figure 5.2 shows the portable T-LSPR setup. The NIs layers evaporated on slides are placed between the array of LEDs and a photodetector that detects the light intensity transmitted through the sample. The LEDs and the photodiode are mounted on a system of two printed circuit boards (PCBs), whose power supply is provided by

## 5.1. T-LSPR based setup

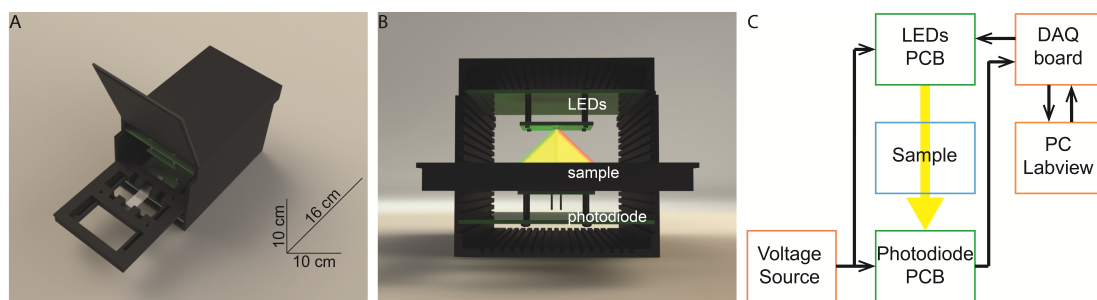


Figure 5.2: (A) Digital rendering of our transmission setup. (B) Frontal view showing the location of the light sources, sample and photodetector. (C) Schematic view of the setup.

an Agilent E3631A. The two PCBs are placed inside an aluminum box that has been treated with an anodization process to make it matte black, such that the light emitted by the LEDs is not reflected by the internal walls and that the external light is screened at the same time. The box presents sets of parallel lateral grooves in the internal walls for PCB holding.

In between, there is a tray equipped with a sample holder adaptable to different sample dimension by means of moving elements and screws. The setup is equipped with a low noise and low vibration fan (Multicomp GM0500PEV Series) to maintain the LEDs at a constant temperature. In fact, measurements conducted with a thermocouple placed inside the instrument showed that the LEDs luminous intensity decreases by about 0.4% for the green LED and 0.8% for the yellow and red LEDs per degree of temperature with respect to the LEDs emission at 25°C. We measured a shift of 1 nm for a variation of 0.43%, 0.63% and 0.39% of the light intensity emission for the green, yellow and red LEDs respectively. Overall, 1°C of temperature increase leads to a 0.6 nm shift, therefore, if not controlled, a temperature variation could lead to a false peak estimation.

The LEDs are current-supplied by a high-speed JFET-input operational amplifier (TL081) and controlled independently by means of 2N7000 N-Channel FETs, so as to illuminate alternatively the sample with spectral distributions centred on the three different wavelengths. The LEDs are spaced by 2.2 mm. The voltage at the non-inverting input of the amplifier is obtained through a voltage divider, dimensioned taking into account the maximum forward currents of the LEDs.

The light intensity can be tuned in real-time by a Data Acquisition Board (NI USB 6281 M Series) that controls the voltage divider and the activation of the LEDs. The LEDs are switched on with a cycle time of 45 seconds and a duty cycle of 33%. The light transmitted through the NIs-coated slides is detected by a photodiode (HAMAMATSU S1337-33BR) operating in the photovoltaic mode mounted on the second PCB. The photodiode has a quantum efficiency ranging from 0.25 to 0.45 in the plasmon peak region.

The photovoltaic configuration is particularly suitable for our low-frequency setup, leading to low noise output and reduced dark current. The current generated by the photodiode in

response to the transmitted light is then converted to voltage by a transimpedance amplifier, whose gain can be adjusted by selecting the proper resistance out of four possible values (10kOhm ÷ 80 kOhm) available in the feedback loop. The OPAMP CA3140EZ is a BiMOS operational amplifier featuring input gate-protected MOSFETs, which allows the measurement of very low input currents (stray input current 10 pA).

A capacitor connected in parallel to the resistances is added to filter out high frequency noise. The output voltage of the amplifier is measured by the DAQ board setup and presents a noise level of about 15  $\mu V$  (see Section 5.3).

### 5.2 The algorithm for peak extraction

Our system aims at characterizing the surface plasmon peak shift observed in the extinction spectrum in response to a biochemical event, by illuminating the sample with a limited number of LEDs.

This shift is estimated by identifying the peak location before and after the NIs surface modification with organic molecules. We developed an algorithm that extracts the peak location employing the LEDs transmittance measurements. The presence of molecular layers on the surface of gold NIs determines a red shift on the SPR spectrum but does not affect its shape significantly.

In order to fit the experimental data, the algorithm employs a curve representing qualitatively the typical plasmon peak shape ( $T_{NI}(\lambda)$ ). Such a curve can be obtained by the extinction spectrum of any sample of the batch, since the shape is not significantly sample-dependent. However, in this work we obtain the peak-shape representative curve by averaging extinction spectra obtained on several samples, to smooth sample variability effects.

The algorithm takes into account the non-ideal spectral characteristics of the light sources and of the photodetector, as they contribute to the transfer function of our system. In fact, the LEDs have bell-shaped spectra  $f_{LED}(\lambda)$  normalized to their maximum emission value with a specific FWHM. Besides, the photodetector has a quantum efficiency spectrum  $f_{PH}(\lambda)$  variable in the SP peak range.

Therefore, for a given LED 'i', the following expression corresponds to the  $T_{NI}(\lambda)$  read by the system of that LED and photodetector:

$$\sum_{j=\lambda_1}^{\lambda_2} T_{NI}(\lambda) \cdot f_{LED,i}(\lambda) \cdot f_{PH}(\lambda) \cdot \Delta(\lambda_j) \quad (5.1)$$

Here we approximate the integral over  $\lambda$  with a summation as the discretization error is negligible if we take fine-grained samples (in this case we took 4'000 samples in a 400 nm range), while computational speed significantly improves. The mathematical expression of



### 5.3. Repeatability of the peak wavelength determination

the transmittance of the reference sample is:

$$T_{LED,i} = \frac{\sum_{j=\lambda_1}^{\lambda_2} T_{NI}(\lambda) \cdot f_{LED,i}(\lambda) \cdot f_{PH}(\lambda) \cdot \Delta(\lambda_j)}{\sum_{j=\lambda_1}^{\lambda_2} f_{LED,i}(\lambda) \cdot f_{PH}(\lambda) \cdot \Delta(\lambda_j)} \quad (5.2)$$

where  $\lambda_1$  and  $\lambda_2$  are the extremes of the considered wavelength range, and  $\Delta\lambda$  is the wavelength increment.  $T_{LED,i}$  represents the theoretical transmittance value calculated for the LED 'i'. The algorithm iteratively translates  $T_{NI}(\lambda)$  in the x and y directions, i.e. wavelengths and transmittance values, respectively, with small increments  $\delta_x$  and  $\delta_y$ :

$$T_{NI}(\lambda, \delta_x, \delta_y) = \delta_y + T_{NI}(\lambda + \delta_x) \quad (5.3)$$

This iterative translation is carried out in the 350 nm - 750 nm range where the SPR occurs. At each translation step,  $T_{LED,i}$  is calculated and compared to the experimental measurements. The algorithm determines the translation parameters that minimize the root mean square error between the set of theoretical values and the experimental ones. The curve obtained by the corresponding translation provides the best estimation of the peak location of the transmittance spectrum.

At every translation step along the x axis, the  $T_{LED,i}$  points are calculated for all the LEDs for every possible translation in the y axis; the algorithm computes the root mean square error between those points and the experimental values  $y_{LED,i}$ .

In other words, the optimization routine tries to identify the parameters  $\delta_x$  and  $\delta_y$  that minimize the Euclidean distance between the vector  $(y_{LED,1}, \dots, y_{LED,i}, \dots, y_{LED,N})$  and the vector  $(T_{LED,1}, \dots, T_{LED,i}, \dots, T_{LED,N})$ .

This procedure can be mathematically expressed by the following formula:

$$\operatorname{argmin}_{\delta_x, \delta_y} \left\{ \sqrt{\sum_{i=1}^N [y_{LED,i} - T_{LED,i}]^2} \right\} \quad (5.4)$$

At the end of the elaboration, the optimal  $\delta_x^*$  and  $\delta_y^*$  parameters are found and the wavelength corresponding to the peak of the curve is extracted (Figure 5.3).

### 5.3 Repeatability of the peak wavelength determination

The portable system for T-LSPR has been characterized in terms of measurement error on a NIs FTO-coated glass slide.

The output of the system is a voltage ranging from few volts to tens of volts depending on the active LED. The average output voltage over 6 subsequent measurements is  $12.17 \text{ mV} \pm 14.64 \text{ } \mu\text{V}$  for the green LED,  $3.28 \text{ mV} \pm 19.12 \text{ } \mu\text{V}$  for the yellow LED, and  $8.18 \text{ mV} \pm 15.26 \text{ } \mu\text{V}$  for the

## Chapter 5. Peak shift determination with T-LSPR setup

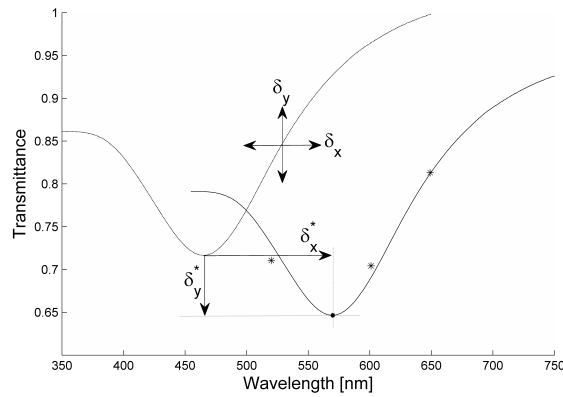


Figure 5.3: Fitting of the LEDs experimental data. The three stars represent the intensity measured by enlightening the sample with the LEDs and they are plotted at the LEDs effective wavelengths. The dashed curve represents the typical plasmon peak shape ( $T_{NI}(\lambda)$ ) and the two double arrows,  $\delta_x$  and  $\delta_y$ , indicate the direction in which the curve is shifted in order to fit the experimental data.  $\delta_x^*$  and  $\delta_y^*$  are the optimal values extracted by the algorithm that correspond to the best data fitting.

red LED. Each measurement is an average of 40 kSamples taken at a rate of 100 kSamples/s.

The peak wavelengths extracted by means of the algorithm (see Section 5.2) from these 6 measurements have a maximum deviation of 1.1 nm as shown in Figure 5.4 A.

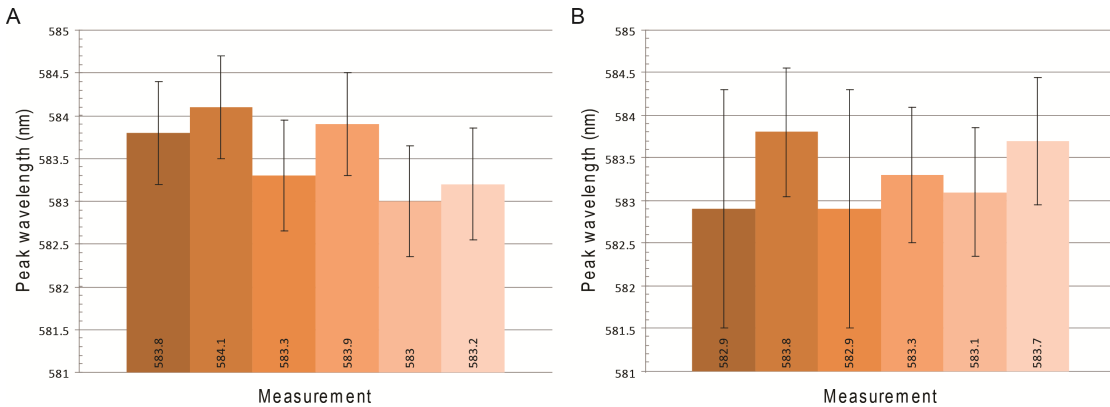


Figure 5.4: (A) The measurement and extraction of the peak location of a NIs coated slide has been repeated 6 subsequent times. The maximum deviation among the 6 measurements is 1.1 nm. Each measurement has an error bar between 1.2 nm and 1.3 nm given by the standard deviation over the 40000 samples. (B) The NIs-coated slide has been removed from the sample holder and place it back in between each of the 6 measurements [1].

To evaluate the error due to a different positioning of the NIs-coated slide on the sample holder, we removed the slide from the holder and placed it back in between each measurement for 6 times. The peak wavelengths extracted by the algorithm have a maximum deviation of 0.9 nm, while the error bars range from 1.5 nm to 2.8 nm. The results are shown in Figure 5.4B.

## 5.4. Measurement of the peak shift due to a ssDNA layer formation

In order to test the impact of the choice of the fitting curve representing the typical peak shape (Section 5.2), we compared the results obtained using the same identical spectrum for any sample with respect to the employment of the spectrum corresponding to a specific sample. The two procedures do not lead to significant difference in the value of the extracted peak. In this work, we used a spectrum obtained from averaging all the samples of the batch.

### 5.4 Measurement of the peak shift due to a ssDNA layer formation

A batch of 11 NIs-coated slides has been prepared with the self-assembly process in order to obtain a layer of ssDNA on the gold surface. The peak locations have been determined for every sample before and after surface modification by means of the LEDs-based measurement setup and by the extraction algorithm described in Section 5.1 and 5.2, respectively. The average peak shift obtained upon DNA immobilization on the 11 samples corresponds to 7.24 nm with a standard deviation of 1.65 nm. A typical peak shift is shown in Figure 5.5.

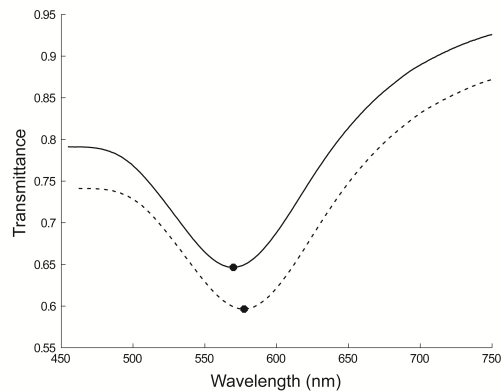


Figure 5.5: Peak shift of a NIs sample before (solid line) and after surface modification with ssDNA (dotted line) as extracted by means of our LEDs-based setup and extraction algorithm. Transmission is calculated with respect to a FTO-coated slide.

The same samples have been also characterized by means of a Jasco V-570 Spectrophotometer (Perkin Elmer). The obtained average peak shift after the molecular layer formation corresponds to 5.18 nm with a standard deviation of 1.94 nm (instrument bandwidth 1 nm). We consider the difference in the average peak shift estimated by our LEDs-based setup and by the spectrophotometer to be due to a different contribution of the scattering effects in the two sample cells.

In order to evaluate the stability of the NIs peak in liquid environment we measured a reference sample prior and after incubation in Phosphate Buffered Saline solution 1X. The incubation did not lead to an appreciable peak shift. This measurement demonstrates that the peak shift observed after ssDNA immobilization is actually due to the presence of the molecular layer and not to conformational changes of the NIs in a buffer solution.

Other works based on T-LSPR that employs single wavelength measurements [39] have been published. The advantage of our instrument compared to single-wavelength measurements is that we have three discrete light sources that enable the identification of the peak position in wavelength. We are interested in this feature for two reasons: 1) we want to compare our setup with a standard UV-Vis spectrophotometer in its ability to describe the full spectrum of the plasmon. 2) Many publications in the surface plasmon field report that the molecular changes at the interface affect directly the plasmon peak position [145]. Moreover, our approach has the advantage to measure and monitor the possible broadening of the plasmon in case the plasmonic structures are unstable.

### 5.5 Summary

We designed and implemented a portable setup for T-LSPR measurements with 1 nm precision on the plasmonic peak extraction. The sensor is fully-portable, low cost and suitable for real-time detection. It is based on electronically-driven power LEDs and integrated instrumentation amplifiers. We developed a novel data analysis approach that extracts the key signature of the LSPR spectrum from the measurements with a set of three LEDs, emitting in the visible region.

In this work, we tested our LEDs-based setup on NIs FTO-coated slides. The accuracy in the peak location determination has been characterized. The uncertainty due to the measurement error and the software extraction procedure leads to a 1.1 nm maximum deviation over 6 repeated measurements. NIs have been modified with ssDNA and the resultant LSPR peak redshift has been characterized over 11 samples. We found that the response of our LEDs-based device combined with the fast algorithm tracks very well the plasmonic shift extracted by standard UV-Vis spectrophotometer.

The results presented demonstrated the remarkable performance of our simple, low-cost setup and peak extraction algorithm with respect to a high-end spectrophotometer. The system was tested on evaporated gold NIs on FTO-coated glass slides, nevertheless it is compatible with any surface exhibiting a localized SPR effect. Furthermore, the T-LSPR configuration is suitable to be scaled down to sub-micrometer detection areas and parallelized as a detector array. The choice of using low power-consumption components makes the device suitable for low-cost and portable bioanalytics applications, as in the case of POCs.

## 6 Plasmon shift determination in array format with CMOS image sensor

An improved version of the T-LSPR setup presented in the previous chapter has been designed and developed in order to perform parallel array measurements. The goal is to characterize in real-time multiple binding events occurring on the same biosensor surface. The improved system features a broad spectrum LED and a CMOS image sensor, it is scaled down to a palm size and it is powered by computer via USB connection.

In this chapter, a complete description of the system is presented. The peak extraction algorithm has been adapted to the new features of the T-LSPR system and a new parameter for the wavelength evaluation, the hue, is introduced. At last, the characterization of the NIs biosensor response to bulk refractive index changes is presented and the calibration curves and figure of merit are calculated.

### 6.1 Optical setup for real-time detection

The T-LSPR setup is a self-contained system that employs a non-polarized white light LED (Cree Lamp XP-E supplied by 2.49V) as excitation source and a CMOS image sensor (ST Microelectronics VW6558) as a light detector. The transmitted light through the NIs coated slides is affected by the plasmonic resonance phenomenon occurring at the NIs-solution interface.

The light is collected by the CMOS detector through a plano-convex lens (Thorlabs LA1270-A) that reduces the focal distance between the NIs coated slide and the CMOS sensor. Relative distances among the elements of the optical setup are represented in scale in Figure 6.1 A) and 6.1 B).

The use of an image sensor allows for arrays spotting enabling to monitor multiple surface reactions at the same time. The dimensions of the CMOS sensor are  $3.5 \times 3.03 \times 2.5 \text{ mm}^3$ . It has an integrated lens with focal length of 1.25 mm and horizontal field of view (HFOV) of  $60^\circ$ . The resolution is 648x488 pixels with red (R), green (G) and blue (B) filters in a Bayer pattern configuration. The size of each pixel is  $2.2 \mu\text{m} \times 2.2 \mu\text{m}$ .

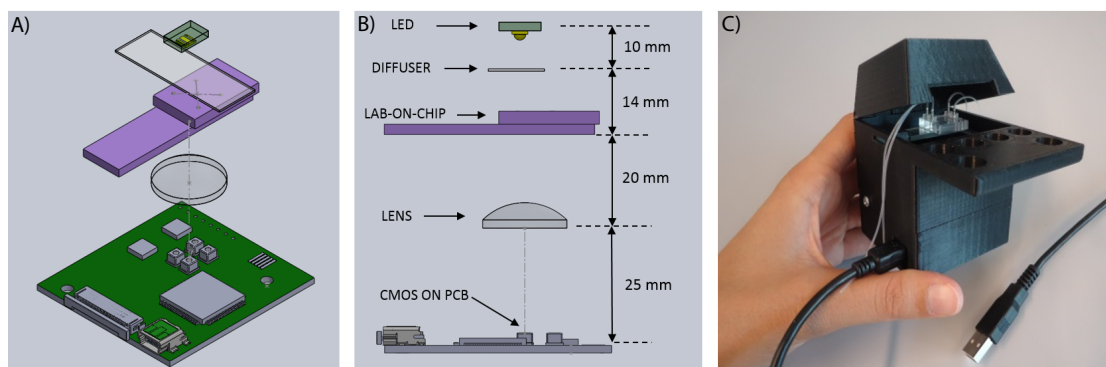


Figure 6.1: A) Digital rendering of the components of the optical setup. B) Side view with relative distances in scale among the components. C) Picture of the T-LSPR setup.

A diffuser is placed at 10 mm distance from the LED to improve the light uniformity and to prevent hot spots on the image. All the setup components are placed inside a 3D printed case of size 5.5 cm x 6 cm x 8.5 cm (Figure 6.1 C)). The black material is chosen in order to have very low internal reflections.

### 6.2 Microfluidic plasmonic chip for molecular analytics

The microfluidic chip is composed of a glass slide coated with gold NIs (described in Section 4.3) and a microfluidic module.

Microfluidic channels for the delivery of Tobramycin solutions to the DNA aptamer on the surface are built by mounting a cover plate on top of the NIs FTO-glass slide. The cover plate is made out of Polymethyl Methacrylate (PMMA) and it is held on the NIs FTO-glass slide by a double coated tape (3M High Performance Double Coated Tape 9086). The channels' size (2 mm x 14 mm x 150  $\mu\text{m}$ ) corresponds to the pattern on the tape by laser micromachining (Figure 6.2).

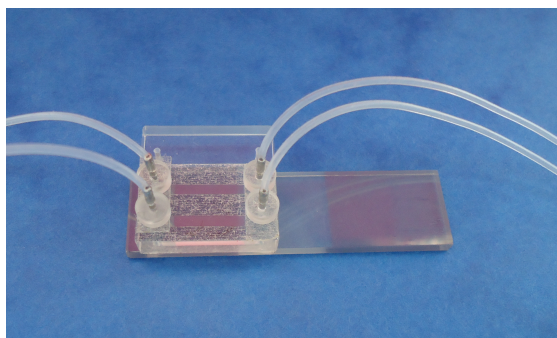


Figure 6.2: Picture of the microfluidic plasmonic chip.

Inlets and outlets are 0.8 mm in diameter such that microfluidics connections are possible from standard syringe needles (Terumo) connected to the syringe pump (Harvard Apparatus

11 Elite Nanomite Programmable Syringe Pump) via flexible silicon tubes (Sani-Tech STHT-C).

### 6.3 Data analysis

Images of 200x300 pixels were recorded at 8 frames per second with an analog gain set to 1, they were saved in a sequential order in bitmap format and were displayed in real-time on the screen. Regions of interest (ROIs) of about 800 pixels were manually selected on the images in order to include the functionalized areas (Figure 6.3). RGB intensities were then averaged for each ROI yielding to the corresponding output signal used for further data analysis.

Image analysis was then performed by either determining the plasmonic peak location (wavelength) using an algorithm we developed (5.2), or by calculating the hue change.

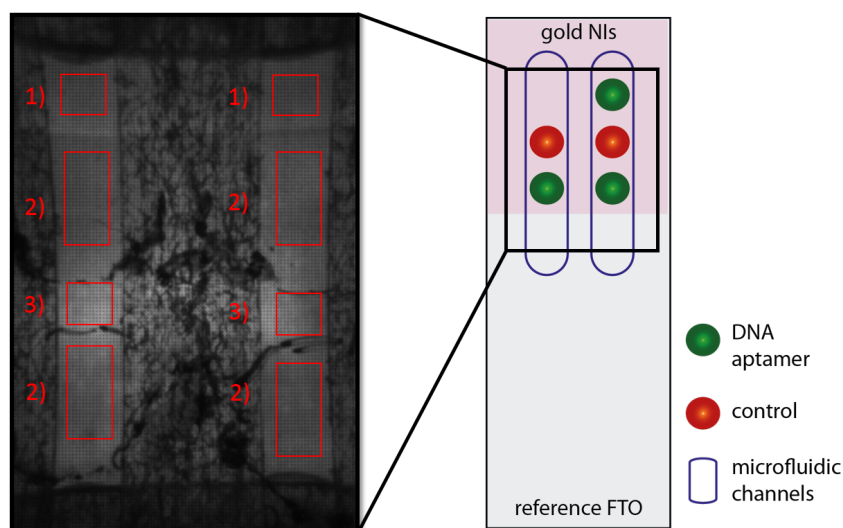


Figure 6.3: Schematic representation of a NIs FTO glass slide indicating the spots on surface and the areas exposed to the microfluidic channels (right). Example of image acquired by the CMOS camera (left). The ROIs are selected during the data processing. 1) Reference FTO surface. 2) Aptamer spots. 3) MCH control spots.

### 6.4 Adaptation of the algorithm to the new setup

For each ROI of each image, the R, G and B values for light transmittance are mediated over the ROI. This set of three discrete points is used by the algorithm to extract the plasmon peak location in wavelength.

The biomolecular binding event on the surface induces a redshift of the plasmon peak without altering its shape, the latter being an intrinsic characteristic of the gold NIs. The characteristic plasmon resonance of the gold NIs FTO-coated glass slide is used as a reference curve in the algorithm. The algorithm takes into account the spectral characteristics of the white LED and

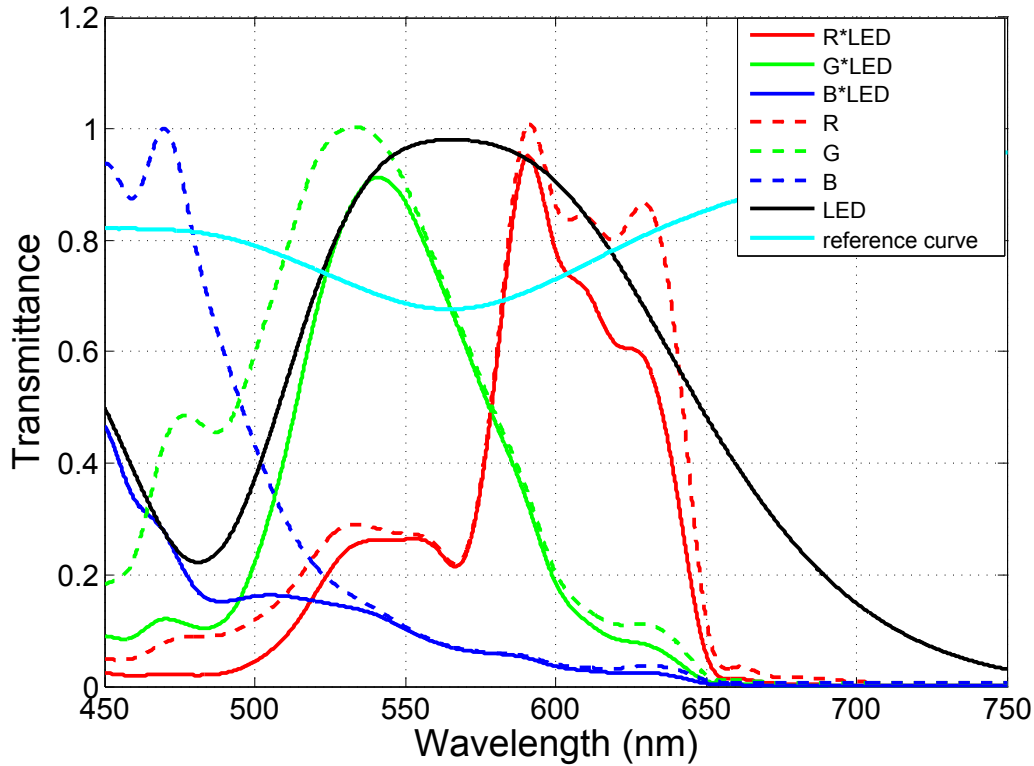


Figure 6.4: Example of a typical gold NIs spectrum (blue dashed line) measured with a UV-Vis-NIR spectrophotometer Jasco V-570 in transmittance mode with a scan speed of 200 nm/min, bandwidth 1 nm. The solid line black line represents the white LED emission. The dashed blue, green and red lines represent the RGB filters of the CMOS image sensor normalized at their respective maximum values and the continuous blue, green and red lines are the same curves convoluted with the LED spectrum.

the RGB filters used in the optical setup.

At each iteration, the reference curve is shifted in wavelength and transmittance until the best fit with the set of three measured points is reached and the peak location is estimated. The detailed description of the algorithm can be found in 5.2.

## 6.5 Hue calculation

Raw data were first converted from Bayer pattern to RGB values and then converted into the HSV (Hue, Saturation, Value) color-space. In the HSV colorspace the hue (H) value corresponds to the perceived color tone and thus indirectly to the physical wavelength, therefore it is a candidate parameter to evaluate the spectral variations of the plasmon resonance peak in the spectrum. It uniquely depends on the measured combination of red, green and blue pixel values and it is independent of the overall luminous intensity, as proven experimentally and



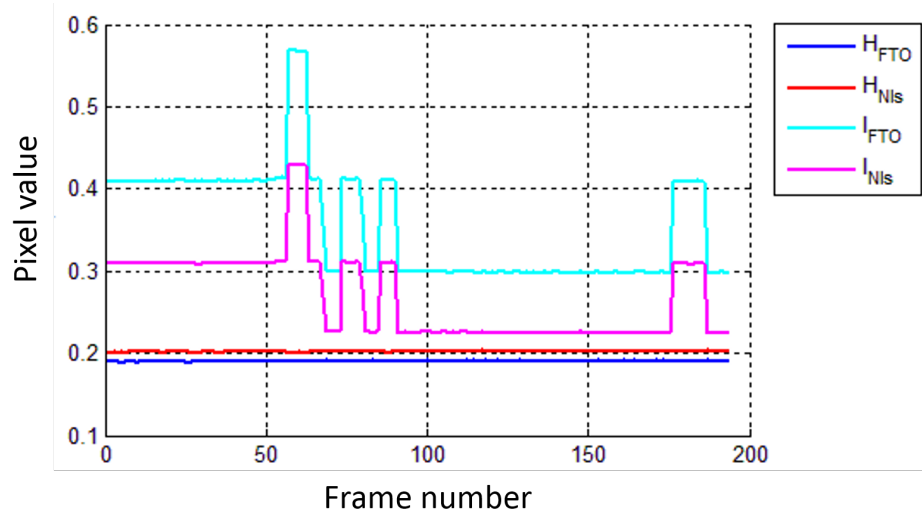


Figure 6.5: Hue calculation for different light intensities. The pink and cyan lines represent the light intensity for a NIs and a bare FTO spot on surface, respectively, modified by changing the LED feeding current. The corresponding hue is represented by the red and blue lines and it is independent on the luminous intensity of the light.

shown in Figure 6.5.

A 2 hours experiment conducted by varying the feeding current of the LED, such to increase and decrease the luminous intensity reaching the CMOS pixels, proved that the hue remains constant independently from any light intensity variation.

For each image and for each selected ROI, the hue of the average of the selected pixels is calculated (as in Equation 6.3) and low-pass filtered (filter order of 126, cutoff frequency of 0.00438 Hz). The variation of the hue was then used to display the plasmonic changes over time.

$$\text{MAX} = \text{MAX}(R, G, B) \quad (6.1)$$

$$\text{min} = \text{min}(R, G, B) \quad (6.2)$$

$$H' = \left\{ \begin{array}{ll} \frac{G-B}{\text{MAX}-\text{min}} & \text{if MAX=R} \\ \frac{B-R}{\text{MAX}-\text{min}} + 2 & \text{if MAX=G} \\ \frac{R-G}{\text{MAX}-\text{min}} + 4 & \text{if MAX=B} \end{array} \right\} \quad (6.3)$$

$$H = \frac{H'}{6} \quad (6.4)$$

$$H = H + 1 \quad \text{if } H < 0 \tag{6.5}$$

### 6.6 Stability of the NIs layer in aqueous solution

The stability of the gold NIs was tested by measuring the NIs FTO-glass prior and after 24 hours immersion in TE 1X buffer. Extinction spectra measured with a commercial spectrophotometer (Ocean Optics 2000+) show no appreciable shift.

In order to test the NIs adhesion in presence of a flow of solution, the microfluidic module was mounted on the NIs FTO-glass slide, as described in 6.2, and TE buffer is flushed for 10 minutes at 5  $\mu\text{l}/\text{min}$ . The absence of change in the signal proves the stability of the gold NIs under flow.

### 6.7 Refractive index sensing in bulk

In order to determine the sensitivity of the NIs FTO-coated slides to bulk refractive index changes, the microfluidic module is mounted on the slides, as described in paragraph 6.2, and solutions with diverse RI values, prepared as reported in [160], are delivered to their surface.

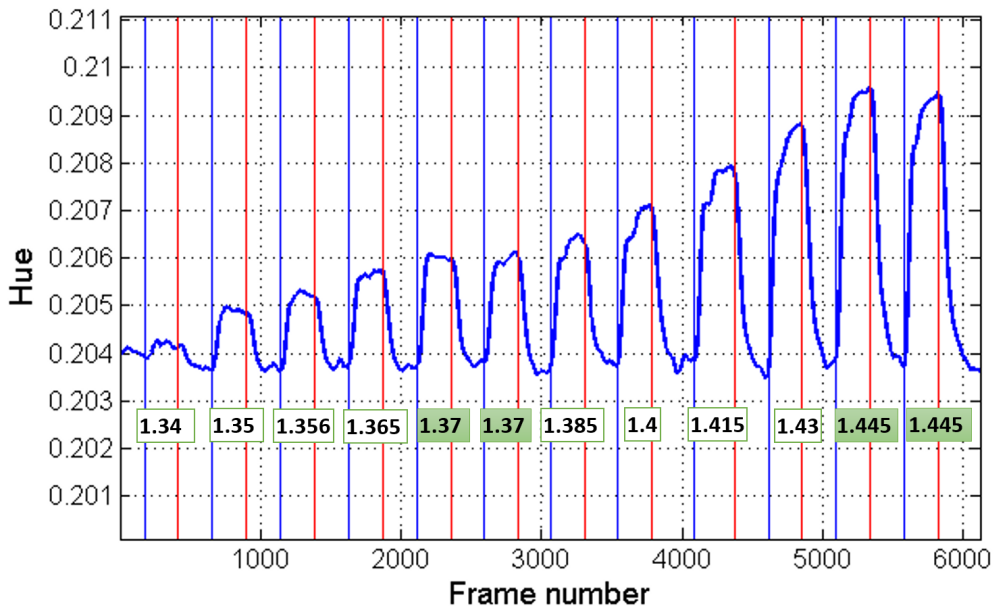


Figure 6.6: Bulk Refractive Index response of the NIs FTO-coated glass slide to glucose/sucrose solutions injections with increasing RI values expressed in hue variation. The blue and red vertical lines indicate when the glucose/sucrose solution and the ultra pure water reach the sensor’s surface, respectively.

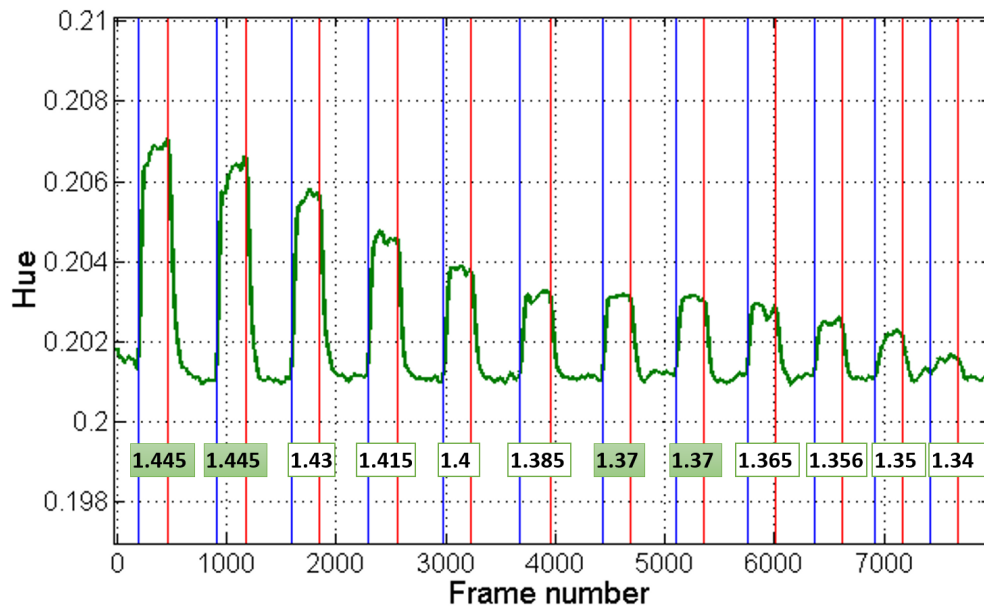


Figure 6.7: Bulk Refractive Index response of the NIs FTO-coated glass slide to glucose/sucrose solutions injections with decreasing RI values. The blue and red vertical lines indicate when the glucose/sucrose solution and the ultra pure water reach the sensor's surface, respectively.

Ultra pure water, that has RI of 1.33, is used as reference solution. For RI between 1.34 and 1.37, the solutions are prepared by glucose dilutions in ultra pure water. From 1.385 to 1.445 the solutions are prepared by sucrose dilutions in ultra pure water.

Every glucose/sucrose injection is alternated with an injection of ultra pure water, that is referred to as the baseline of the experiment. The presence of solutions with higher RI with respect to water in contact with the NIs surface makes the plasmon peak location to redshift.

Figures 6.6 and 6.7 show the glucose/sucrose injections delivered to the surface in increasing and decreasing concentrations, respectively. During the experiments, the solutions with RI 1.37 and 1.445 have been repeated twice consecutively in order to verify that the plasmon peak shift measured was not due to a drift or instability of the nanostructures.

Solutions with high RI values present increased viscosity, as it is visible in Figure 6.6 starting from RI 1.385, where the transition from the glucose solution to the water baseline is slower. In Figure 6.7 the water injections in between two consecutive glucose/sucrose high RI solutions have been prolonged in order to reach a stable baseline before the next glucose/sucrose injection. Also in this case, the high viscosity is evident as a smoother transition from the glucose/sucrose solution to water.

The plasmon shift has been evaluated in term of plasmon peak location, as extracted with the algorithm (6.4), and as related to the hue (6.5). A direct comparison between peak location

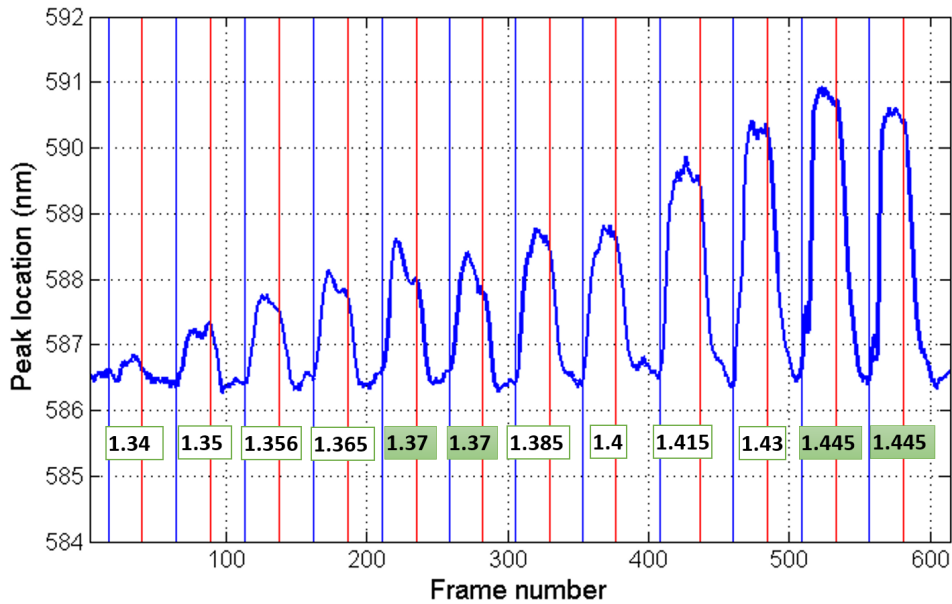


Figure 6.8: Bulk Refractive Index response of the NIs FTO-coated glass slide to glucose/sucrose solutions injections with increasing RI values expressed in peak location shift (nm). The blue and red vertical lines indicate when the glucose/sucrose solution and the ultra pure water reach the sensor's surface, respectively.

extraction and hue calculation is discussed in the next chapter (7.3).

### 6.7.1 Calibration curve and figure of merit

The bulk RI plasmon peak shifts plotted against RI value show a linear trend with a sensitivity of 36.7 nm/RI (Figure 6.9).

The characteristic plasmon shape of the gold NIs FTO-coated glass sensor has a FWHM of 150 nm (Figure 4.2). In order to be able to compare the performance of our sensor with other different structures, the FOM (see section 3.3) of the NIs FTO-coated glass slide sensor to bulk RI sensing, calculated as in Equation 3.10, is 0.24.

The sensitivity of LSPR sensors to changes in RI is highly dependent on the plasmon characteristics such as the penetration depth, spectral linewidth and electromagnetic field strength (see section 3.2). In order to increase the FOM of a LSPR sensor, the sensitivity should be increased or the FWHM should be reduced, that can be achieved by improving the regularity of the nanostructures in shape and pattern.

Many groups investigated various nanostructures with different techniques in order to increase the sensor performance, as it is the case of C. Huang [161] that fabricated gold nanorings on quartz using NSL featuring RI sensitivity of 350 nm/RIU (Refractive Index Unit) with a FOM

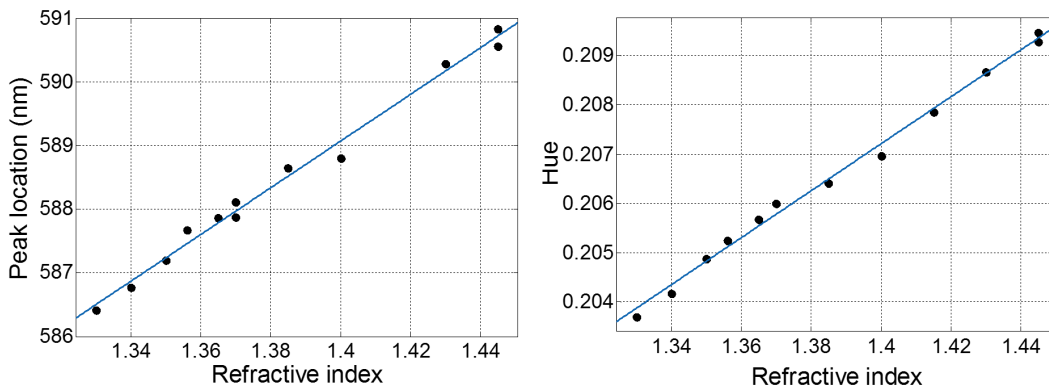


Figure 6.9: Bulk Refractive Index sensitivity expressed in peak location wavelength (left) and in hue variation (right).

of 3.1. The group of R. Van Duyne [162] developed LSPR sensor based on nanowell surfaces covered by a silver film exhibiting a sensitivity of 538 nm/RIU and a FOM of 14.5. The same group developed silver triangular nanoprisms [88] featuring a sensitivity of 205 nm/RIU and a FOM of 3.3.

More complex structures, as the case of plasmonic mushrooms composed of a gold cap on a photoresist pillar located on a gold film [102] and featuring a FOM of 108 (FWHM 10 nm and 1010 nm/RIU) tested in dry conditions, and other systems with very narrow FWHM and high FOM, as in the case of EOT systems [109, 110, 112] have been presented.

The evaluation of sensitivity in dry conditions is only partially relevant in biosensing. First of all, the stability of the biosensor to solvents should be verified as the nanostructures must not undergo conformational changes, afterwards, measurements conducted in wet environment can change the overall conditions of the measurement system (as for example light scattered, light transmitted, ...).

With respect to the above mentioned sensors, our NIs FTO-coated slides have a much higher FWHM and lower bulk RI sensitivity, leading to an overall low FOM. This is mainly attributed to the limited-controlled in size NIs fabrication process and to the irregular FTO surface on top of which the gold is evaporated (Figure 4.1).

Nevertheless, the presence of the irregular structure of the FTO layer is fundamental for the stability of the NIs in wet environment. The stability of the nanostructures and their resistance in solvents and in high ionic strength solutions is the most critical feature [161, 88, 156, 96, 130].

The gold NIs employed in this work can withstand high ionic strength solutions for long time and under continuous flow without any passivation or other surface modification needed (see Section 4.2), while keeping unaltered the nanostructures and their sensing properties.



## **7 Real-time direct detection of small molecule binding in saline buffer and in serum**

In this chapter the real-time experiments of biomolecular binding conducted with the T-LSPR setup are presented. In particular, a selected DNA aptamer developed in our laboratory is tested on the NIs FTO-coated to recognize tobramycin, a small molecule drug (467 Da) via a label-free direct assay. The experiments have been conducted, at first, in saline buffer and, then, in undiluted serum.

### **7.1 NIs surface functionalization and samples preparation**

The DNA aptamer specific for tobramycin was previously developed in our lab [47] (5'-TCCGTGTATAGGTCGGGTCTCTTGCCAACTGATTCGTTGAAAAGTATAGCCCCGCAGGG-3') and it was purchased from Sigma (Switzerland) with a 5'-thiolated end.

DNA aptamers were immobilized on gold via sulfur-gold bonds. The NIs FTO glass slides were incubated at room temperature for 16 hours in a PBS buffer solution of DNA aptamer 3  $\mu$ M. After the incubation, the slides were rinsed with ultra-pure water and gently dried with nitrogen.

The surface was then passivated with mercapto-6-hexanol (MCH, Sigma) 1mM in TE 1X for 30 minutes. The prepared slides were then thoroughly rinsed with ultra-pure water and dried by nitrogen stream.

NaCl, PBS, and Fetal Bovine Serum (FBS) were purchased from Sigma (Switzerland), while TE buffer was purchased from Applichem.

Tobramycin samples were prepared in either TE1X buffer or in FBS, in which case they were subsequently filtered with Amicon Ultra Filter (Milli-pore, Switzerland) with 3 kDa cut-off in order to remove most of the protein content.

## **7.2 Handling of solutions by microfluidics**

Microfluidics was built on top of the NIs FTO-glass slide such that two independent channels are covering the areas spotted with the DNA aptamer, the MCH reference spots, a bare gold NIs area and a blank FTO area (Figure 6.3).

For all the experiments, surface conditioning was performed by injecting 1M NaCl regeneration solution followed by running buffer. Solutions with different concentrations of tobramycin were tested. After every injection of tobramycin, TE 1X buffer was injected in order to observe tobramycin dissociation from the surface. Eventually, NaCl was used to remove the remaining tobramycin molecules on the surface, thereby regenerating the surface.

## **7.3 Small molecule analysis with a custom made T-LSPR system and DNA aptamers**

The selected DNA aptamer was tested on a planar gold surface with a standard propagating SPR based system [47], however it was never tried on non-connected patterns and detected by a custom made T-LSPR system. Our T-LSPR setup consists of FTO glass slides covered with non-connected gold NIs.

In order to assess the T-LSPR setup capability to detect surface binding of small drugs, the gold NIs were functionalized with the DNA aptamers for tobramycin. The surface binding of tobramycin is detected by monitoring the refractive index (RI) change in the proximity of the NIs by looking at the plasmon resonance wavelength shift. The binding of biomolecules on surface induces an increase of the local RI that is proportional to the concentration of the captured tobramycin, resulting in a redshift of the plasmon peak. The plasmon peak extraction was performed by a custom made algorithm, which has already been validated in dry conditions in [1].

In order to verify if our setup is able to detect small molecule binding, a tobramycin solution 10  $\mu$ M in TE buffer was injected in the microfluidic channel of the L-TSPR system at 5  $\mu$ l/min. Tobramycin binding to the DNA aptamers was followed in real-time with the peak extraction algorithm (Figure 7.1).

Despite the small molecular weight of tobramycin (467Da), a binding/dissociation curve is clearly detectable, while the control spot (MCH) shows no apparent binding (Figure 7.1, black lines). The signal baseline shows a standard deviation of  $2.2 \times 10^{-5}$ , that allows to clearly distinguish the association and dissociation binding interactions.

Although the plasmonic peak extraction algorithm is able to precisely detect the peak shift in order to follow tobramycin binding/dissociation kinetics, the long elaboration time required (maximum of only 4 frames analyzed per second versus 8 frames per second acquired) is not recommended in real-time measurement experiments. Furthermore, the peak extraction



### 7.3. Small molecule analysis with a custom made T-LSPR system and DNA aptamers

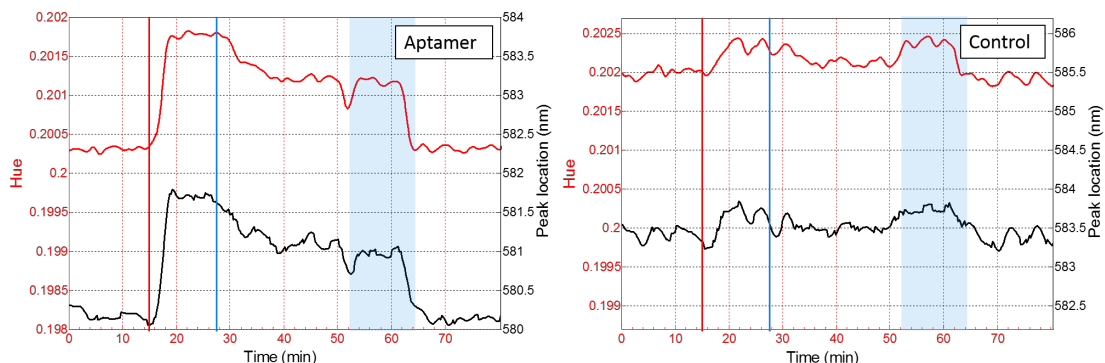


Figure 7.1: 70  $\mu\text{l}$  Tobramycin 10  $\mu\text{M}$  in TE 1X delivered to the DNA aptamers and to a control MCH on surface at 5  $\mu\text{l}/\text{min}$ . Peak location (black line) and hue (red line) are extracted from the same RGB data collected by the CMOS image sensor. The red and blue vertical lines represent the start of the association and dissociation phases, respectively. The light blue area represents the regeneration step thanks to NaCl solution. The control spot does not show any specific response to the injection of Tobramycin indicating that the small molecule drug is recognized and bound to the DNA aptamer only.

algorithm is sensitive to the spatial distribution of light over the CMOS image sensor and therefore requires a reference image as blank FTO-glass slide (with microfluidics channels filled with running buffer) in order to normalize the RGB data.

As an alternative, hue analysis has already been used by the group of Lin [163] to detect plasmonic changes, even though only for bulk RI measurements. The advantage of hue calculation is that it only requires a quick conversion of the RGB values and it is therefore possible to plot it in real-time during the experiment.

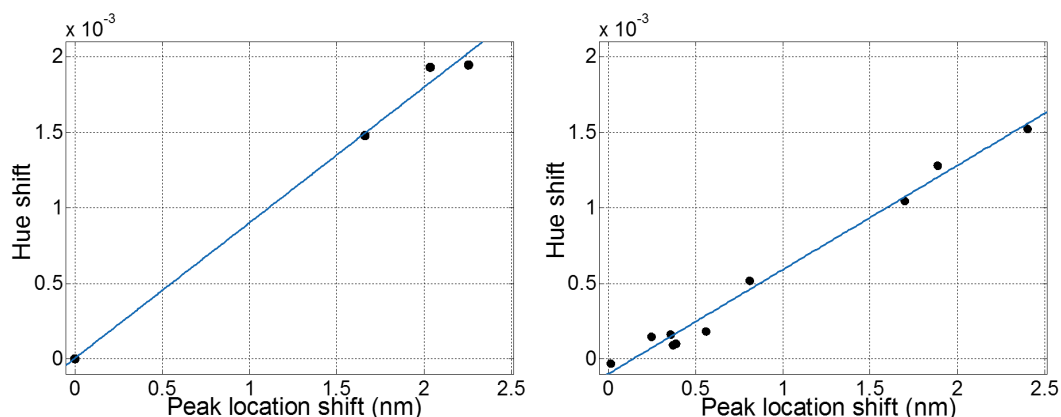


Figure 7.2: Correlation between hue shift and peak location shift in TE buffer (left) and in serum (right).

In order to use the hue analysis for our experiments, we evaluated the correlation between the extracted peak shift and the hue variation. First, hue analysis on the abovementioned raw data

## Chapter 7. Real-time direct detection of small molecule binding in saline buffer and in serum

produces a binding/dissociation curve almost identical to the peak extraction (Figure 7.1, red lines). Second, a linear relationship between hue value and peak location is found for different concentrations of tobramycin and in different matrices (TE buffer and serum) (Figure 7.2).

Therefore, hue variation analysis can be safely used to measure and display in real-time the binding of tobramycin on the surface of our T-LSPR system.

### 7.4 Real-time sensing of tobramycin in TE buffer

In order to confirm the ability of our gold NIs FTO-coated slides to quantify tobramycin binding on the DNA aptamers, we sequentially injected tobramycin at different concentrations (0.5  $\mu\text{M}$ , 1  $\mu\text{M}$ , 2  $\mu\text{M}$ , 5  $\mu\text{M}$  and 10  $\mu\text{M}$ ), TE buffer and regeneration solution (1M NaCl) on the sensing areas array via the microfluidic module at 5  $\mu\text{l}/\text{min}$  (Figure 7.3).

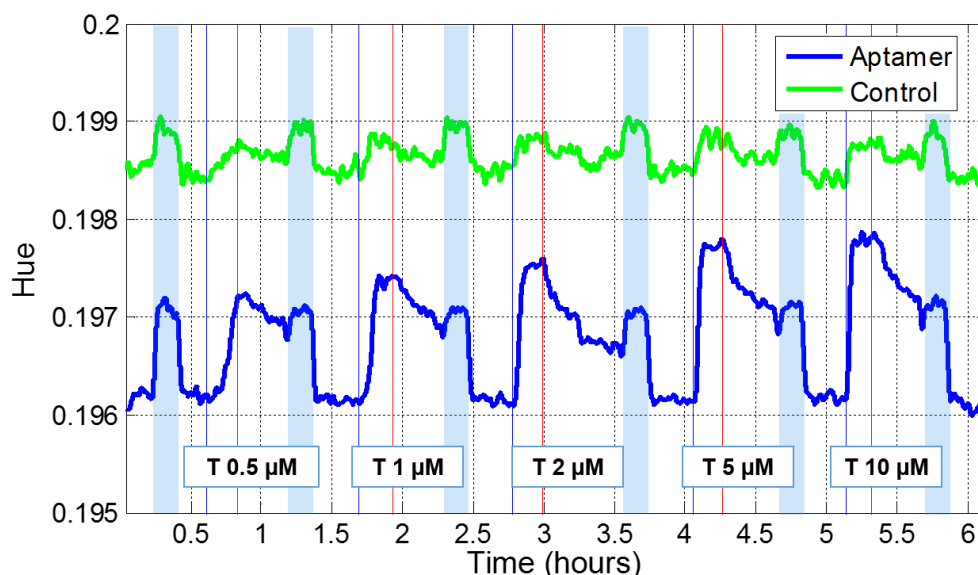


Figure 7.3: Real-time association and dissociation of Tobramycin recognized by the selected DNA aptamer (blue line) attached to the surface. 70  $\mu\text{l}$  of tobramycin in concentrations of 0.5  $\mu\text{M}$ , 1  $\mu\text{M}$ , 2  $\mu\text{M}$ , 5  $\mu\text{M}$  and 10  $\mu\text{M}$  in TE 1X are delivered to the surface at 5  $\mu\text{l}/\text{min}$ . The green line represents the control measurement performed with a layer of MCH on the NIs, which allows to cancel out the signal of the bulk effect and to verify the occurrence of non-specific binding. The blue and red vertical lines indicate the start of the association and dissociation phases, respectively. The light blue areas correspond to the injection of NaCl as a regeneration step.

The hue variation of the DNA aptamer-functionalized NIs (blue line) and of the control-functionalized NIs (MCH, green line) was then followed in real-time. A signal proportional to the amount of bound tobramycin is clearly visible in the aptamer-functionalized spots, while the control spot only shows a slight variation of signal probably due to some non-specific

#### 7.4. Real-time sensing of tobramycin in TE buffer

binding and bulk effect. NaCl drives the baseline to its original value prior to the injection of tobramycin, proving that tobramycin bound to the surface is removed and the DNA aptamers are available for capturing drug molecules during the following cycle.

The importance of regeneration of the surface is fundamental in biosensing assays as it allows of reusing the same surface without the need of re-functionalization of a new NIs FTO-coated glass slide.

Looking at the association and dissociation phases for the different concentrations of tobramycin tested, Figure 7.4 shows that at  $0.5 \mu\text{M}$  of tobramycin the association rate is slow and it is evidently affected from the mass transport effect. At increasing concentrations of tobramycin the association rate becomes faster and the saturation value is reached quicker.

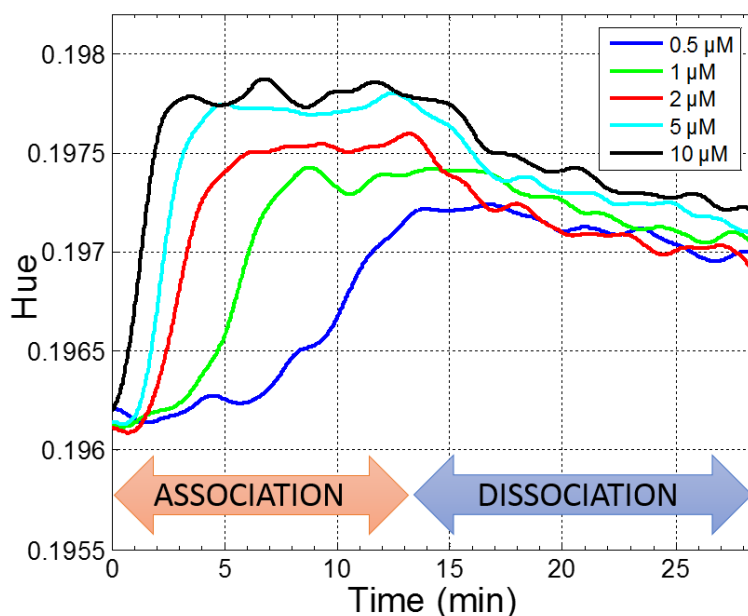


Figure 7.4: Kinetics association and dissociation of tobramycin for the different concentrations tested.

Plotting the association signal values with respect to the concentration of tobramycin injected (Figure 7.5) allows us to fit the points using the Langmuir equation, and hence to calculate the equilibrium binding constant,  $K_D$ .  $K_D$  represents the concentration of tobramycin needed to achieve a half-maximum binding and in our case corresponds to  $0.26 \mu\text{M}$ .

The same analysis performed with a commercial SPR gives a  $K_D$  of  $0.23 \mu\text{M}$  for the same aptamer [47]. The high similarity of the  $K_D$  obtained with our T-LSPR and the commercial SPR indicates that the DNA aptamers are comparably functionalized on the surface, while retaining their ability to recognize tobramycin. Moreover, this clearly shows that the T-LSPR signal is equivalent to the commercial SPR signal for the tested concentrations.

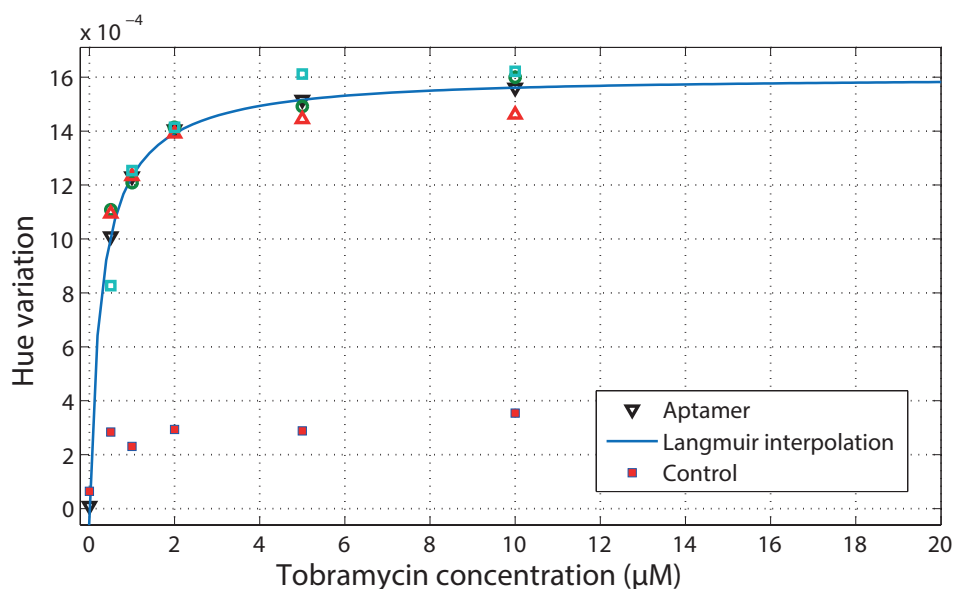


Figure 7.5: Hue variation for different concentrations of tobramycin averaged over 4 independent DNA aptamer spots on the same NIs FTO glass slide (black dots) and for the MCH control spot (red squares).

## 7.5 Real-time sensing of tobramycin in undiluted serum

A POC system intended to analyze patients' blood giving a fast and precise response needs to be able to measure tobramycin with the DNA aptamer in a more complex matrix than TE buffer. Therefore we tested our T-LSPR set up for tobramycin detection in undiluted Fetal Bovine Serum (FBS) as human serum surrogate. Because our system is a label-free and thus prone to be sensitive to unspecific binding, FBS was filtered with a 3KDa cut off membrane in order to remove most of the proteins (7.1).

Several tobramycin concentrations (10 µM, 20 µM, 40 µM, 60 µM and 80 µM) were then spiked in filtered FBS, and injected at 10 µl/min over the sensing areas in order to be measured with our portable T-LSPR setup (Figure 7.6).

Real-time measurements show the tobramycin detection in undiluted FBS in the DNA aptamer spot, while the control spot shows no clear binding (data not shown). The raw data are affected by a decreasing drift of the baseline which is compensated using the regeneration injection signals (NaCl 1M, pure bulk) that is assumed to remain constant during the experiment.

In order to verify non-specific binding of the proteins and substances present in the serum, and to evaluate its bulk effect, tobramycin injections were alternated with FBS without tobramycin. Because of the higher RI of serum with respect to TE buffer, the control injections show a pronounced bulk effect (Figure 7.6). When tobramycin is delivered to the surface (blue vertical lines), the binding association is not evident because it is masked by the serum bulk effect. Nevertheless, the tobramycin captured by the DNA aptamer is visible and measurable from the

## 7.5. Real-time sensing of tobramycin in undiluted serum

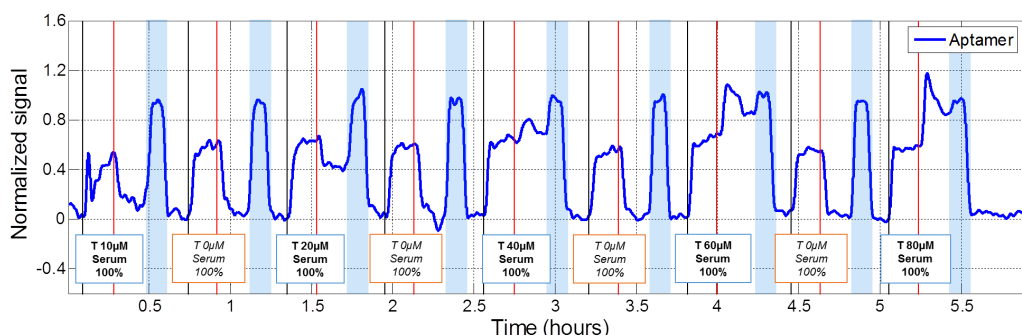


Figure 7.6: Real-time association and dissociation of tobramycin recognized by the selected DNA aptamer attached to the surface. 70  $\mu\text{l}$  of tobramycin in the concentrations of 10  $\mu\text{M}$ , 20  $\mu\text{M}$ , 40  $\mu\text{M}$ , 60  $\mu\text{M}$  and 80  $\mu\text{M}$  in undiluted serum, alternated with control injections serum without tobramycin, are delivered to the surface at 10  $\mu\text{l}/\text{min}$ . The black and red vertical lines indicate the start of the association and dissociation phases, respectively. The light blue areas correspond to the injection of NaCl as a regeneration step.

start of the dissociation phase (red vertical lines), when TE buffer is injected in the channels removing the serum bulk effect. The tobramycin signal exhibit a sharp increase to a value proportional to the amount of Tobramycin injected, from which the dissociation phase begins.

Why is the serum totally masking the binding of tobramycin to the DNA aptamers? It does not seem to be a matter of noise, as tobramycin injection at 80  $\mu\text{M}$  gives a smaller signal than its subsequent dissociation. We wondered if the serum could absorb light in the wavelengths needed for plasmon generation. FBS absorbance spectrum measured with a commercial spectrophotometer (Nanodrop 2000c Thermo Scientific) only shows peaks at 200 nm and 300 nm (data not shown), which is out of the range of the NIs plasmon and therefore cannot be the cause of the masking effect.

Another possible explanation could come from the literature. The group of Vörös [164] shows the effect of charges on plasmonics combined with electrochemistry detection. We wondered what the electrical behavior of the small particles in serum is. A paper from the group of Szoka [165] reports the electrical properties of molecules in solutions and how the presence of serum alters their charge. It is possible that proteins, hormones and other molecules present in serum have a strong impact on the dielectric environment surrounding the NIs, causing a damping of the plasmon and reducing its penetration depth into the dielectric. However, this hypothesis needs further investigation.

For the DNA aptamers spots, a linear trend with a sensitivity of 0.0123 (hue variation per  $\mu\text{M}$ ) is observed for the increasing concentrations of Tobramycin (Figure 7.7). In order to evaluate the detection resolution for tobramycin in undiluted serum, we calculated the standard deviation of the measured signal among 4 different aptamer spots for all the concentrations. The signal corresponding to twice the average standard deviation indicates that the theoretical minimum resolvable concentration of tobramycin is 3.4  $\mu\text{M}$ .

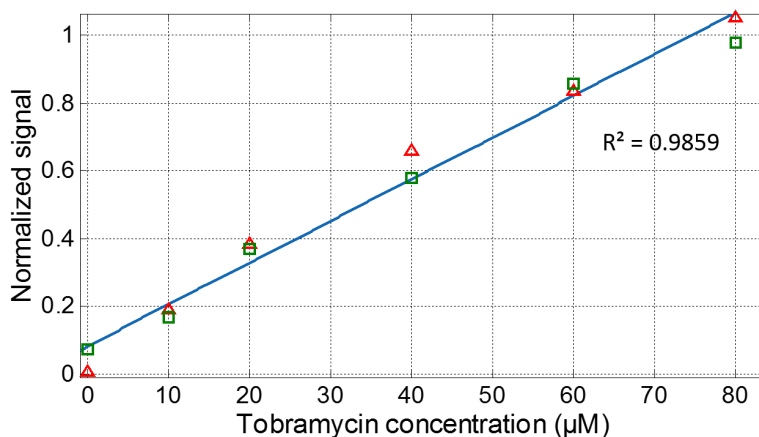


Figure 7.7: Hue variation for different concentrations of tobramycin averaged over 2 independent DNA Aptamer spots on the same NIs FTO glass slide normalized over NaCl injections.

Nevertheless, the binding/dissociation curve at the lowest concentration of tobramycin shows a lower signal to noise ratio which, with the present system configuration, probably will hinder the detection at lower concentrations of tobramycin.

Currently measured concentrations of tobramycin in patients' blood range between 1  $\mu\text{M}$  and 80  $\mu\text{M}$  (Prof. Thierry Buclin, University Hospital of Lausanne, personal communication), which is less than one order of magnitude below our minimum detectable concentration.

In fact, one big component of the noise comes from the bit noise of CMOS image sensor, that can be reduced with a more stable power supply (that is, battery). Additionally, we can increase the overall signal by increasing the light source intensity, therefore further increasing the signal to noise ratio.

On the other hand, the capability of our T-LSPR sensor to resolve small RI changes is mainly limited by the NIs FTO-glass sensor. More regular structures and patterns have been reported to increase the sensitivity (see Section 3.2). In fact, the irregularity in size and pattern of the NIs, together with the irregular shape of the FTO layer on glass, contribute to increase the surface roughness and broaden the plasmon, thus reducing its sensitivity. Nevertheless, the stability over time of these NIs and their resistance to high ionic strength solutions, critical in biosensing [161, 117], allows to perform long time measurements and surface regeneration.

## 8 Conclusions and future perspectives

This thesis is a multidisciplinary work that combines the technical design and implementation of a portable label-free detection system with the use of DNA aptamers to recognize small molecules in undiluted serum.

The attention on T-LSPR was motivated by the possibility to scale down the detection system and to employ low-cost available components. The system is T-LSPR-based and made of off-the-shelf components, LEDs, and CMOS image sensor, which make it compact and suitable as a POC.

Because of the high sensitivity of the CMOS sensor in the visible range, a suitable biosensor exhibiting LSPR in the visible spectrum was chosen. The non-connected patterns are extremely flexible in that the plasmon resonance can be tuned by modifying the material, size, and shape of the nanostructures. The two major constraints in the choice of the gold NIs were the material and the stability of the nanostructures in solvents. Gold represents the most-used material in biosensing, as it is inert and easy to functionalize via thiols. The employed NIs on FTO-covered glass showed very high stability in solvents and in high ionic strength solutions and proved to be suitable for surface modification and in-flow experiments.

The goal was to probe the performance of the detection principle with low-molecular-mass molecules; for this, a direct assay, label-free configuration was chosen. In addition, such conditions required almost no manipulation of the sample. For assay performed in TE buffer, concentrations of tobramycin down to  $0.5 \mu\text{M}$  were measured and the real-time kinetics of the binding was extracted. The calculated  $K_D$  matched the results obtained with a high-end SPR system.

Motivated by the results obtained in saline buffer, the recognition of tobramycin by the DNA aptamer was tested in undiluted serum. The presence of a complex matrix is known to be the cause of several interfering signals, such as non-specific binding on the sensor surface, concentration-dependent effects, and bulk effects. Particularly in label-free assays, the serum would severely diminish the performance in terms of limit of detection. However, the detection

## Chapter 8. Conclusions and future perspectives

---

of 10  $\mu$ M concentration of tobramycin was possible with our portable T-LSPR setup and, more importantly, the sensing nanopattern demonstrated excellent stability and regenerability in such a matrix.

Although the serum masks the binding association of tobramycin, the information of the captured tobramycin is visible and measurable from the start of the dissociation phase and leads to a linear calibration curve. The complete masking of the association phase by the presence of serum is not reported elsewhere, and the physical effect responsible of the hindering is still subject to discussion. In fact, the same experiment on the high-end SPR system could not be performed, as the output signal was not readable. Whether this is a matter of detection system or if the type of biosensor (NIs vs planar gold layer) remains to be investigated, as 20% diluted serum was not yet detectable in the standard SPR system.

In the portable T-LSPR setup, tobramycin detection in serum was possible because of the NIs FTO-coated glass slides that make it possible to regenerate their surface and allow repeated serum injection/NaCl regeneration cycles in continuous flow (up to 20 hours continuous monitoring tested) without losing their sensing capabilities or degrading the recognition properties of the DNA aptamer bound to their surface.

Because of the discrete nature of the exciting light and detector, a custom-made algorithm for the reconstruction of the plasmon resonance and the identification of its peak location has been developed. The setup and the algorithm were first validated in dry conditions on single-stranded DNA-modified NIs. However, the algorithm applied to the real-time monitoring of the plasmonic shift of binding events was too slow. Therefore, hue was studied as a substitutive parameter and improved the speed of elaboration by a factor of four.

Currently, the major limitation in the measurements is represented by the low signal-to-noise ratio of the CMOS image sensor output signal, which leads to an overall noisy hue. One major component of the noise comes from the bit noise of the CMOS image sensor, which can be reduced with a more stable power supply (that is, a battery). Additionally, we can increase the overall signal by increasing the light source intensity, thereby further increasing the signal-to-noise ratio.

On the other hand, the capability of our T-LSPR sensor to resolve small RI changes is mainly limited by the NIs FTO-glass sensor. More regular structures and patterns can increase the sensitivity, as the irregular size and pattern of the NIs, together with the irregular shape of the FTO layer on glass, help increase the surface roughness and broaden the plasmon, thereby reducing the overall sensitivity. Nevertheless, the possibility of exploring new more sensitive structures is not excluded, as long as they guarantee high stability to solvents and a simple and cost-effective fabrication process, with the potential for one-step surface functionalization.

POCs are rapidly growing in popularity because of the numerous advantages they offer compared to conventional systems, such as the possibility for personalized medicine and in situ diagnostics. The presented T-LSPR system still requires further optimization in order to fully



---

work as a POC. At present, the delivery of reagents to surface is controlled by syringe pumps placed externally to the case of the POC. The possibility of including small automatic piezoelectric pumps inside the POC has been considered, although the flow-rate employed for the presented measurements,  $10 \mu\text{l}/\text{min}$ , is too low to be controlled with the commercial piezoelectric pumps explored so far, as the fluid is pushed in gradual steps instead of continuous flow.

In addition, the possibility of increasing the flow-rate for delivery of reagents to surface is also considered. From one side, the mass transport effect visible at low concentrations could be improved, but on the other side the dead volume in the tubing system will lead to a higher consumption of reagents, as experimented in a preliminary test not shown here.

The NIs FTO-coated glass slide can host multiple spots of the DNA aptamer, allowing for parallel monitoring of the different sites during the same measurement. The maximum throughput reachable in the sensor was not exploited in the present study; instead, the focus was on the real-time observation and quantification of tobramycin in serum.

Implementation of multiple arrays detection, together with the compact dimensions of the system, allowed by the usage of low-power components, makes our device fitting the requirements for a POC. In conclusion, this is the first work reporting on a portable T-LSPR system that is able to measure small molecules in undiluted serum via label-free direct assay. We are currently approximately one order of magnitude above the minimum concentration, but it is not too optimistic to envision that our portable T-LSPR system will soon be able to measure through the whole clinical range.



# Bibliography

- [1] Cappi, G., Accastelli, E., Cantale, V., Rampi, M. A., Benini, L., and Guiducci, C.: Peak shift measurement of localized surface plasmon resonance by a portable electronic system. *Sensors and Actuators B: Chemical* 176, 225–231 (2013)
- [2] Ahmed, M. U., Saaem, I., Wu, P. C., and Brown, A. S.: Personalized diagnostics and biosensors: a review of the biology and technology needed for personalized medicine. *Critical Reviews in Biotechnology* 0, 1–17
- [3] Schneider, T., Wirth, J., Garwe, F., Csaki, A., and Fritzsche, W.: Plasmonic nanoparticles for bioanalytics and therapy at the limit. vol. 8311 of *Proceedings of SPIE*, 83110F. Optical Society of America
- [4] Yager, P., Domingo, G. J., and Gerdes, J.: Point-of-Care Diagnostics for Global Health. *Annual Review of Biomedical Engineering* 10, 107–144 (2008)
- [5] Brennan, D., Justice, J., Corbett, B., McCarthy, T., and Galvin, P.: Emerging optofluidic technologies for point-of-care genetic analysis systems: a review. *Analytical and Bioanalytical Chemistry* 395, 621–636 (2009)
- [6] Gubala, V., Harris, L. F., Ricco, A. J., Tan, M. X., and Williams, D. E.: Point of Care Diagnostics: Status and Future. *Analytical Chemistry* 84, 487–515 (2012)
- [7] Neuzil, P. and Reboud, J.: Palm-Sized Biodetection System Based on Localized Surface Plasmon Resonance. *Analytical Chemistry* 80, 6100–6103 (2008)
- [8] Xie, L., Yan, X., and Du, Y.: An aptamer based wall-less LSPR array chip for label-free and high throughput detection of biomolecules. *Biosensors and Bioelectronics* 53, 58–64 (2014)
- [9] Stevens, R. C., Soelberg, S. D., Near, S., and Furlong, C. E.: Detection of Cortisol in Saliva with a Flow-Filtered, Portable Surface Plasmon Resonance Biosensor System. *Analytical Chemistry* 80, 6747–6751 (2008)
- [10] Zheng, D., Zou, R., and Lou, X.: Label-Free Fluorescent Detection of Ions, Proteins, and Small Molecules Using Structure-Switching Aptamers, SYBR Gold, and Exonuclease I. *Analytical Chemistry* 84, 3554–3560 (2012)

## Bibliography

---

- [11] Baker, B. R., Lai, R. Y., Wood, M. S., Doctor, E. H., Heeger, A. J., and Plaxco, K. W.: An Electronic, Aptamer-Based Small-Molecule Sensor for the Rapid, Label-Free Detection of Cocaine in Adulterated Samples and Biological Fluids. *J Am Chem Soc* 128, 3138–3139 (2006)
- [12] Zayats, M., Huang, Y., Gill, R., Ma, C.-a., and Willner, I.: Label-Free and Reagentless Aptamer-Based Sensors for Small Molecules. *J Am Chem Soc* 128, 13666–13667 (2006)
- [13] Ferapontova, E. E., Olsen, E. M., and Gothelf, K. V.: An RNA Aptamer-Based Electrochemical Biosensor for Detection of Theophylline in Serum. *J Am Chem Soc* 130, 4256–4258 (2008)
- [14] Xia, F., Zuo, X., Yang, R., Xiao, Y., Kang, D., Vallee-Balisle, A., Gong, X., Yuen, J. D., Hsu, B. B. Y., Heeger, A. J., and Plaxco, K. W.: Colorimetric detection of DNA, small molecules, proteins, and ions using unmodified gold nanoparticles and conjugated polyelectrolytes. *Proceedings of the National Academy of Sciences* 107, 10837–10841 (2010)
- [15] Zhu, H., Dale, P. S., Caldwell, C. W., and Fan, X.: Rapid and Label-Free Detection of Breast Cancer Biomarker CA15-3 in Clinical Human Serum Samples with Optofluidic Ring Resonator Sensors. *Analytical Chemistry* 81, 9858–9865 (2009)
- [16] Washburn, A. L., Gunn, L. C., and Bailey, R. C.: Label-Free Quantitation of a Cancer Biomarker in Complex Media Using Silicon Photonic Microring Resonators. *Analytical Chemistry* 81, 9499–9506 (2009)
- [17] von Muhlen, M. G., Brault, N. D., Knudsen, S. M., Jiang, S., and Manalis, S. R.: Label-Free Biomarker Sensing in Undiluted Serum with Suspended Microchannel Resonators. *Analytical Chemistry* 82, 1905–1910 (2010)
- [18] Huang, Y.-W., Wu, C.-S., Chuang, C.-K., Pang, S.-T., Pan, T.-M., Yang, Y.-S., and Ko, F.-H.: Real-Time and Label-Free Detection of the Prostate-Specific Antigen in Human Serum by a Polycrystalline Silicon Nanowire Field-Effect Transistor Biosensor. *Analytical Chemistry* 85, 7912–7918 (2013)
- [19] Luo, X., Xu, Q., James, T., and Davis, J. J.: Redox and Label-Free Array Detection of Protein Markers in Human Serum. *Analytical Chemistry* 86, 5553–5558 (2014)
- [20] Lai, R. Y., Plaxco, K. W., and Heeger, A. J.: Aptamer-Based Electrochemical Detection of Picomolar Platelet-Derived Growth Factor Directly in Blood Serum. *Analytical Chemistry* 79, 229–233 (2006)
- [21] Xiao, Y., Qu, X., Plaxco, K. W., and Heeger, A. J.: Label-Free Electrochemical Detection of DNA in Blood Serum via Target-Induced Resolution of an Electrode-Bound DNA Pseudoknot. *J Am Chem Soc* 129, 11896–11897 (2007)
- [22] Chin, C. D., Linder, V., and Sia, S. K.: Commercialization of microfluidic point-of-care diagnostic devices. *Lab on a Chip* 12, 2118–2134 (2012)

- [23] Chin, C. D., Laksanasopin, T., Cheung, Y. K., Steinmiller, D., Linder, V., Parsa, H., Wang, J., Moore, H., Rouse, R., Umvilighozo, G., Karita, E., Mwambarangwe, L., Braunstein, S. L., van de Wijgert, J., Sahabo, R., Justman, J. E., El-Sadr, W., and Sia, S. K.: Microfluidics-based diagnostics of infectious diseases in the developing world. *Nat Med* 17, 1015–1019 (2011). 10.1038/nm.2408
- [24] Breslauer, D. N., Maamari, R. N., Switz, N. A., Lam, W. A., and Fletcher, D. A.: Mobile Phone Based Clinical Microscopy for Global Health Applications. *PLoS One* 4, e6320 (2009)
- [25] Netra: <http://eyenetra.com/product-netrag.html>
- [26] Linder, V.: Microfluidics at the crossroad with point-of-care diagnostics. *Analyst* 132, 1186–1192 (2007)
- [27] Peeling, R. W. and Mabey, D.: Point-of-care tests for diagnosing infections in the developing world. *Clinical Microbiology and Infection* 16, 1062–1069 (2010)
- [28] Lu, Y., Shi, W., Qin, J., and Lin, B.: Low cost, portable detection of gold nanoparticle-labeled microfluidic immunoassay with camera cell phone. *Electrophoresis* 30, 579–582 (2009)
- [29] Long, K., Gallegos, D., Yu, H., Clark, P., Lin, Y., George, S., Nath, P., and Cunningham, B. T.: Label-Free Biodetection using a Smartphone. *Lab on a Chip* (2013)
- [30] Martinez, A. W., Phillips, S. T., Carrilho, E., Thomas, S. W., Sindi, H., and Whitesides, G. M.: Simple Telemedicine for Developing Regions: Camera Phones and Paper-Based Microfluidic Devices for Real-Time, Off-Site Diagnosis. *Analytical Chemistry* 80, 3699–3707 (2008)
- [31] Homola, J.: *Surface Plasmon Resonance Based Sensors*, vol. 4 of *Springer Series on Chemical Sensors and Biosensors* (2006)
- [32] Goncalves, M. S. T.: Fluorescent Labeling of Biomolecules with Organic Probes. *Chemical Reviews* 109, 190–212 (2009)
- [33] Dorfman, A., Kumar, N., and Hahn, J.-i.: Highly Sensitive Biomolecular Fluorescence Detection Using Nanoscale ZnO Platforms. *Langmuir* 22, 4890–4895 (2006)
- [34] Lian, W., Litherland, S. A., Badrane, H., Tan, W., Wu, D., Baker, H. V., Gulig, P. A., Lim, D. V., and Jin, S.: Ultrasensitive detection of biomolecules with fluorescent dye-doped nanoparticles. *Analytical Biochemistry* 334, 135 – 144 (2004)
- [35] Chen, Y., Munechika, K., and Ginger, D. S.: Dependence of Fluorescence Intensity on the Spectral Overlap between Fluorophores and Plasmon Resonant Single Silver Nanoparticles. *Nano Letters* 7, 690–696 (2007)

## Bibliography

---

- [36] Touahir, L., Galopin, E., Boukherroub, R., Gouget-Laemmel, A. C., Chazalviel, J.-N., Ozanam, E., and Szunerits, S.: Localized surface plasmon-enhanced fluorescence spectroscopy for highly-sensitive real-time detection of DNA hybridization. *Biosensors and Bioelectronics* 25, 2579 – 2585 (2010)
- [37] Thompson, R. E., Larson, D. R., and Webb, W. W.: Precise Nanometer Localization Analysis for Individual Fluorescent Probes. *Biophysical journal* 82, 2775–2783 (2002)
- [38] Gartia, M. R., Hsiao, A., Sivaguru, M., Chen, Y., and Liu, G. L.: Enhanced 3D fluorescence live cell imaging on nanoplasmonic substrate. *Nanotechnology* 22, 365203 (2011)
- [39] Myers, F. B. and Lee, L. P.: Innovations in optical microfluidic technologies for point-of-care diagnostics. *Lab on a Chip* 8, 2015–2031 (2008)
- [40] Abdiche, Y., Malashock, D., Pinkerton, A., and Pons, J.: Determining kinetics and affinities of protein interactions using a parallel real-time label-free biosensor, the Octet. *Analytical Biochemistry* 377, 209–217 (2008)
- [41] Xiao, Y., Lubin, A. A., Heeger, A. J., and Plaxco, K. W.: Label-Free Electronic Detection of Thrombin in Blood Serum by Using an Aptamer-Based Sensor. *Angewandte Chemie International Edition* 44, 5456–5459 (2005)
- [42] Tombelli, S. and Mascini, M.: Aptamers as molecular tools for bioanalytical methods. *Curr Opin Mol Ther* (2009)
- [43] Tombelli, S. and Mascini, M.: Aptamers Biosensors for Pharmaceutical Compounds. *Combinatorial Chemistry & High Throughput Screening* 13, pp. 641–649(9) (2010)
- [44] Jayasena, S. D.: Aptamers: An Emerging Class of Molecules That Rival Antibodies in Diagnostics. *Clinical Chemistry* 45, 1628–1650 (1999)
- [45] Mascini, M., Palchetti, I., and Tombelli, S.: Nucleic Acid and Peptide Aptamers: Fundamentals and Bioanalytical Aspects. *Angewandte Chemie International Edition* 51, 1316–1332 (2012)
- [46] PerezRuiz, E., Kemper, M., Spasic, D., Gils, A., van Ijzendoorn, L. J., Lammertyn, J., and Prins, M. W. J.: Probing the Force-Induced Dissociation of Aptamer-Protein Complexes. *Analytical Chemistry* 86, 3084–3091 (2014)
- [47] Spiga, F. M., Maietta, P., Valencia, A., and Guiducci, C.: Opening the box of DNA aptamers for small drugs: a novel capture SELEX coupled with Surface Plasmon Resonance and High Throughput Sequencing. *Submitted to Nucleic Acid Research* (2014)
- [48] Cappi, G., Moncada, Y., Spiga, F. M., Ferretti, A., Beyeler, M., Bianchessi, M., and Guiducci, C.: Label-free detection of Tobramycin in serum by Transmission-LSPR. *In preparation* (2014)

- [49] Liedberg, B., Nylander, C., and Lunstrom, I.: Surface plasmon resonance for gas detection and biosensing. *Sensors and Actuators* 4, 299–304 (1983)
- [50] Rich, R. L. and Myszka, D. G.: Grading the commercial optical biosensor literature Class of 2008: The Mighty Binders. *Journal of Molecular Recognition* 23, 1–64 (2010)
- [51] Piliarik, M. and Homola, J. .: Surface plasmon resonance (SPR) sensors: approaching their limits? *Optics Express* 17, 16505–16517 (2009)
- [52] Abbas, A., Linman, M. J., and Cheng, Q.: New trends in instrumental design for surface plasmon resonance-based biosensors. *Biosensors and Bioelectronics* 26, 1815–1824 (2011)
- [53] Chiavaioli, F., Biswas, P., Trono, C., Bandyopadhyay, S., Giannetti, A., Tombelli, S., Basumallick, N., Dasgupta, K., and Baldini, F.: Towards sensitive label-free immunosensing by means of turn-around point long period fiber gratings. *Biosensors and Bioelectronics* 60, 305 – 310 (2014)
- [54] Beusink, J. B., Lokate, A. M., Besselink, G. A., Pruijn, G. J., and Schasfoort, R. B.: Angle-scanning SPR imaging for detection of biomolecular interactions on microarrays. *Biosensors and Bioelectronics* 23, 839 – 844 (2008)
- [55] Homola, J., Vaisocherova, H., Dostalek, J., and Piliarik, M.: Multi-analyte surface plasmon resonance biosensing. *Methods* 37, 26–36 (2005)
- [56] Hoa, X. D., Kirk, A. G., and Tabrizian, M.: Towards integrated and sensitive surface plasmon resonance biosensors: A review of recent progress. *Biosensors and Bioelectronics* 23, 151–160 (2007)
- [57] Retra, K., Irth, H., and van Muijlwijk-Koezen, J. E.: Surface Plasmon Resonance biosensor analysis as a useful tool in FBDD. *Drug Discovery Today: Technologies* 7, e181–e187 (2010)
- [58] Seattle Sensor Systems. <http://seattlesensors.com/products.html>
- [59] Chinowsky, T. M., Soelberg, S. D., Baker, P., Swanson, N. R., Kauffman, P., Mactutis, A., Grow, M. S., Atmar, R., Yee, S. S., and Furlong, C. E.: Portable 24-analyte surface plasmon resonance instruments for rapid, versatile biodetection. *Biosensors and Bioelectronics* 22, 2268–2275 (2007)
- [60] Reichert Technologies. <http://www.reichertspr.com/spr-systems/sr7000dc/>
- [61] Shankaran, D. R., Gobi, K. V., and Miura, N.: Recent advancements in surface plasmon resonance immunosensors for detection of small molecules of biomedical, food and environmental interest. *Sensors and Actuators B: Chemical* 121, 158–177 (2007)

## Bibliography

---

- [62] Rebe Raz, S., Bremer, M. G. E. G., Giesbers, M., and Norde, W.: Development of a biosensor microarray towards food screening, using imaging surface plasmon resonance. *Biosensors and Bioelectronics* 24, 552–557 (2008)
- [63] Smith, E. A., Thomas, W. D., Kiessling, L. L., and Corn, R. M.: Surface plasmon resonance imaging studies of protein-carbohydrate interactions. *J Am Chem Soc* 125, 6140–8 (2003). Smith, Emily A Thomas, William D Kiessling, Laura L Corn, Robert M GM49975/GM/NIGMS NIH HHS/ GM59622/GM/NIGMS NIH HHS/ J Am Chem Soc. 2003 May 21;125(20):6140-8.
- [64] Lee, H. J., Goodrich, T. T., and Corn, R. M.: SPR Imaging Measurements of 1-D and 2-D DNA Microarrays Created from Microfluidic Channels on Gold Thin Films. *Analytical Chemistry* 73, 5525–5531 (2001)
- [65] Shumaker-Parry, J. S., Aebersold, R., and Campbell, C. T.: Parallel, Quantitative Measurement of Protein Binding to a 120-Element Double-Stranded DNA Array in Real Time Using Surface Plasmon Resonance Microscopy. *Analytical Chemistry* 76, 2071–2082 (2004)
- [66] Steiner, G.: Surface plasmon resonance imaging. *Analytical and Bioanalytical Chemistry* 379, 328–331 (2004)
- [67] Yao, J., Stewart, M., Maria, J., Lee, T.-W., Gray, S., Rogers, J., and Nuzzo, R.: Seeing Molecules by Eye: Surface Plasmon Resonance Imaging at Visible Wavelengths with High Spatial Resolution and Submonolayer Sensitivity. *Angewandte Chemie International Edition* 47, 5013–5017 (2008)
- [68] Boozer, C., Kim, G., Cong, S., Guan, H., and Londergan, T.: Looking towards label-free biomolecular interaction analysis in a high-throughput format: a review of new surface plasmon resonance technologies. *Current Opinion in Biotechnology* 17, 400 – 405 (2006). Protein technologies
- [69] Raphael, M. P., Christodoulides, J. A., Mulvaney, S. P., Miller, M. M., Long, J. P., and Byers, J. M.: A New Methodology for Quantitative LSPR Biosensing and Imaging. *Analytical Chemistry* 84, 1367–1373 (2012)
- [70] Lee, S. H., Lindquist, N. C., Wittenberg, N. J., Jordan, L. R., and Oh, S.-H.: Real-time full-spectral imaging and affinity measurements from 50 microfluidic channels using nanohole surface plasmon resonance. *Lab on a Chip* 12, 3882–3890 (2012)
- [71] Horiba: HORIBA scientific. <http://www.horiba.com/scientific/products/surface-plasmon-resonance-imaging-spri/spri-technology/the-principle-of-spri/>
- [72] IBIS Technologies. <http://www.ibis-spr.nl/>
- [73] Chinowsky, T., Quinn, J., Bartholomew, D., Kaiser, R., and Elkind, J.: Performance of the Spreeta 2000 integrated surface plasmon resonance affinity sensor. *Sensors and Actuators B: Chemical* 91, 266 – 274 (2003)



- [74] SPRmicro K-MAC. <http://www.kmac.to/eng/products.php?cid=sprmicro>
- [75] Capitan-Vallvey, L. F. and Palma, A. J.: Recent developments in handheld and portable optosensing A review. *Analytica Chimica Acta* 696, 27 – 46 (2011)
- [76] Piliarik, M., Parova, L., and Homola, J.: High-throughput SPR sensor for food safety. *Biosensors and Bioelectronics* 24, 1399–1404 (2009)
- [77] Fernandez, E, Hegnerovaj, K., Piliarik, M., Sanchez-Baeza, F, Homola, J., and Marco, M.-P.: A label-free and portable multichannel surface plasmon resonance immunosensor for on site analysis of antibiotics in milk samples. *Biosensors & Bioelectronics* 26, 1231–1238 (2010)
- [78] Sipova, H., Zhang, S., Dudley, A. M., Galas, D., Wang, K., and Homola, J.: Surface Plasmon Resonance Biosensor for Rapid Label-Free Detection of Microribonucleic Acid at Subfemtomole Level. *Analytical Chemistry* 82, 10110–10115 (2010)
- [79] Duval, D. and Lechuga, L. M.: Breakthroughs in photonics 2012: 2012 breakthroughs in lab-on-a-chip and optical biosensors. *IEEE Photonics Journal* 5 (2013). Export Date: 26 June 2013 Source: Scopus Art. No.: 6472721
- [80] Estevez, M. C., Otte, M. A., Sepulveda, B., and Lechuga, L. M.: Trends and challenges of refractometric nanoplasmonic biosensors: A review. *Anal Chim Acta* 806, 55–73 (2014)
- [81] Endo, T., Kerman, K., Nagatani, N., Takamura, Y., and Tamiya, E.: Label-Free Detection of Peptide Nucleic Acid DNA Hybridization Using Localized Surface Plasmon Resonance Based Optical Biosensor. *Analytical Chemistry* 77, 6976–6984 (2005)
- [82] Hong, Y., Huh, Y.-M., Yoon, D. S., and Yang, J.: Nanobiosensors Based on Localized Surface Plasmon Resonance for Biomarker Detection. *Journal of Nanomaterials* 2012, 13 (2012)
- [83] Larsson, E. M., Alegret, J., Kall, M., and Sutherland, D. S.: Sensing Characteristics of NIR Localized Surface Plasmon Resonances in Gold Nanorings for Application as Ultrasensitive Biosensors. *Nano Letters* 7, 1256–1263 (2007)
- [84] Breault-Turcot, J. and Masson, J.-F.: Nanostructured substrates for portable and miniature SPR biosensors. *Analytical and Bioanalytical Chemistry* 403, 1477–1484 (2012)
- [85] Otte, M. A., Sepulveda, B., Ni, W., Juste, J. P., Liz-Marzan, L. M., and Lechuga, L. M.: Identification of the Optimal Spectral Region for Plasmonic and Nanoplasmonic Sensing. *ACS Nano* 4, 349–357 (2009)
- [86] Svedendahl, M., Chen, S., Dmitriev, A., and Kaell, M.: Refractometric Sensing Using Propagating versus Localized Surface Plasmons: A Direct Comparison. *Nano Letters* 9, 4428–4433 (2009)

## Bibliography

---

- [87] Haynes, C. L. and Van Duyne, R. P.: Nanosphere Lithography A Versatile Nanofabrication Tool for Studies of Size-Dependent Nanoparticle Optics. *The Journal of Physical Chemistry B* 105, 5599–5611 (2001)
- [88] Sherry, L. J., Jin, R., Mirkin, C. A., Schatz, G. C., and Van Duyne, R. P.: Localized Surface Plasmon Resonance Spectroscopy of Single Silver Triangular Nanoprisms. *Nano Letters* 6, 2060–2065 (2006)
- [89] Kelly, K. L., Coronado, E., Zhao, L. L., and Schatz, G. C.: The Optical Properties of Metal Nanoparticles The Influence of Size, Shape, and Dielectric Environment. *The Journal of Physical Chemistry B* 107, 668–677 (2002)
- [90] Bolduc, O. R. and Masson, J.-F.: Advances in Surface Plasmon Resonance Sensing with Nanoparticles and Thin Films: Nanomaterials, Surface Chemistry, and Hybrid Plasmonic Techniques. *Analytical Chemistry* 83, 8057–8062 (2011)
- [91] Cao, C., Zhang, J., Wen, X., Dodson, S. L., Dao, N. T., Wong, L. M., Wang, S., Li, S., Phan, A. T., and Xiong, Q.: Metamaterials-Based Label-Free Nanosensor for Conformation and Affinity Biosensing. *ACS Nano* 7, 7583–7591 (2013)
- [92] Liu, Y. and Zhang, X.: Metamaterials: a new frontier of science and technology. *Chem Soc Rev* 40, 2494–2507 (2011)
- [93] Henzie, J., Lee, M. H., and Odom, T. W.: Multiscale patterning of plasmonic metamaterials. *Nat Nano* 2, 549–554 (2007). 10.1038/nnano.2007.252
- [94] Trekker, J., Leten, C., Struys, T., Lazenka, V. V., Argibay, B., Micholt, L., Lambrichts, I., Van Roy, W., Lagae, L., and Himmelreich, U.: Sensitive in vivo cell detection using size-optimized superparamagnetic nanoparticles. *Biomaterials* 35, 1627–1635 (2014)
- [95] Doron-Mor, I., Cohen, H., Barkay, Z., Shanzer, A., Vaskevich, A., and Rubinstein, I.: Sensitivity of Transmission Surface Plasmon Resonance (T-SPR) Spectroscopy: Self-Assembled Multilayers on Evaporated Gold Island Films. *Chemistry European Journal* 11, 5555–5562 (2005)
- [96] Lahav, M., Vaskevich, A., and Rubinstein, I.: Biological Sensing Using Transmission Surface Plasmon Resonance Spectroscopy. *Langmuir* 20, 7365–7367 (2004)
- [97] Ruach-Nir, I., Bendikov, T. A., Doron-Mor, I., Barkay, Z., Vaskevich, A., and Rubinstein, I.: Silica-Stabilized Gold Island Films for Transmission Localized Surface Plasmon Sensing. *J Am Chem Soc* 129, 84–92 (2006)
- [98] Hutter, E. and Pileni, M.-P.: Detection of DNA Hybridization by Gold Nanoparticle Enhanced Transmission Surface Plasmon Resonance Spectroscopy. *The Journal of Physical Chemistry B* 107, 6497–6499 (2003)

- [99] Lodewijks, K., Ryken, J., Van Roy, W., Borghs, G., Lagae, L., and Van Dorpe, P.: Tuning the Fano Resonance Between Localized and Propagating Surface Plasmon Resonances for Refractive Index Sensing Applications. *Plasmonics* 8, 1379–1385 (2013)
- [100] Kegel, L. L., Boyne, D., and Booksh, K. S.: Sensing with Prism-Based Near-Infrared Surface Plasmon Resonance Spectroscopy on Nanohole Array Platforms. *Analytical Chemistry* (2014)
- [101] Chung, P.-Y., Wang, P.-Y., Dou, X., and Jiang, P.: Templated Nanodimple Arrays with Tunable Nanostructures for Sensitive Surface Plasmon Resonance Analysis. *The Journal of Physical Chemistry C* 117, 8933–8940 (2013)
- [102] Shen, Y., Zhou, J., Liu, T., Tao, Y., Jiang, R., Liu, M., Xiao, G., Zhu, J., Zhou, Z.-K., Wang, X., Jin, C., and Wang, J.: Plasmonic gold mushroom arrays with refractive index sensing figures of merit approaching the theoretical limit. *Nat Commun* 4 (2013)
- [103] Verellen, N., Van Dorpe, P., Huang, C., Lodewijks, K., Vandenbosch, G. A. E., Lagae, L., and Moshchalkov, V. V.: Plasmon Line Shaping Using Nanocrosses for High Sensitivity Localized Surface Plasmon Resonance Sensing. *Nano Letters* 11, 391–397 (2011)
- [104] Kharissova, O. V., Kharisov, B. I., Garcia, T. H., and Mendez, U. O.: A Review on Less-common Nanostructures. *Synthesis and Reactivity in Inorganic, Metal-Organic, and Nano-Metal Chemistry* 39, 662–684 (2009)
- [105] Acimovic, S. S., Ortega, M. A., Sanz, V., Berthelot, J., Garcia-Cordero, J. L., Renger, J., Maerkl, S. J., Kreuzer, M. P., and Quidant, R.: LSPR Chip for Parallel, Rapid and Sensitive Detection of Cancer Markers in Serum. *Nano Letters* (2014)
- [106] Malic, L., Morton, K., Clime, L., and Veres, T.: All-thermoplastic nanoplasmonic microfluidic device for transmission SPR biosensing. *Lab on a Chip* (2013)
- [107] Huang, C., Bonroy, K., Reekmans, G., Laureyn, W., Verhaegen, K., De Vlaminck, I., Lagae, L., and Borghs, G.: Localized surface plasmon resonance biosensor integrated with microfluidic chip. *Biomedical Microdevices* 11, 893–901 (2009)
- [108] Gallegos, D., Long, K. D., Yu, H., Clark, P. P., Lin, Y., George, S., Nath, P., and Cunningham, B. T.: Label-free biodetection using a smartphone. *Lab Chip* 13, 2124–2132 (2013)
- [109] Chang, T.-Y., Huang, M., Yanik, A. A., Tsai, H.-Y., Shi, P., Aksu, S., Yanik, M. F., and Altug, H.: Large-scale plasmonic microarrays for label-free high-throughput screening. *Lab Chip* 11, 3596–3602 (2011)
- [110] Im, H., Lee, S. H., Wittenberg, N. J., Johnson, T. W., Lindquist, N. C., Nagpal, P., Norris, D. J., and Oh, S. H.: Template-stripped smooth Ag nanohole arrays with silica shells for surface plasmon resonance biosensing. *ACS Nano* 5, 6244–6253 (2011). Cited By (since 1996):31 Export Date: 28 January 2014 Source: Scopus

## Bibliography

---

- [111] Cetin, A. E., Coskun, A. F., Galarreta, B. C., Huang, M., Herman, D., Ozcan, A., and Altug, H.: Handheld high-throughput plasmonic biosensor using computational on-chip imaging. *Light Sci Appl* 3, e122 (2014). Supplementary information available for this article at <http://www.nature.com/lsa/journal/v3/n1/supinfo/lsa20143s1.html>
- [112] Im, H., Sutherland, J. N., Maynard, J. A., and Oh, S.-H.: Nanohole-Based Surface Plasmon Resonance Instruments with Improved Spectral Resolution Quantify a Broad Range of Antibody-Ligand Binding Kinetics. *Analytical Chemistry* 84, 1941–1947 (2012)
- [113] Yanik, A. A., Huang, M., Artar, A., Chang, T.-Y., and Altug, H.: Integrated nanoplasmonic-nanofluidic biosensors with targeted delivery of analytes. *Applied Physics Letters* 96, 021101 (2010)
- [114] Eftekhari, E., Ferreira, J., Santos, M. L. J., Escobedo, C., Brolo, A. G., Sinton, D., and Gordon, R.: Development of portable SPR sensor devices based on integrated periodic arrays of nanoholes. *Proc SPIE* 7356, 73560C–73560C–7 (2009)
- [115] Patskovsky, S., Blanchard-Dionne, A.-P., Rousset, N., and Meunier, M.: Double peak nanoplasmonic sensor for multiple biosensing. *NSTI-Nanotech* 3 (2011)
- [116] Sannomiya, T., Scholder, O., Jefimovs, K., Hafner, C., and Dahlin, A. B.: Investigation of Plasmon Resonances in Metal Films with Nanohole Arrays for Biosensing Applications. *Small* 7, 1653–1663 (2011)
- [117] Barik, A., Otto, L. M., Yoo, D., Jose, J., Johnson, T. W., and Oh, S.-H.: Dielectrophoresis-Enhanced Plasmonic Sensing with Gold Nanohole Arrays. *Nano Letters* 14, 2006–2012 (2014)
- [118] Xu, M., Luo, X., and Davis, J. J.: The label free picomolar detection of insulin in blood serum. *Biosensors and Bioelectronics* 39, 21–25 (2013)
- [119] Luo, X., Xu, M., Freeman, C., James, T., and Davis, J. J.: Ultrasensitive Label Free Electrical Detection of Insulin in Neat Blood Serum. *Analytical Chemistry* 85, 4129–4134 (2013)
- [120] Cottier, K., Wiki, M., Voirin, G., Gao, H., and Kunz, R. E.: Label-free highly sensitive detection of (small) molecules by wavelength interrogation of integrated optical chips. *Sensors and Actuators B: Chemical* 91, 241–251 (2003)
- [121] Yao, G.-H., Liang, R.-P., Huang, C.-F., Wang, Y., and Qiu, J.-D.: Surface Plasmon Resonance Sensor Based on Magnetic Molecularly Imprinted Polymers Amplification for Pesticide Recognition. *Analytical Chemistry* 85, 11944–11951 (2013)
- [122] Polonschii, C., David, S., Tombelli, S., Mascini, M., and Gheorghiu, M.: A novel low-cost and easy to develop functionalization platform. Case study: Aptamer-based detection of thrombin by surface plasmon resonance. *Talanta* 80, 2157 – 2164 (2010)

- [123] Tombelli, S., Minunni, M., Luzi, E., and Mascini, M.: Aptamer-based biosensors for the detection of HIV-1 Tat protein. *Bioelectrochemistry* 67, 135 – 141 (2005). {NABB} 2003: New Trends in Nucleic Acid Based Biosensors
- [124] Bini, A., Minunni, M., Tombelli, S., Centi, S., and Mascini, M.: Analytical Performances of Aptamer-Based Sensing for Thrombin Detection. *Analytical Chemistry* 79, 3016–3019 (2007)
- [125] White, R. J., Phares, N., Lubin, A. A., Xiao, Y., and Plaxco, K. W.: Optimization of Electrochemical Aptamer-Based Sensors via Optimization of Probe Packing Density and Surface Chemistry. *Langmuir* 24, 10513–10518 (2008)
- [126] Chang, A. L., McKeague, M., Liang, J. C., and Smolke, C. D.: Kinetic and Equilibrium Binding Characterization of Aptamers to Small Molecules using a Label-Free, Sensitive, and Scalable Platform. *Analytical Chemistry* (2014)
- [127] Jang, H. R., Wark, A. W., Baek, S. H., Chung, B. H., and Lee, H. J.: Ultrasensitive and Ultrawide Range Detection of a Cardiac Biomarker on a Surface Plasmon Resonance Platform. *Analytical Chemistry* 86, 814–819 (2013)
- [128] Miller, M. M. and Lazarides, A. A.: Sensitivity of Metal Nanoparticle Surface Plasmon Resonance to the Dielectric Environment. *The Journal of Physical Chemistry B* 109, 21556–21565 (2005)
- [129] Szunerits, S., Praig, V. G., Manesse, M., and Boukherroub, R.: Gold island films on indium tin oxide for localized surface plasmon sensing. *Nanotechnology* 19, 195712 (2008)
- [130] Malinsky, M. D., Kelly, K. L., Schatz, G. C., and Van Duyne, R. P.: Chain Length Dependence and Sensing Capabilities of the Localized Surface Plasmon Resonance of Silver Nanoparticles Chemically Modified with Alkanethiol Self-Assembled Monolayers. *J Am Chem Soc* 123, 1471–1482 (2001)
- [131] Homola, J.: Present and future of surface plasmon resonance biosensors. *Analytical and Bioanalytical Chemistry* 377, 528–539 (2003)
- [132] Thost, J.-P., Krieger, W., Kroo, N., Szentirmay, Z., and Walther, H.: Determination of the propagation length of surface plasmons with the scanning tunneling microscope. *Optics Communications* 103, 194 – 200 (1993)
- [133] Kim, D.-K., Kerman, K., Saito, M., Sathuluri, R. R., Endo, T., Yamamura, S., Kwon, Y.-S., and Tamiya, E.: Label-Free DNA Biosensor Based on Localized Surface Plasmon Resonance Coupled with Interferometry. *Analytical Chemistry* 79, 1855–1864 (2007)
- [134] Hutter, E. and Fendler, J. H.: Exploitation of Localized Surface Plasmon Resonance. *Advanced Materials* 16, 1685–1706 (2004)

## Bibliography

---

- [135] Lopatynskiy, A. M., Lopatynska, O. G., Guo, L. J., and Chegel, V. I.: Localized Surface Plasmon Resonance Biosensor-Part I: Theoretical Study of Sensitivity-Extended Mie Approach. *Sensors Journal, IEEE* 11, 361–369 (2011)
- [136] Gao, S., Koshizaki, N., Koyama, E., Tokuhisa, H., Sasaki, T., Kim, J.-K., Cho, Y., Kim, D.-S., and Shimizu, Y.: Innovative Platform for Transmission Localized Surface Plasmon Transducers and Its Application in Detecting Heavy Metal Pd(II). *Analytical Chemistry* 81, 7703–7712 (2009)
- [137] Shao, Y., Xu, S., Zheng, X., Wang, Y., and Xu, W.: Optical Fiber LSPR Biosensor Prepared by Gold Nanoparticle Assembly on Polyelectrolyte Multilayer. *Sensors* 10, 3585–3596 (2010)
- [138] Haes, A. J. and Van Duyne, R. P.: A Nanoscale Optical Biosensor: Sensitivity and Selectivity of an Approach Based on the Localized Surface Plasmon Resonance Spectroscopy of Triangular Silver Nanoparticles. *Journal of the American Chemical Society* 124, 10596–10604 (2002). PMID: 12197762
- [139] Yonzon, C. R., Stuart, D. A., Zhang, X., McFarland, A. D., Haynes, C. L., and Van Duyne, R. P.: Towards advanced chemical and biological nanosensors An overview. *Talanta* 67, 438–448 (2005)
- [140] Anker, J. N., Hall, W. P., Lyandres, O., Shah, N. C., Zhao, J., and Van Duyne, R. P.: Biosensing with plasmonic nanosensors. *Nat Mater* 7, 442–453 (2008). 10.1038/nmat2162
- [141] Kedem, O., Tesler, A. B., Vaskevich, A., and Rubinstein, I.: Sensitivity and Optimization of Localized Surface Plasmon Resonance Transducers. *ACS Nano* 5, 748–760 (2011)
- [142] Zhu, S., Li, F., Du, C., and Fu, Y.: A localized surface plasmon resonance nanosensor based on rhombic Ag nanoparticle array. *Sensors and Actuators B: Chemical* 134, 193–198 (2008)
- [143] Myroshnychenko, V., Rodriguez-Fernandez, J., Pastoriza-Santos, I., Funston, A. M., Novo, C., Mulvaney, P., Liz-Marzan, L. M., and Garcia de Abajo, F. J.: Modelling the optical response of gold nanoparticles. *Chemical Society Reviews* 37, 1792–1805 (2008)
- [144] Hong, Y., Huh, Y.-M., Yoon, D. S., and Yang, J.: Nanobiosensors Based on Localized Surface Plasmon Resonance for Biomarker Detection. *Journal of Nanomaterials* 2012, 13 (2012)
- [145] Willets, K. A. and Van Duyne, R. P.: Localized surface plasmon resonance spectroscopy and sensing. *Annu Rev Phys Chem* 58, 267–97 (2007). Willets, Katherine A Van Duyne, Richard P 4R33 DK 066990-02/DK/NIDDK NIH HHS/ U54 CA 119341/CA/NCI NIH HHS/ Annu Rev Phys Chem. 2007;58:267-97.
- [146] Shon, Y.-S., Choi, H., Guerrero, M., and Kwon, C.: Preparation of Nanostructured Film Arrays for Transmission Localized Surface Plasmon Sensing. *Plasmonics* 4, 95–105 (2009)

- [147] Haes, A. J., Zou, S., Schatz, G. C., and Van Duyne, R. P.: A Nanoscale Optical Biosensor: The Long Range Distance Dependence of the Localized Surface Plasmon Resonance of Noble Metal Nanoparticles. *The Journal of Physical Chemistry B* 108, 109–116 (2003)
- [148] Boardman, A. D.: *Electromagnetic surface modes*. Wiley (1982)
- [149] Kvasnicka, P. and Homola, J.: Optical sensors based on spectroscopy of localized surface plasmons on metallic nanoparticles: Sensitivity considerations. *Biointerphases* 3, FD4–FD11 (2008)
- [150] Mayer, K. M. and Hafner, J. H.: Localized Surface Plasmon Resonance Sensors. *Chemical Reviews* 111, 3828–3857 (2011)
- [151] Siegfried, T., Ekinici, Y., Solak, H. H., Martin, O. J. F., and Sigg, H.: Fabrication of sub-10nm gap arrays over large areas for plasmonic sensors. *Applied Physics Letters* 99, 263302 (2011)
- [152] Abasahl, B., Santschi, C., and Martin, O. J. F.: Plasmonic break junctions: Controlling optical nanostructures with dimensions between atomic contact and a few Angstroms. Int. Conf. on Nanoscience and Technology ICNT 2012 (2012)
- [153] Zhang, N., Su, X., Free, P., Zhou, X., Neoh, K. G., Teng, J., and Knoll, W.: Plasmonic metal nanostructure array by glancing angle deposition for biosensing application. *Sensors and Actuators B: Chemical* 183, 310–318 (2013)
- [154] Yao, J., Le, A.-P., Gray, S. K., Moore, J. S., Rogers, J. A., and Nuzzo, R. G.: Functional Nanostructured Plasmonic Materials. *Advanced Materials* 22, 1102–1110 (2010)
- [155] Siegfried, T., Ekinici, Y., Martin, O. J., and Sigg, H.: Engineering Metal Adhesion Layers That Do Not Deteriorate Plasmon Resonances. *ACS Nano* 7, 2751–2757 (2013)
- [156] Galopin, E., Touahir, L., Niedziolka-Jonsson, J., Boukherroub, R., Gouget-Laemmel, A. C., Chazalviel, J.-N., Ozanam, F., and Szunerits, S.: Amorphous silicon-carbon alloys for efficient localized surface plasmon resonance sensing. *Biosensors and Bioelectronics* 25, 1199 – 1203 (2010)
- [157] Huang, C., Bonroy, K., Reekman, G., Verstreken, K., Lagae, L., and Borghs, G.: An on-chip localized surface plasmon resonance-based biosensor for label-free monitoring of antigen–antibody reaction. *Microelectronic Engineering* 86, 2437 – 2441 (2009)
- [158] Cantale, V., Simeone, F. C., Gambari, R., and Rampi, M. A.: Gold nano-islands on FTO as plasmonic nanostructures for biosensors. *Sensors and Actuators B: Chemical* 152, 206–213 (2011)
- [159] Montmeat, P., Marchand, J.-C., Lalauze, R., Viricelle, J.-P., Tournier, G., and Pijolat, C.: Physico-chemical contribution of gold metallic particles to the action of oxygen on tin dioxide sensors. *Sensors and Actuators B: Chemical* 95, 83–89 (2003)

## Bibliography

---

- [160] Yunus, W. M. b. M. and Rahman, A. b. A.: Refractive index of solutions at high concentrations. *Applied Optics* 27, 3341–3343 (1988)
- [161] Huang, C., Ye, J., Wang, S., Stakenborg, T., and Lagae, L.: Gold nanoring as a sensitive plasmonic biosensor for on-chip DNA detection. *Applied Physics Letters* 100, – (2012)
- [162] Hicks, E. M., Zhang, X., Zou, S., Lyandres, O., Spears, K. G., Schatz, G. C., and Duyne, R. P. V.: Plasmonic Properties of Film over Nanowell Surfaces Fabricated by Nanosphere Lithography. *Journal of Physical Chemistry B* 109, 22351–22358 (2005)
- [163] Ho, H. P., Wong, C. L., Chan, K. S., Wu, S. Y., and Lin, C.: Application of two-dimensional spectral surface plasmon resonance to imaging of pressure distribution in elastohydrodynamic lubricant films. *Appl Opt* 45, 5819–5826 (2006)
- [164] Dahlin, A. B., Zahn, R., and Voros, J.: Nanoplasmonic sensing of metal-halide complex formation and the electric double layer capacitor. *Nanoscale* 4, 2339–2351 (2012)
- [165] Zelphati, O., Uyechi, L. S., Barron, L. G., and Jr., F. C. S.: Effect of serum components on the physico-chemical properties of cationic lipid/oligonucleotide complexes and on their interactions with cells. *Biochimica et Biophysica Acta (BBA) - Lipids and Lipid Metabolism* 1390, 119 – 133 (1998)



# Giulia Cappi

Italian Nationality  
Born on March 16<sup>th</sup>, 1984  
Av. Vinet 23, 1004 Lausanne, Switzerland  
[giulia.cappi@gmail.com](mailto:giulia.cappi@gmail.com)  
+41 762441603

## Education

---

### 2010- 2014 **PhD Student in Biotechnology and Bioengineering**

Swiss Federal Institute of Technology (EPFL), Lausanne, Switzerland  
Laboratory of Life Science Electronics (CLSE), Prof. Carlotta Guiducci

- Bioanalytical parallel systems based on Transmission Localized Surface Plasmon Resonance. The project involves the design and development of portable and low cost platforms for real-time measurements of biomolecular interactions (DNA, RNA, pharmaceutical drugs). Measurement of spectral emissions, optical and electronic characterization, microfabrication, data analysis and algorithms development via MATLAB.

### 2007- 2009 **M.Sc. in Biomedical Engineering**

University of Rome "Sapienza", Rome, Italy

### 2003- 2006 **B.Sc. in Clinical Engineering**

University of Rome "Sapienza", Rome, Italy

## Projects and Internships

---

### 2010 **University of Rome "Sapienza", Rome, Italy**

Scientific Collaboration at the Electronics Engineering Department (3 months)

- Design and development of electrowetting devices for Lab-on-a-chip. The project involved microfabrication and electrical characterization.

### 2009 **PHILIPS Research Europe, Eindhoven, The Netherlands**

Internship at the Molecular Diagnostics Department (6 months)

- Optimization of a Compact Confocal Scanner for quantitative Polymerase Chain Reaction monitoring. Functionality test, thermal characterization and COMSOL simulations.

### 2006 **Istituto Superiore di Sanità, Rome, Italy**

Internship at the Health and Technology Department (5 months)

- Measurement and Data Processing of pressure waves non-invasively recorded in order to synthesize the aortic pressure. The objective was to derive the system transfer function starting from radial pressure measurements and to study how age and drugs affect the pressure waveform.

## Languages

---

**ITALIAN** mother tongue

**ENGLISH** full working proficiency

**FRENCH** full working proficiency (C1 level)

**GERMAN** personal proficiency (B1 level)

## Publications

---

### Journal papers

1. G. Cappi, E. Accastelli, V. Cantale, M. A. Rampi, L. Benini, C. Guiducci, "Peak shift measurement of localized surface plasmon resonance by a portable electronic system", *Sensors and Actuators, B*. Volume 176, January 2013, Pages 225–231.
2. G. Cappi, Y. Moncada, F. M. Spiga, A. Ferretti, M. Beyeler, M. Bianchessi, C. Guiducci, "Label-free detection of Tobramycin in Serum by Transmission- LSPR", In preparation, 2014.

**Oral presentations  
and conference  
proceedings**

1. E. Accastelli, G. Cappi, J. Buckley, C. Guiducci, "Comparison between front- and back-gating of Silicon Nanoribbons in real-time sensing experiments". The 13th IEEE International Conference on Nanotechnology, August 5-8, 2013, Beijing, China.
2. G. Cappi, E. Accastelli, L. Benini, C. Guiducci, "A portable setup for molecular detection based on transmission LSPR". XXI International Materials Research Congress, Cancún, Mexico, August 12-17, 2012. Nanostructured Materials and Nanotechnology Symposium- MRS Proceedings from IMRC 2012.
3. G. Cappi, E. Accastelli, V. Cantale, M. A. Rampi, L. Benini, C. Guiducci, "A Portable Biomolecular Interaction Sensor based on Localized SPR on Gold Nanoislands". In SPP5 - The Fifth International Conference on Surface Plasmon Photonics, Busan, South Korea, 15th-20th May 2011.
4. C. Guiducci, Y. Temiz, Y. Leblebici, E. Accastelli, A. Ferretti, G. Cappi, E. Bianchi, "Integrating Bio-sensing Functions on CMOS Chips". Asia Pacific Conference on Circuits and Systems (APCCAS 2010), Kuala Lumpur, Malaysia, December 6th – 9th, 2010.

**Posters**

1. G. Cappi, E. Accastelli, F. Spiga, C. Guiducci, "LSPR-based system for high-throughput real-time measurements of biomolecular interactions". In SPP6 - The Sixth International Conference on Surface Plasmon Photonics, Ottawa, Canada, 26th-31st May 2013.
2. E. Accastelli, G. Cappi, J. Buckley, B. De Salvo, C. Guiducci, "Characterization of Silicon Nanoribbons". Nanobiotech, Montreux, November 12th-14th, 2012.